Master of Science Thesis

Model Predictive Control for optimum integration of Active and Passive Energy sources

Naveen Rajappa

Submitted to obtain the degree of Master of Science in
Mechanical Engineering at the Delft University of Technology

June 14, 2023

Thesis Committee:

Dr. R.M.J. Bokel
Prof.dr. L.C.M. Itard
Dr. B.P. Tighe
Prof. Dr. K. Hooman

The work in this thesis was carried out in collaboration with:

Brains4Buildings
www.brains4buildings.org

Thesis Committee :
Prof.dr. L.C.M Itard
Prof.dr. R.M.J Bokel
Dr. B.P Tighe
Prof.dr. K. Hooman

Contents

List of Figures

List of Tables

Acronyms

List of Symbols

Symbol	Quantity	Unit
μ	Dynamic viscosity	Pa.s
ν	Kinematic viscosity	J. s kg^1
Nu	Nusselt number	-
Pr	Prandtl number	-
Ra	Rayleigh number	-
Re	Reynolds number	-
ρ	Density	kg m^3
A	Area	m^2
c_p	Specific heat capacity	J kg^1 K^{-1}
V	Volume	m^3
g	Acceleration due to gravity	m s^2
h	Convective heat transfer coefficient	W K^1 m^2
$\dot{m}$	Mass flow rate	Kg/s
$\dot{Q}_{sol}$	Energy gain rate by solar irradiation	W
$\dot{Q}_{conv}$	Energy gain rate by convection	W
$\dot{Q}_{cond}$	Energy gain rate by conduction	W
$\dot{Q}_{rad}$	Energy gain rate by long wave IR radiation	W
$\dot{Q}_{adv}$	Energy gain rate by advection	W
$\dot{Q}_{vent}$	Energy gain rate by ventilation	W
$\dot{Q}_{adv}$	Energy gain rate by advection	W

Symbol	Quantity	Unit
$\dot{Q}_{gen}$	Internal Energy gain rate	W
$\dot{Q}_{hp}$	Energy supply rate by heat pump	W
n	Number of glazings in series before a component	-
T_{amb}	Ambient air temperature	K
T_z	Indoor air temperature	K
T_r	Roof temperature	K
T_c	Ceiling temperature	K
$T_{n,i}$ [i=1,2,3]	Glazing temperature (north)	K
$T_{s,i}$ [i=1,2,3]	Glazing temperature (south)	K
$T_{e,i}$ [i=1,2,3]	Glazing temperature (east)	K
$T_{w,i}$ [i=1,2,3]	Glazing temperature (west)	K
T_{deck}	Air temperature in deck	K
T_{rf}	Raised floor temperature	K
T_{bf}	Basement floor temperature	K
T_h	Inlet air temperature after heat recovery	K
T_{pcm}	Temperature of PCM battery	K
$T_{air,pcm}$	Temperature of air via PCM battery	K
y_{pcm}	Liquid fraction of PCM	-
H_{pcm}	Latent heat capacity of PCM	J/Kg
T_g	Ground temperature	K
T_{mix}	Temperature of air entering the heat pump	K
T_{hp}	Temperature of air after passing through heatpump	K

Symbol	Quantity	Unit
x_h	Position of solar blinds	-
x_{sw}	Aperture fraction of Sky windows	-
x_{pcm}	Fraction of air stream passing through PCM	-
x_{rec}	Fraction of heat recuperation	-
α	Solar irradiance absorptance	-
α_o	Oriented Solar irradiance absorptance	-
λ	Thermal conductivity of fluid or gas	-
σ	Stefan–Boltzmann constant	W/m^2K^{-4}
β	Angle between a surface and horizontal	Degrees
θ_n	Angle between surface normal and solar beam	Deg
ρ_g	Ground reflectance	Albedo
θ_z	Zenith angle	Deg
G_{sc}	Solar constant	kW/m^2
h	convective heat transfer coefficient	$W/(m^2K)$
$\mathcal{F}$	Radiation view factor between two surfaces	-
X	Component Width	m
Y	Component Length	m
Z	Component Height	m
ϵ	Surface emissivity	-
ϵ_{low}	Surface emissivity for low ϵ glass	-
ξ	Effective optical transparency	-
k	Thermal conductivity	$W\ K^1\ m^1$
η	efficiency	-

Abstract

The primary objective of this research is to develop an energy management system for the Co-creation center (CCC) that maximizes the use of passive energy sources while maintaining indoor thermal comfort. Passive energy sources have the potential to significantly reduce the energy consumption of the building. However, to achieve optimal energy savings, it is necessary to integrate multiple passive energy sources and develop a control strategy that can manage them effectively.

Model Predictive Control (MPC) strategies have been extensively researched in the literature as a means of optimizing energy consumption in buildings. However, most studies only consider a single passive energy source or energy distribution in multiple zones. There is limited research on the optimal management of multiple passive energy sources.

To address this gap, this thesis investigates the use of an MPC strategy to optimize the operation of multiple passive energy sources in a building. Specifically, the research focuses on four solar blinds, a Phase Change Material (PCM) battery, sky windows, heat recuperation, natural ventilation, and an active energy source. Grey-box modeling is used to model the building, and the model is calibrated using experimental data.

The MPC problem is then set up to minimize energy supplied by Heat pump (HP) while ensuring indoor thermal comfort during occupied periods. An adaptive comfort model is used as a criterion to satisfy during occupied periods. The proposed MPC control is then implemented in the building.

The results show that the proposed MPC outperforms the rule-based controller in terms of energy consumption and maintaining thermal comfort. The research further provides insights into the potential of MPC strategy to increase the energy flexibility of buildings. The final parts of this research focused on varying the PCM temperatures and using a more flexible thermal comfort model and studying its effects on the energy demand of the building. The findings could be used to inform the design of energy-efficient buildings and the development of smart energy management systems.

Acknowledgements

Writing this master's thesis has been an unforgettable journey, filled with both challenges and triumphs. I am incredibly grateful for the support and motivation provided by the wonderful individuals who surrounded me throughout this process. Their guidance and encouragement made this accomplishment possible.

First and foremost, I extend my deepest gratitude to Professor Regina Bokel for her invaluable role as one of my direct supervisors. The regular discussions we had were instrumental in shaping this thesis and fueled my determination to strive for the desired outcomes. I would like to extend my heartfelt gratitude to Prof. Laure Itard for her invaluable guidance and mentorship throughout my research journey, as well as for sparking my passion for the field of building physics. Her expertise and support have played a pivotal role in shaping this thesis. Furthermore, I extend my thanks to Professor Brian Tighe for accepting the role of the supervisor from EFPT and ensuring a seamless completion of this thesis. His guidance and support were invaluable. I would also like to thank Professor Kamel Hooman for accepting the last-minute invite to be a part of the graduation committee.

Special thanks go to Yun Li, who introduced me to the world of Model Predictive Control. The discussions we shared had a profound impact on shaping the content of this thesis. I am also grateful for the warm welcome and invaluable experience provided by the Brains4Buildings group, which allowed me to delve into the fascinating realm of smart buildings. Their support and guidance were instrumental in shaping my understanding of this field. I extend my heartfelt thanks to Tim Jonathan from The Green Village for his patience in handling my numerous requests and entrusting me with important responsibilities

Finally, I want to express my heartfelt gratitude to my parents for their unwavering support throughout this journey, despite the distance that separated us. Their belief in me empowered me to pursue my dreams. I would also like to extend my thanks to my friends and colleagues for their unwavering support during these challenging times.

I would like to conclude this acknowledgment section with a quote that resonated deeply with me throughout this endeavor:

"I have not failed. I've just found 10,000 ways that won't work."
- Thomas Edison

1 Introduction

1.1 Building energy demand

The depletion of fossil resources is largely caused by the increasing energy consumption in modern times. Urban areas are responsible for about 40% of total energy consumption in the EU [4]., with two-thirds of that energy being used for Heating Ventilation and Air Conditioning (HVAC). This results in 25% of total energy consumption being used to maintain pleasant indoor temperatures. In 2015, the Dutch government implemented Building regulations to reduce energy consumption in the sector, and as of 2021, all new constructions must meet the requirements for Nearly Energy-Neutral Buildings (BENG). The BENG has a three-step approach to decrease CO_2 consumption[5]:

- Limit the energy consumption per built area
- Limit the maximum primary fossil energy consumption.
- Increase the share of renewable energy

According to BENG regulations [6], the average consumption for a newly constructed office building is 90 kWh/m2 per year. Of this amount, a maximum of 40 kWh/m^2 can come from non-renewable sources, and at least 30% must be sourced from renewable energy.

1.2 CONVERGE project

The feasibility of meeting BENG standards varies depending on the type of building; for example, a terraced building may find it easier to meet the requirements due to less surface area for energy loss, while a standalone office building may have a higher energy demand in the range of 100-150 kWh/m^2 per year [7], requiring technical innovations to reduce energy consumption. An initiative aimed at finding innovative solutions for building energy is the TU Delft CONVERGE project (www.thegreenvillage.org/project/converge/).

Passive climate control methods have been identified as a potential means of decreasing energy consumption in buildings. Such strategies include the use of operable windows, solar blinds, phase change materials, and heat recovery systems. In 2018, the Green Village foundation of TU Delft began a project aimed at researching and developing a nearly zero-energy building, which was originally based on the "Earth, Wind Fire" project. The project, called CONVERGE (short for COmfortable Natural Ventilation and Energy REduction), has two primary objectives:

- Optimum integration of passive climate control systems into Building energy management system (BEMS) to reduce at least 80 % of energy demand
- To serve as a test bed to gain insights and apply this knowledge in practice

The Co-Creation Centre serves as both a gathering place and a research hub. It features a spacious conference room that can accommodate various events like conferences, educational seminars, and office meetings. The number of attendees can range from a small group to a full house. The conference room, which is visible in Figure 3.3 features large glass walls. On the right side, the service cabin is equipped with a kitchen, restrooms, and technology facilities. The building features cutting-edge glass engineering, as evidenced by its fully

Figure 1.1: Co-creation center

transparent triple-glazed facades and glass columns. To mitigate overheating, the building was designed with large overhangs and automated outdoor sunshades. Originally intended for a capacity of 30 individuals, the building was later modified to accommodate up to 240 attendees in a meeting setting prior to the imposition of Covid restrictions. The building's climate is maintained by a climate tower, which can be seen on the left in Figure 1, and its energy performance is further enhanced through the installation of PV panels on the tower. The building aspires to achieve energy neutrality or even a positive energy balance, which exceeds the Dutch BENG standard. Additionally, the building serves as a research facility to study the feasibility of passively heating, cooling, and ventilating a transparent building while maintaining comfort levels. The building is continuously monitored through an extensive sensor network.

The TU Delft plays a significant role in the CONVERGE project by dedicating its researchers and students to it. Additionally, companies such as Van Dorp, Priva, and Hunter Douglas

provide the necessary hardware and software for the project to be executed. The Green Village also comprises a wide range of stakeholders, which is leveraged to raise awareness about the project.

1.3 Research Question

The research question is "How to design an efficient model predictive control strategy to the Co-creation center which integrates solar shading with passive ventilation and phase change materials with the goal of optimizing the passive energy utilization ratio while maintaining indoor thermal comfort ?". In order to effectively tackle the primary research questions, it is essential to break them down into smaller objectives. These sub-questions act as stepping stones, providing a framework for the research and serving as a structured approach to direct our inquiry. The sub-questions are :

1. How well does the developed building model compare to the thermal behavior in an actual building?
2. How can a building's model be created to be both accurate and not overly complex for model-based control?
3. How does the created model predictive control strategy effectively combine passive and active energy sources while still ensuring thermal comfort?
4. Is it possible to decrease energy consumption in a building by using this strategy compared to a rule-based controller in a real-case scenario?

1.4 Report Outline

The report is structured as follows: It begins with Chapter 1, which introduces the CONVERGE project and outlines the research objectives. Chapter 2 focuses on the application of the adaptive thermal comfort model within the project. Moving on to Chapter 3 provides an overview of the existing control system and the established benchmark for this research. In Chapter 4, the report delves into the thermodynamic modeling of the various components of the Co-creation center, followed by a chapter dedicated to the validation of this model. From Chapter 6 onwards, the report shifts its focus to the development of the control systems' MPC problem setup. The subsequent chapter discusses the practical implementation and application of the developed MPC. Chapters 8 and 9 examine the performance improvements resulting from the implementation of the MPC, while Chapters 10 and 11 explore potential modifications to further enhance the system. Finally, the last chapter provides the report's conclusions, along with recommendations for future work.

2 Adaptive thermal comfort models

The primary purpose of a building is human habitation. Moreover, people spend almost 90% of their time in buildings. Numerous researchers have shown that indoor comfort plays a crucial role in occupants' health, morale, productivity, and satisfaction. It is thus essential to preserve a comfortable indoor environment whilst trying to reduce the energy consumption of the HVAC systems [8]. Appendix B explains the various aspects of indoor comfort.

The Netherlands has established a number of guidelines for the indoor thermal comfort of buildings since the 1970s [9] , with Fanger's comfort model [10] serving as the foundation for these guidelines. However, it has been revealed through comprehensive experimentation by de Dear et al. [11] that individuals have varying evaluations of indoor climate, particularly when they possess the ability to control or influence the indoor climate. The phenomenon of thermal adaptability, driven by factors such as expectations of indoor climate, has led to the development of flexible temperature ranges in building design [12] , with the potential to reduce the energy consumption of heating, ventilation, and air conditioning systems.

As a result, new adaptive indoor thermal climate directives have been formulated for the Netherlands [13] , in alignment with ASHRAE 55-2004 [14] based on experiments by de Dear and Brager [11]. In recent years, thermal comfort models have increasingly taken human adaptability into account, with adaptive thermal comfort being defined as the ability of individuals to re-establish comfort through various means such as behavioral adaptation, which can include personal, environmental, technical and organizational adjustments [15] . This can include actions such as adjusting window openings, dressing according to external weather conditions and making dietary adjustments. It is important to note that physiological adaptation does not affect an individual's neutrality. But psychological adaptation corresponds to altered perception or response to sensory information [16].

2.1 Adaptive temperature limits (ATG)

The ASHRAE 55-2004 standard outlines a method for determining appropriate thermal conditions in naturally conditioned spaces, however, this method is only relevant for certain types of buildings where the indoor thermal climate is primarily influenced by the occupants (through operable windows, for example) and mechanical air conditioning is not utilized. Brager and de Dear define air-conditioned buildings as sealed, centrally air-conditioned spaces with open floor plans, in which occupants are not able to open or close windows.

In the Netherlands and similar climatic zones, this distinction proves to be impractical as

most buildings fall somewhere between these two extremes. To address this issue, two building types referred to as alpha and beta were introduced by Van der Linden[12]. According to the classification scheme provided by them, if a building has a sealed facade and if two occupants have no more than one operable window, the building belongs to type beta. The CCC hence belongs to type beta.

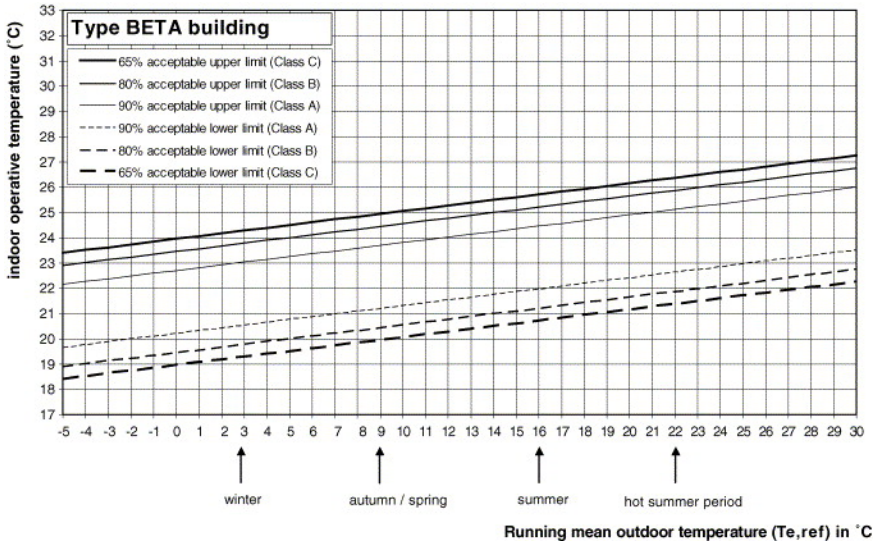

Figure 2.1: Adaptive thermal comfort model (beta)

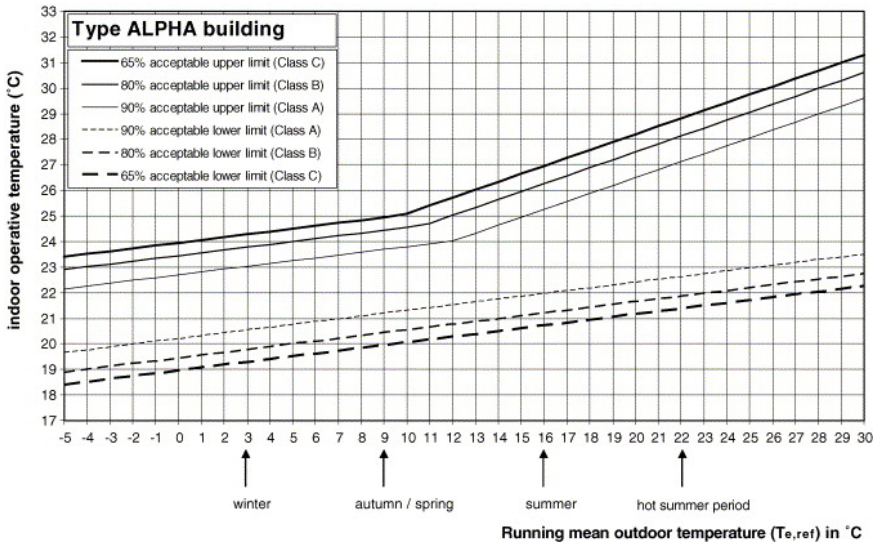

Figure 2.2: Adaptive thermal comfort model (alpha)

In Figure 2.2 and Figure 2.1, along the horizontal axis, $T_{e,ref}$ is to be found and $T_{e,ref}$ is the adapted version of T_{RMO}. The temperature limits have been described for acceptability limits of 65, 80 and 90% respectively. In the ATG method, $T_{e,ref}$ is calculated as:

$$T_{e,ref} = \frac{T_{today} + 0.8T_{yesterday} + 0.4T_{day\ before\ yesterday} + 0.2T_{before\ two\ days}}{2.4} \tag{2.1}$$

Considering the building type to be BETA, the target indoor temperature can be calculated as shown in Equation 2.2 . Assuming 80 % acceptability criteria, the allowable temperature band is $\pm 2^oC$.

$$T_{target} = 21.45 + 0.11T_{e,ref} \pm 2 \quad in\ ^oC \tag{2.2}$$

Considering the building to be belonging to ALPHA (as discussed in Chapter 11), the target temperature and the lower limit of operating temperature would be the same, but the upper limit would be modified if $T_{e,ref}$ is greater than 11^oC as:

$$T_{upper} = T_{target} + 0.21 * (T_{e,ref} - 11) + 2 \quad in\ ^oC \tag{2.3}$$

The adaptive comfort limits can be applied to office buildings where the activity level of occupants is in the range of 1.0-1.4 met and clothing values are between 0.5-1.0 clo and hence it is suitable to be applied to CCC.

2.1.1 Conclusion

To ensure the comfort of occupants, an adaptive comfort model has been studied and is to be applied to this thesis. According to the classification criteria provided by Van der Linden[12], the CCC belongs to the category BETA and the target indoor temperature can be estimated using Equation 2.2. However, the application of ALPHA model will be also discussed in Chapter 11. One of the main advantages of the adaptive comfort model is that it allows for more energy-efficient building design and operation by allowing for a wider range of temperatures, as the occupants have the ability to adapt to the thermal environment.

3 Existing energy components and control options of Co-creation center

3.1 The building energy components

A unique feature of the CONVERGE project is that it combines multiple passive climate control sources and an online control system. The building is equipped with hundreds of sensors and actuators that provide the data for accurate measurement and control. The main focus of the project is on developing an online smart energy management system that ensures occupants' comfort while being energy efficient. The project includes the design of a climate tower, which integrates heat recovery systems, phase change materials, and a heat pump for air conditioning and ventilation as shown in Figure 3.2. The building has

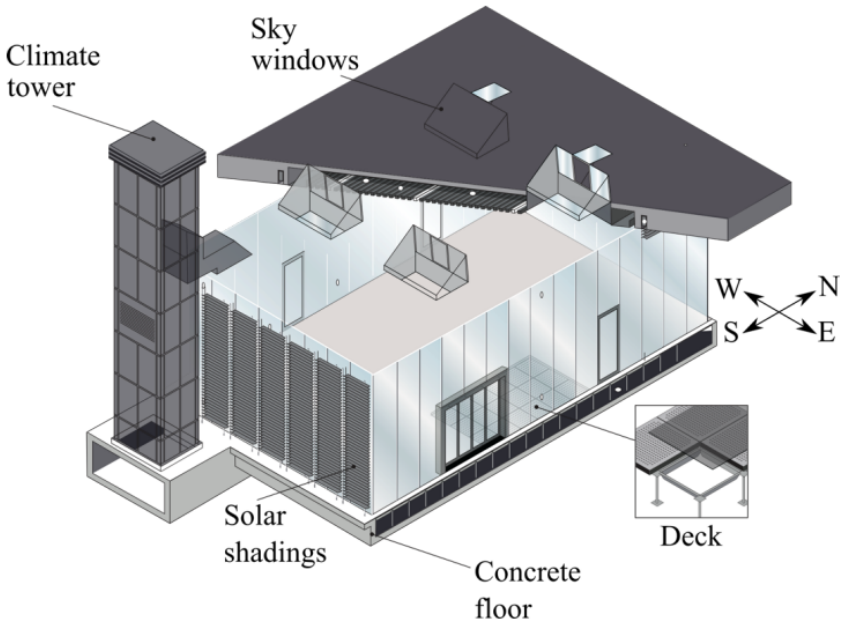

Figure 3.1: General overview of the Co-creation center

fully transparent triple-glazed facades, which are used in conjunction with solar blinds to

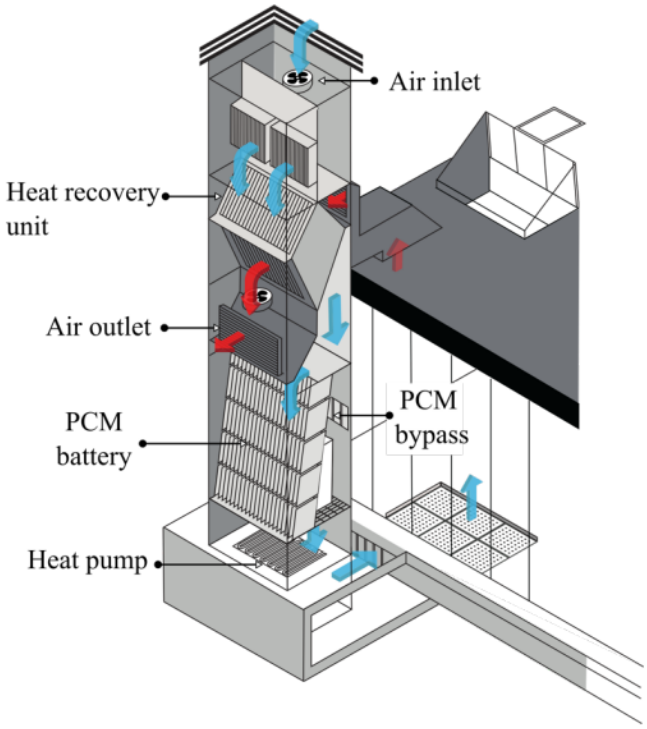

Figure 3.2: An overview of the HVAC components installed in CCC

passively regulate the indoor climate. The building has a floor area of 315m^2, and the facades have a U-value of 0.53 W/m^{2}K. The building is also equipped with 34 photovoltaic panels, each with a maximum output of 300 W, located on the climate tower, which have an estimated annual electricity production range of 6,000 to 7,000 kWh. [17]

The building utilizes a combination of passive solar heating and active heating systems to maintain thermal comfort during the winter months. The transparent facade allows for solar gain, while preheated displacement ventilation is utilized via the floor to further enhance the heating of the interior spaces. An air-based heat pump located in the climate tower serves as the primary heating source for the building. The climate tower, which serves as a large air handling unit, also controls the ventilation system which is monitored by the indoor CO_2 concentration to minimize the number of air changes during the heating season. Additionally, a counter-flow heat exchanger with heat recovery is implemented to further reduce the energy consumption required for ventilation [17].

During the summer months, the building employs a variety of strategies to mitigate solar load and maintain thermal comfort. One such strategy is the use of shading devices such as blinds, as depicted in Figure 3.1. Additionally, overhangs are employed to reduce the amount of direct sunlight entering the building. A phase change material (PCM) battery is

also utilized, consisting of 1,170 panels (totaling 2,106 kg, 181 kWh) [17] of calcium chloride hexahydrate, with a phase change temperature between 20 and 23 °C [17], to provide additional cooling or heating capacity to the building. The PCM battery can be cooled by ventilation during the night and heated by warm return air.

Furthermore, during the cooling season (summer and spring), natural ventilation through skylights and doors can be employed during the day and at night to provide additional cooling. Additional cooling can also be achieved through the use of a heat pump, utilizing return air as a cold source. [17].

A simplified model of the Co-creation center is presented in Figure 3.3, consisting of dif-

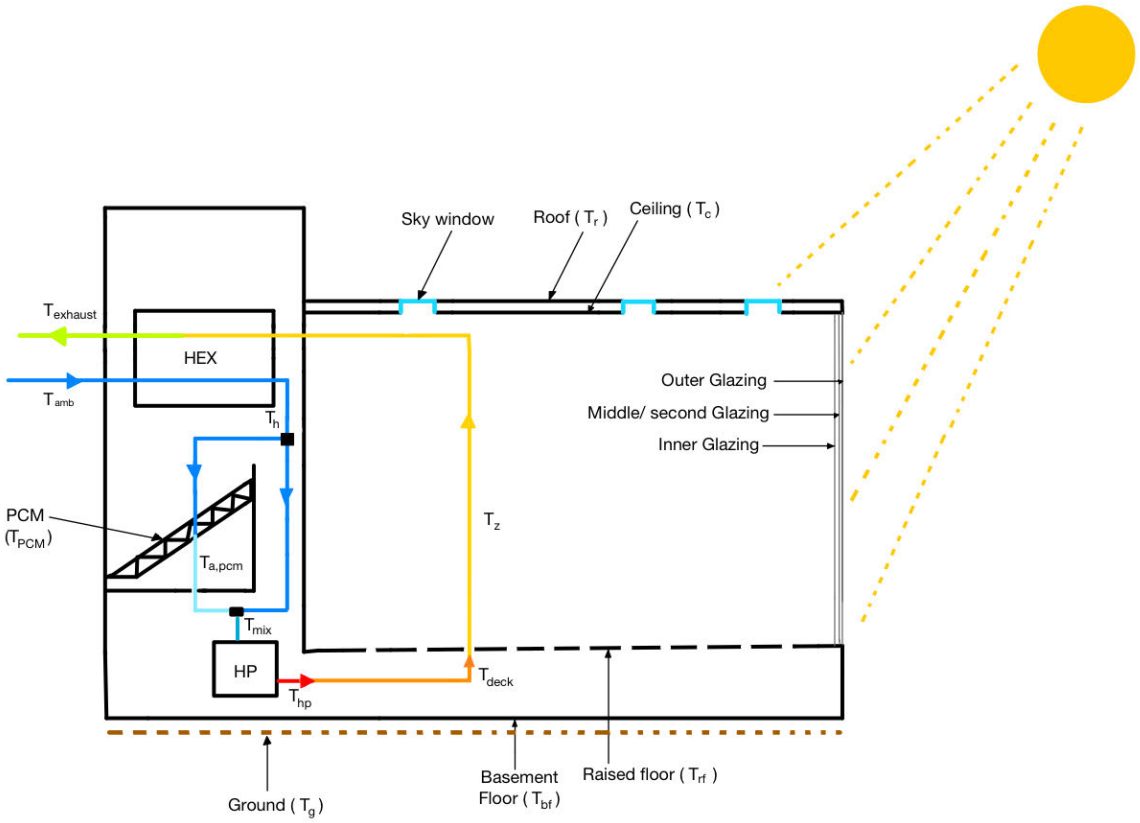

Figure 3.3: Simplified model of CCC various energy components

ferent components such as the roof, ceiling, raised floor, basement floor, four walls made of

State Units	Material -	X m	Y m	Z m	ρ Kg/m^3	c_p J/(KgK)	κ W/(mK)	α -	ξ -	ϵ -	ϵ_{low} -
T_z	Air	13.5	22.5	5.2	1.225	1000	-	-	-	-	-
T_r	Bitmen	13.5	22.5	0.004	1050	1800	0.167	0.87	-	0.92	-
T_c	Steel	13.5	22.5	0.003	7850	840	0.167	-	-	-	-
$T_{n,i}, T_{s,i}$	Glass	13.5	5.2	0.008	2470	792	-	0.078	0.78	0.77	0.16
$T_{e,i}, T_{w,i}$	Glass	22.5	5.2	0.008	2470	792	-	0.078	0.78	0.77	0.16
T_{rf}	Calcium Sulphate	13.5	22.5	0.038	1550	800	-	0.2	-	-	
T_{bf}	Concrete	13.5	22.5	0.225	2000	840	0.313	-	-	-	
T_{pcm}	CCH	0.198	0.57	0.013	1300	1400	-	-	-	-	-

Table 3.1: Dimensions and thermo-physical properties of the building components

triple-glazed glass, an inner zone, and separate nodes representing the flow of air, HEX represents the heat exchanger for heat recovery and HP represents the heat pump. The different geometrical dimensions (length, width and depth represented by X, Y and Z respectively) and physical properties of the various states are represented in Table 3.1 To simplify the model, the significant components were discretized into a single node, and an assumption of uniform temperature throughout was made. This approach was aimed at reducing the complexity of the model by simplifying its components while retaining the essential features needed to analyze the system. These components are affected by disturbances such as :

- Ambient temperature
- Ground temperature
- Ambient Wind speed
- Solar irradiance components (I_d and I_b)
- Occupancy
- Dew point temperature

3.2 Control system: PID controller

The described control system is used to regulate the temperature within a building by considering various factors such as solar irradiation, exterior temperature, and wind conditions. The system utilizes temperature measurements collected in situ and algorithms to keep the tracking error e (the difference between the actual temperature and the desired temperature) close to zero.

One method that has been implemented for this purpose is a PID (Proportional-Integral-Derivative) controller. PID controllers are widely used in control systems due to their accuracy and reliability in maintaining a desired set point [18]. The controller continuously balances the selected inputs, such as shades aperture, ventilation flow rates, and heat pump power, by adjusting a correction factor u that depends on the tracking error feedback.

In more detail, the PID controller is composed of three main components: the proportional, integral and derivative terms. The proportional term is responsible for providing a correction factor that is proportional to the error, the integral term accumulates the error over time, and the derivative term predicts the future error based on the current rate of change. These three terms are combined together to form the control signal. The controller continuously monitors the error and adjusts the correction factor u in real-time to maintain a stable temperature within the building.

$$u = K_p e + K_i \int_0^t e\,dt \; + K_p \frac{de}{dt} \tag{3.1}$$

where K_p and K_p are control parameters tuned for the current controller.

Control of indoor thermal comfort

The indoor thermal comfort is managed by controlling the air temperature set-point. A separate set-point is selected for summer and winter seasons [17]. The air temperature set-point also takes into account the radiant temperature of the glass, which is the temperature that one feels when standing next to the glass, to maintain the operative temperature above 21°C during the winter season [17]. This ensures that the indoor environment is comfortable for the building's occupants.

Solar blinds control

The building is equipped with individually controllable shading devices, i.e blinds, on all four facades. These shading devices can be adjusted to various tilt angles and vertical heights to provide precise control of solar radiation entering the building. Four different shading control strategies were developed and evaluated to optimize the building's thermal comfort [17]:

1. Fixed passive strategy: This strategy involves pre-determined fixed positions for the shading devices and does not involve any active or automated adjustments based on real-time conditions.

2. Sun-tracking dynamic control: This strategy is based on a traditional sun-tracking algorithm, which involves the active and automated control of the tilt of the shading devices, such as blinds, to block direct sunlight at all times.

3. Energy-based dynamic control strategy: This strategy involves the active and automated control of the shading devices based on the amount of available solar energy and the thermal load within the building at any given time. This strategy aims to optimize the use of solar energy and manage the heat requirements of the building by adjusting the position of the shading devices.

4. Visual comfort-based dynamic control: This strategy involves the active and automated control of the shading devices based on the combined requirements of preventing discomfort glare and maximizing the view out. The control of the shading devices is based on illuminance data obtained from sensors installed on the roof of the building. The strategy aims to balance the visual comfort of the building's occupants and the natural light in the space by adjusting the position of the shading devices.

To begin controlling the blinds, the focus should be on using energy-based dynamic control, which has the potential to save energy. However, it is crucial to integrate visual-comfort-based dynamic control into the strategy to avoid direct glare and provide a comfortable environment for the occupants.

Fresh air control

The fresh air supply system in the building is primarily controlled based on the concentration of CO2 in the air when the building is occupied. When the CO_2 concentration falls below 800 parts per million (ppm), the airflow can follow different paths through the climate tower, which is a large air handling unit. The main goal of this system is to provide healthy indoor air quality by maintaining the CO2 concentration in the building under 800 ppm.

Heat recuperation control

The airflow control system for passive heating and cooling in the building has the capability to regulate the operation of the heat exchanger between 0 and 100%. Additionally, the system allows for the option of directing the exhaust air through or bypassing the PCM (Phase Change Material) battery. This allows for the optimization of the building's thermal comfort by adjusting the airflow and utilizing the PCM battery as a thermal storage.

PCM Heating and cooling control

The fundamentals of Phase Change materials is presented in Appendix D. The airflow control system for PCM heating and cooling in the building allows for the regulation of the air passing through the PCM to heat or cool the inlet air. The airflow percentage through the PCM can be adjusted between 0 and 100%. This control strategy is implemented when the building is occupied and the goal is to achieve thermal comfort. When the building is unoccupied or when the indoor air temperature is within the desired range, a portion of the air can pass through the PCM to either heat or cool the PCM, thus storing heat or cold for later use [17].

Heat pump control

The heat pump is used to provide additional heating or cooling to the building's HVAC system based on the calculated thermal load requirements. However, a limitation is imposed on the exhaust temperature of the heat pump to prevent overloading the system and to maintain its efficiency. This limits the maximum amount of energy that can be extracted from the heat pump, which in turn affects the overall performance of the building's HVAC system. The nominal capacity of the heat pump for cooling is 30 kW and for heating is 15 kW.

3.3 Existing models of the building

The present study involves the use of two separate models to simulate the thermal dynamics of a building and its HVAC system. The first model is a Matlab-based multi-node RC network model, which is obtained by utilizing the concept of lumped parameter modeling. This method involves the simplification of the building's thermal dynamics by dividing it into a limited number of "nodes" and approximating the thermal properties of each node. The parameters of the model have been optimized using data, hence it is a $grey-box$ model. However, the current version of the model in Matlab is dependent on elementary weather data, which does not account for the actual occupancy and weather conditions of the building. In order to evaluate the accuracy of the Matlab model, it is necessary to incorporate actual occupancy and weather data and validate it with a white-box model.

The second model, which serves as the validation tool, is a *white-box* model developed in EnergyPlus software. This model has been previously validated with sensor data [17] and has been demonstrated to provide a high level of accuracy in the design of artificial lighting components for the building. By inputting identical weather data and occupancy data into both the Matlab and EnergyPlus models, the Matlab model can be validated by comparing its predictions with those of the EnergyPlus model.

4 Building Energy Modeling

Efficiently capturing the thermal response of a building to external weather conditions and occupancy requires a precise model of the building. While external weather data, such as global horizontal irradiance (GHI), wind characteristics, and outdoor temperatures, can be obtained through available sensors and through proprietary software (as discussed in Section 6.3.4), the measurements are general and may not provide a precise understanding of the amount of sunlight received. To develop an accurate model of the system, it is essential to consider the orientation and location of the building.

Static parameters, such as geometrical and thermo-physical values, can be used to establish a baseline model, which can be refined by tweaking the values of unknown parameters. Starting with a thermal model of the system can provide a solid foundation for parameter adjustments, allowing for greater accuracy in the model's predictions. A wide range of modeling approaches have been investigated to accurately represent the dynamics of energy flow, and these can be broadly classified into three paradigms: white-box, grey-box, and black-box modeling as discussed in Appendix C. In this research, the grey-box modeling approach has been chosen due to its capability to be calibrated using limited data and its appropriateness for applications such as building energy demand estimation, fault detection, and model-based control.

To simplify the complexity of the model, it is assumed that only components in series, such as the roof and ceiling, are thermally coupled, and no direct energy transfer (via conduction) is considered between components such as walls and floors, or between walls and ceilings. In addition, energy transfer through radiation is neglected, as the difference in energy of the internal surfaces is mostly a small quantity and the large inner zone results in a low viewing factor.

It is to be noted that the model has been developed based on the model created by L.A de Araujo Passos and some alterations have been made to few components that are represented by (*)

Roof and Ceiling *

The roof is composed of thin bitumen layer, while the ceiling is constructed of corrugated galvanized steel sheets. Heat transfer between the roof and its surroundings is simulated using Zhukauskas' correlation for forced convection. The model also accounts for solar irradiation and radiation heat transfer between the roof and sky. The approach to model the sky temperature is discussed in Algorithm 1. Additionally, heat transfer between the

ceiling and roof occurs through an insulation layer with a thermal conductivity (κ_{ins}) of 0.167 W/(m.K). The heat transfer between the ceiling and inner zone is modeled using McAdams' convection correlations [19] for downward-facing horizontal surfaces. The roof's heat balance is discretely modeled within the time step Δt as:

$$\Delta T_r = (\dot{Q}_{sol} - \dot{Q}_{cond} - \dot{Q}_{rad} - \dot{Q}_{conv})\frac{\Delta t}{\rho V c_p} \tag{4.1}$$

$$\dot{Q}_{sol} = I_o A_r \alpha_r \tag{4.2}$$

$$\dot{Q}_{cond} = \frac{\kappa_{ins}.A(T_r - T_c)}{d} \tag{4.3}$$

$$\dot{Q}_{rad} = \epsilon\sigma A({T_r}^4 - {T_{sky}}^4) \tag{4.4}$$

$$\dot{Q}_{conv} = \bar{h}_{r,a}.A(T_r - T_a) \tag{4.5}$$

$$\bar{h}_{r,a} = \frac{Nu.\lambda_{air}}{l} \tag{4.6}$$

$$l = \frac{A}{2X + 2Y} \tag{4.7}$$

$$Nu = \begin{cases} 0.664 Re^{0.33} Pr^{0.33} & \text{Re} < 5000 \\ 0.037 Re^{0.62} Pr^{0.333} & 5000 < \text{Re} < 100000 \\ 0.026 Re^{0.8} Pr^{0.333} & \text{Re} > 100000 \end{cases} \tag{4.8}$$

The heat balance of the ceiling is modeled as:

$$\Delta T_c = (-\dot{Q}_{cond} - \dot{Q}_{conv})\frac{\Delta t}{\rho V c_p} \tag{4.9}$$

$$\dot{Q}_{cond} = \kappa.A(T_c - T_r) \tag{4.10}$$

$$\dot{Q}_{conv} = \bar{h}_{c,z}.A(T_c - T_z) \tag{4.11}$$

$$\bar{h}_{c,z} = \frac{\vec{N}u\lambda_{air}}{l} \tag{4.12}$$

$$l = \frac{A}{2X + 2Y} \tag{4.13}$$

$$\vec{N}u = \begin{cases} 0.54Ra^{0.25} & \mathrm{T}_c < \mathrm{T}_z \text{ and Ra} \leq 10^7 \\ 0.15Ra^{0.33} & \mathrm{T}_c < \mathrm{T}_z \text{ and Ra} > 10^7 \\ 0.27Ra^{0.25} & \mathrm{T}_c > \mathrm{T}_z \end{cases} \tag{4.14}$$

Algorithm 1 Sky temperature modeling

Input :T_{dew}, T_a
Output: T_{sky}
procedure
$\varepsilon_{sky} \leftarrow 0.736 + 0.00577T_{dew}$
$I_h \leftarrow \varepsilon_{sky}\sigma((T_a + 273.15)^4)$
$T_{sky} \leftarrow (\frac{I_h}{\sigma})^{0.25} - 273.15$
return T_{sky}

Four triple-glazed walls*

The utilization of fully glazed wall structures comprising triple-glazed glass with Argon gas-filled cavities on all four sides is a modern method that has not been extensively researched. However, this construction approach is not commonly used due to the potential issue of overheating caused by excessive sunlight penetration, which cannot be effectively controlled without proper management of blinds or shading devices.

The transfer of heat between the environment and the glazings is modeled using convection and radiation relations. Forced convection between the external glazing and the environment is modeled using the Chilton-Colburn correlation, while natural convection inside the large, narrow vertical cavities formed between the glazings is modeled using McGregor's correlation [20]. Churchill and Chu correlation for vertical surfaces [21] is used to model the convective heat transfer between the interior glazing and the inner zone. Additionally, the radiative heat transfer between the glazings is also considered due to the relatively high emissivity of glass.

However, an innovative low ϵ glass is used in the CCC. Low ϵ glass is manufactured by

coating the glass with metal oxide coatings that reduce the surface emissivity without significantly reducing transparency. These coatings are only applied on the cavity side of the interior and exterior glazing, but not on the middle glazing.Thus, radiative heat transfer in the cavities is significantly reduced due to the low ϵ glass. In the following equations, the subscript i represents the side (north, south,east or west) and j=1,2,3 represent the exterior, middle, and interior glazings, respectively.

$$\Delta T_{i,j} = (\dot{Q}_{sol} - \dot{Q}_{rad} - \dot{Q}_{conv})\frac{\Delta t}{\rho V c_p} \tag{4.15}$$

$$\dot{Q}_{sol} = \begin{cases} (I_{o,b}\alpha_o + (I_{o,r}I_{o,d})\alpha)A & \text{j=1} \\ (I_{o,b}\xi_o\alpha_o + (I_{o,r}I_{o,d})\xi\alpha)A & \text{j=2} \\ (I_{o,b}\xi_o^2\alpha_o + (I_{o,r}I_{o,d})\xi^2\alpha)A & \text{j=3} \end{cases} \tag{4.16}$$

$$\dot{Q}_{rad} = \begin{cases} \sigma A(\epsilon(T_{i,1}^4 - T_{sky}^4) + \mathcal{F}(T_{i,1}^4 - T_{i,2}^4)) & \text{j=1} \\ \sigma A\mathcal{F}(2T_{i,2}^4 - T_{i,1}^4 - T_{i,3}^4) & \text{j=2} \\ \sigma A\mathcal{F}(T_{i,3}^4 - T_{i,2}^4) & \text{j=3} \end{cases} \tag{4.17}$$

$$\mathcal{F} = \frac{1}{\frac{1}{\epsilon} + \frac{1}{\epsilon_{low}} - 1} \tag{4.18}$$

$$\dot{Q}_{conv} = \begin{cases} A(\bar{h}_{1,a}(T_{i,1} - T_a) + \bar{h}_{1,2}(T_{i,1} - T_{i,2})) & \text{j=1} \\ A(\bar{h}_{2,1}(T_{i,2} - T_{i,1}) + \bar{h}_{2,3}(T_{i,2} - T_{i,3})) & \text{j=2} \\ A(\bar{h}_{3,2}(T_{i,3} - T_{i,2}) + \bar{h}_{3,z}(T_{i,3} - T_z)) & \text{j=3} \end{cases} \tag{4.19}$$

$$\bar{h}_{j,k} = \begin{cases} \frac{Nu_j.\lambda_{air}}{Y} & \text{if k=a,z and j} \neq \text{k} \\ \frac{Nu_k.\lambda_{Argon}}{Y} & \text{if k=1,2,3 and j} \neq \text{k} \end{cases} \tag{4.20}$$

The expressions for Nusselt number for various scenarios are :

$$\text{Chilton-Colburn for k=a} \qquad Nu_k = 0.664Re^{0.5}Pr^{0.333} \tag{4.21}$$

$$\text{McGregor for k=1,2,3:} \quad Nu_k = 0.42Pr^{0.012}Ra^{0.25}(\frac{Y}{D})^{-0.3} \tag{4.22}$$

$$\text{Churchill and Chu for k=z:} \quad Nu_k = \begin{cases} 0.68 + (\frac{0.67Ra^{0.25}}{1+(\frac{0.492}{Pr})^{0.5625}})^{0.4444} & \text{Ra} < 10^9 \\ 0.825 + (\frac{0.387Ra^{0.167}}{1+(\frac{0.492}{Pr})^{0.5625}})^{0.5926} & \text{Ra} \geq 10^9 \end{cases} \tag{4.23}$$

Raised and basement floor

The raised floor is constructed using Calcium sulfate tiles that are upheld by steel pedestals. Certain tiles have perforations that allow for air movement from the deck below. As a result, the raised floor is considered a floating plate that separates the interior zone from the deck, absorbs incoming solar radiation, and interacts with the interior zone through convection on its upper surface while also interacting with the lower deck through its lower surface. To model the heat balance of the raised floor, the McAdams' relation for horizontal surfaces that face upwards and downwards is employed.

$$\Delta T_{rf} = (\dot{Q}_{sol} - \dot{Q}_{conv})\frac{\Delta t}{\rho V c_p} \tag{4.24}$$

$$\dot{Q}_{sol} = x_h I_o A_{floor} \xi_0^3 \alpha \tag{4.25}$$

$$\dot{Q}_{conv} = \bar{h}_{rf,z}.A(T_rf - T_z) + \bar{h}_{rf,deck}.A(T_{rf} - T_{deck}) \tag{4.26}$$

$$\bar{h}_{rf,z} = \frac{Nu_{rf,z}.\lambda_{air}}{l} \tag{4.27}$$

$$\bar{h}_{rf,deck} = \frac{Nu_{rf,deck}.\lambda_{air}}{l} \tag{4.28}$$

$$l = \frac{A}{2X + 2Y} \tag{4.29}$$

$$Nu_{rf,z} = \begin{cases} 0.54Ra^{0.25}; & \mathrm{T}_{rf} > \mathrm{T}_z \text{ and Ra} \geq 10^7 \\ 0.15Ra^{0.333} & \mathrm{T}_{rf} > \mathrm{T}_z \text{ and Ra} > 10^7 \\ 0.27Ra^{0.25} & \mathrm{T}_{rf} < \mathrm{T}_z \end{cases} \tag{4.30}$$

$$Nu_{rf,deck} = \begin{cases} 0.54Ra^{0.25} & \mathrm{T}_{rf} < \mathrm{T}_{deck} \text{ and Ra} \geq 10^7 \\ 0.15Ra^{0.333} & \mathrm{T}_{rf} < \mathrm{T}_{deck} \text{ and Ra} > 10^7 \\ 0.27Ra^{0.25} & \mathrm{T}_{rf} > \mathrm{T}_{deck} \end{cases} \tag{4.31}$$

Beneath the deck lies the basement floor, which is separated from the ground by an insulation layer. The insulation material used has a thermal conductivity value of 0.344 W/m/K. Therefore, in order to accurately model the basement floor, both the heat transfer that occurs through convection between the deck and the basement floor, as well as the heat transfer

that occurs through the insulation layer between the basement floor and the ground, must be taken into account. The heat balance of the basement floor is modeled as:

$$\Delta T_{bf} = (-\dot{Q}_{conv} - \dot{Q}_{cond})\frac{\Delta t}{\rho V c_p} \tag{4.32}$$

$$\dot{Q}_{cond} = \frac{\kappa A(T_{bf} - T_g)}{d} \tag{4.33}$$

$$\dot{Q}_{conv} = \bar{h}_{bf,deck}.A(T_rf - T_{deck}) \tag{4.34}$$

$$\bar{h}_{bf,deck} = \frac{Nu_{rf,deck}.\lambda_{air}}{l} \tag{4.35}$$

$$l = \frac{A}{2X + 2Y} \tag{4.36}$$

$$Nu_{bf,deck} = \begin{cases} 0.54Ra^{0.25} & \mathrm{T}_{bf} < \mathrm{T}_{deck} \text{ and Ra} \geq 10^7 \\ 0.15Ra^{0.333} & \mathrm{T}_{bf} < \mathrm{T}_{deck} \text{ and Ra} > 10^7 \\ 0.27Ra^{0.25} & \mathrm{T}_{bf} > \mathrm{T}_{deck} \end{cases} \tag{4.37}$$

It is noteworthy that direct measurement of ground temperature (T_g) underneath the Co-Creation center is not possible due to the lack of sensors in that location. Instead, an algorithmic model has been developed by Thomas Ceha et.al [22] using a periodic approach, described in Algorithm 2, which provides an approximation of the daily ground temperature at a depth of one meter. This model utilizes the data collected by the Royal Netherlands Meteorological Institute, representing the average ground temperature observed at the weather stations in Wilhelminadorp and De Bilt.

The available data spanning over three years was randomly split into two sets, where 70% of the data is utilized for training the algorithm. During the training phase, the model optimizes the amplitude a, horizontal shift c, and equilibrium point d parameters, with the day as the sole input parameter. The optimized values of a, c, and d were found to be 5.3 K, 43.9 days, and 88.5 K, respectively. The model's accuracy was assessed using the remaining 30% of the data by calculating the RMSE , which was found to be 0.594 K, indicating good performance.

Inner zone*

The interior of the Co-Creation center is modeled as a single zone where the temperature is affected by various factors including the surrounding components and the energy source.

Algorithm 2 Ground temperature estimation

Input :$\{T_{g,b}, T_{g,w}\} \in$ Data
Output: Optimized values $\{a, c, d\} \in u$
procedure
$T_{g,m} \leftarrow$ **mean**$(T_{g,b}, T_{g,w})$
$l \leftarrow$ **length**$(T_{g,m})$
$t \leftarrow$ **randperm**$(l, 0.7l)$ ▷ training set
$v \leftarrow$ **setdiff**$(1l, t)$ ▷ Validation set
$fun \leftarrow$ @(u)**function**$(u, T_{g,m}(t), t)$
$u_o = [6, 45, 285]$
$u \leftarrow$ **fminsearch**(fun, u_o)
return u
$C =$ **function**$(u, T_{g,m}, Day)$
$T_g \leftarrow -a\ Cos(\frac{2\pi}{365}(Day - c)) + d$
$C \leftarrow$ **VAF**$(T_g, T_{g,m})^{-1} +$ **RMSE**$(T_g, T_{g,m})$
return C

The state of this zone is impacted by the movement of air underneath the deck, interior heat generation, and convection from the walls, roof, and raised floor. The convection phenomenon is described using natural convection correlations from Churchill & Chu [21] and McAdams. It is assumed that each occupant generates 117 W of internal heat and an average electrical lighting is used (as discussed in Section A.1.4). Since the heat pump is linked with an air handling unit, the amount of heat generated by the heat pump ($\dot{Q}_{hp}$) and the rate of fresh air flow ($\dot{m}$) are adjusted to regulate the temperature of the zone.

The natural ventilation through the thermal chimney (sky windows) is modeled using Anderson's fully mixed model [23] with a controllable input for aperture fraction(x_{sw}) ranging from 0 to 1. The coefficient C_d denotes the effectiveness of natural ventilation. A CFD model of this specific model has been developed and validated by De Araujo Passos et al. [24] to estimate the value of C_d as 0.57.

$$\Delta T_z = (\dot{Q}_{hp} + \dot{Q}_{gen} - \dot{Q}_{adv} - \dot{Q}_{vent} - \dot{Q}_{conv})\frac{\Delta t}{\rho V c_p} \tag{4.38}$$

$$\dot{Q}_{int} = 117 * N_{people} + 1458 \tag{4.39}$$

$$\dot{Q}_{adv} = \dot{m} c_p (T_z - T_{deck}) \tag{4.40}$$

$$\dot{Q}_{vent} = x_{sw}(0.57 * \rho_{air} A_{sw} * 9.81 * H * \left|\frac{T_z - T_{ambient}}{T_{ambient}} x\right|)^{0.5} c_{p\ air}(T_z - T_{ambient}) \tag{4.41}$$

$$\dot{Q}_{conv} = \bar{h}_{z,i}.A(T_z - T_i) \qquad i \in (rf, r, n, e, s, w) \tag{4.42}$$

$$\bar{h}_{z,i} = \frac{Nu_i.\lambda_{air}}{l} \qquad i \in (rf, r) \qquad \frac{Nu_i.\lambda_{air}}{Y} \qquad i \in (n, e, s, w) \tag{4.43}$$

$$l = \frac{A_i}{2X + 2Y} \qquad i \in (rf, r) \tag{4.44}$$

$$Nu_{z,i} = \begin{cases} \text{Chuchill and Chu eq. 4.23} & i \in (n, e, s, w) \\ \text{McAdams eq. 4.14} & i \in (c) \\ \text{McAdams eq. 4.30 and 4.31} & i \in (rf) \end{cases} \tag{4.45}$$

Heat recovery system

At the top of a climate tower, there is a heat exchanger that exchanges heat between two air streams: the fresh air stream, which comes from outside and has an ambient temperature $T_{ambient}$, and the return air stream, which comes from the indoor zone and has a temperature T_z. This heat exchanger can potentially pre-heat or pre-cool the outdoor air before it is conditioned by a PCM battery and a heat pump. The heat exchanger can also be bypassed, and the proportion of the fresh air stream that passes through the heat exchanger is denoted by x_{rec}. Assuming the heat transfer efficiency of 80%, the temperature of the fresh air stream after passing through the heat exchanger as T_h, the heat exchanger can be mathematically modeled as:

$$x_{rec} * 0.8(T_z - T_{amb}) = (T_h - T_{amb}) \tag{4.46}$$

PCM battery*

After the heat exchanger, there is a large stack of batteries made up of PCM in the climate tower. Appendix D gives an overview of PCM and its incorporation techniques. The PCM used is Calcium Chloride Hexahydrate (CCH), which is enclosed in High Density Polyethylene (HDPE) crystal storage panels. The melting point range of this PCM is between 20-23 degrees Celsius. The PCM battery has an overall thermal storage capacity of 310 kJ/k, which is calculated based on the phase change process. There is an option for the incoming stream to bypass the PCM battery, and the ratio of the inlet stream entering the PCM battery is denoted by x_{pcm}. The properties of the PCM panel are given in Table 4.1.

Description	Value	Unit
Dimension (W * L * D)	275*570*13	mm
Mass	1.8	kg/panel
Density	980	kg/m^3
Latent energy	310	kJ/kg
specific heat capacity (liquid phase)	2.1	kJ/(kgK)
specific heat capacity (solid phase)	2.1	kJ/(kgK)
Thermal conductivity (liquid phase)	0.5	W/(mK)
Thermal conductivity (solid phase)	1.1	W/(mK)
Kinematic Viscosity	$9.6 * 10^{-6}$	m^2s

Table 4.1: Properties of the CSP Panel

The heat transfer between the air stream and the PCM battery can be modeled as forced ventilation:

$$\bar{Q}_{pcm} = \bar{h}_{pcm} A_{pcm} (T_{air,pcm} - T_{pcm}) \tag{4.47}$$

$$\bar{h}_{pcm} = Nu \frac{\lambda_{air}}{L_{pcm}} = 16.8 W/(m^2.K) \tag{4.48}$$

$$Nu = \begin{cases} 1.62 Re^{0.33} Pr^{0.33} \frac{d}{L_{pcm}}^{-0.33} & \text{if Re} \leq 5722 \\ 0.027 Re^{0.8} Pr^{0.33} & \text{if Re} > 5722 \text{ and Pr} \geq 0.7 \end{cases} \tag{4.49}$$

$$\bar{h}_{pcm} A_{pcm} (T_{air,pcm} - T_{pcm}) = x_{pcm} \dot{m} c_p (T_h - T_{air,pcm}) \tag{4.50}$$

The CFD simulations performed by [25] reveal that a typical test condition's convective heat transfer coefficient can be approximated to be 16.8 W/ m^2K. Moreover, the outgoing stream from the PCM battery is combined with the bypassed stream before it is supplied to the heat pump and is modeled as:

$$x_{pcm} T_{air,pcm} + (1 - x_{pcm}) T_h = T_{mix} \tag{4.51}$$

The temperature of the PCM can be modeled as:

$$\bar{h}_{pcm} A_{pcm} (T_{air,pcm} - T_{pcm}) = (1 - y_{pcm}) m_{pcm} c_{p,solid} \frac{dT_{pcm}}{dt} + m_{pcm} H_{pcm} \frac{dy_{pcm}}{dt} + y_{pcm} m_{pcm} c_{p,liquid} \frac{dT_{pcm}}{dt}$$

where y_{pcm} is the liquid fraction of PCM and H_{pcm} is the latent heat energy accompanying phase transfer. The phase transition of the PCM battery is modeled using Scheil-Gulliver's linear phase transition equation as explained in Appendix D :

$$y_{pcm} = 1 - min(1, max(0, \frac{23 - T_{pcm}}{3})) \tag{4.52}$$

Heat pump

The Co-creation center relies on a heat pump as its primary energy source, which functions to provide a specific temperature to the inner zone based on the decisions of the MPC algorithm. The temperature of the air stream supplied by the heat pump (T_{hp}) serves as a variable that can be controlled by the control algorithm.

$$\dot{Q}_{hp} = \dot{m} c_p (T_{hp} - T_{mix}) \tag{4.53}$$

5 Model Calibration and Validation

As the non-linear model developed serves as a testbed for controller development, it is crucial to ensure the representativeness of the actual building. Hence, to evaluate the accuracy of the model, it was validated using measured data from an extensive list of sensors. These measurements were obtained during the first week of April 2021 (02-04-2021 to 09-04-2021), and the validation process aimed to verify the model's ability to accurately predict the indoor temperature and other relevant parameters.

For this analysis, the first week of April 2021 is selected as the timeframe, as it provides variable temperatures and strong solar irradiance, allowing the study of the system under different conditions. During this test period, the active and passive energy sources were turned off and the building was unoccupied for the entire duration. This was done so that the thermodynamic interaction between the building and its external and internal environment could be well studied.

The CCC building has 35 strategically placed sensors for measuring 8 components, and the average temperature of each component is estimated based on the readings from the sensors. This enables the validation of 8 states of the nonlinear model data and verification of the accuracy of the proposed grey-box model. To validate the model, environmental data is required, which is obtained from the weather station in the EWI building for the selected test period. The obtained data comprises of:

- Ambient temperature
- Wind speed
- Dew point temperature
- Global Horizontal Irradiance (GHI)

However, no DNI and DHI sensors are used to measure the direct beam and diffused horizontal irradiances. But, the splitting of global irradiance into DHI and DNI is challenging. But, it is solvable using the empirical irradiance splitting model by Erbs [26]. This model uses global irradiance, solar inclination (α), solar hour angle (ω), sky diffusivity and other empirical coefficients to estimate the diffuse fraction. Once the diffuse fraction is obtained, DHI and DNI can be directly estimated. From the DNI and DHI values, the oriented solar irradiation components are calculated using Perez model as discussed in Section A.1.5The components whose temperatures are compared between the measured sensor data and the model data are:

- Internal and External glazing temperature

- Roof temperature
- Indoor air temperature
- Raised floor temperature

These temperatures were primarily selected due to the influence in determining the operating temperature of the building. Table 5.1 presents the results of the initial comparison between the measured data and the model's prediction of the temperatures. The analysis

State	RMSE [K]	NRMSE	VAF
T_z	1.92	0.17	63.4
T_c	4.23	0.28	45.8
$T_{ext.walls}$	2.14	0.26	62.5
$T_{int.walls}$	5.53	0.32	18.2
T_{rf}	1.35	0.16	63.4
T_r	2.56	0.12	80.8

Table 5.1: Results of Validation during the first week of April 2021

reveals that the RMSE between the observed and predicted values of indoor air temperatures and floor temperatures falls within a range of 2 ^{o}C. However, the RMSE for internal walls and ceiling temperatures demonstrates significantly higher values. This discrepancy can have a substantial influence on the determination of the operative temperature, as elaborated upon in Section B.2.3. Consequently, it was deemed necessary to undertake parameter optimization for those variables with limited confidence in their known values. The optimization process holds the potential to enhance the accuracy of the building model, thus yielding more precise results.

5.1 Parameter Optimization

5.1.1 Problem setup

An initial list of uncertain parameters was compiled, consisting of the optical properties of glass, the properties of argon gas, and the thermal conductivity of the ceiling insulation.To optimize the parameters, an optimization problem was developed wherein the measured temperatures during the first week of April were used as the training data in order to optimize the parameters. During this period, the actuators were kept constant and heat pump and ventilation is switched off, as shown in Table 5.2, and the developed building model was fed with the initial temperatures of the components, weather data, and occupancy data. the measured temperature of the components and the external weather and occupancy data is known at timesteps of 30 minutes. Thus, the optimization problem tries to minimize the difference between the sum of the differences between measured and predicted indoor

Static inputs	Symbols	Value
Mass flow rate of fresh air	$\dot{m}$	0 Kg/s
Position of solar blinds	x_h	0 (open)
Aperture fraction of sky windows	x_{sw}	0 (closed)
Fraction of airstream exchanging heat with PCM battery	x_{pcm}	0 (bypass)
Fraction of heat recuperation	x_{rec}	0 (bypass)

Table 5.2: Static inputs to the model

temperatures (ceiling, air, raised floor, and internal walls) at subsequent timestep. In other words, the objective function is:

$$Objective function = |T_{z\ measured} - T_{z\ predicted}| + |T_{rf\ measured} - T_{rf\ predicted}| + |T_{i,3\ measured} - T_{i,3\ predicted}| + |T_{c\ measured} - T_{c\ predicted}|$$

where the equation is constrained to minimize the errors between the measured and predicted temperatures individually:

$$c = |T_{x\ measured} - T_{x\ predicted}| \qquad i \in rf, z, c, (i,3) \tag{5.1}$$

The values of the parameters are required to be within the given bounds, as shown in Table 5.3. The error between the measured temperatures and the predicted temperatures of each timestep was iteratively minimized to a global minimum at each timestep using the solver $fmincon$ (which uses SQP as explained in Section E.7.3) as the parameters to be optimized are within 20.
At each time step, a unique value is obtained for each of the parameters. At the end of this process, the values of the parameters are obtained for this training period, and the data is processed to remove the outliers in order to obtain the mean value of each parameter. The outliers can be caused by temperature sensors being susceptible to radiative errors, both from direct irradiation by the Sun and lighting sources, as well as from thermal sources such as the walls of a room.

State	Parameter	Units	Initial value	Lower bound	Upper bound
T_c	κ	W/(m.K)	0.3	0.1	0.5
$T_{i,j}$	α	-	0.16	0.1	0.2
$T_{i,j}$	ϵ	-	0.8	0.6	1
$T_{i,j}$	ϵ_{low}	-	0.2	0.1	0.2
$T_{i,j}$	ξ	-	0.8	0.6	0.9
$T_{i,j}$	c_p	J/(KgK)	800	600	900

Table 5.3: Parameters to be optimized

5.1.2 Results of model calibration

During the parameter optimization process, outliers that were beyond 3 standard deviations (SD) were excluded. As a result of this approach, the optimization produced the following outcomes, as shown in Table 5.4.

State	Parameter	Units	Initial value	Optimized value
T_c	κ	W/(m.K)	0.3	0.344
$T_{i,j}$	α	-	0.16	0.155
$T_{i,j}$	ϵ	-	0.8	0.77
$T_{i,j}$	ϵ_{low}	-	0.2	0.13
$T_{i,j}$	ξ	-	0.8	0.78
$T_{i,j}$	c_p	J/(KgK)	800	792

Table 5.4: Results of optimized parameters

5.2 Model Validation

Upon optimizing the parameters, the validation was performed again for the same period (02-04-2021 to 09-04-2021) and the results are presented as follows:

5.2.1 Results of Validation

Indoor air temperature

Figure 5.1 depicts the comparison in indoor air temperature between the model outputs and the measured sensor data during 02-04-2021 t0 09-04-2021. It can be observed that the model is more reactive to external conditions but overall, the mean indoor temperature is quite similar

Internal and external glazing temperatures

The figures presented demonstrate the degree of similarity in the dynamics of the model and the measured data. The temperature measurements for April 3 and April 4 are used as they offer a comparison of a bright, sunny day and a cloudy day in close succession, providing insight into the system's dynamics and thermal inertia. Figure 5.2 provides the outputs of the model while Figure 5.3 provides the readings of the sensors.

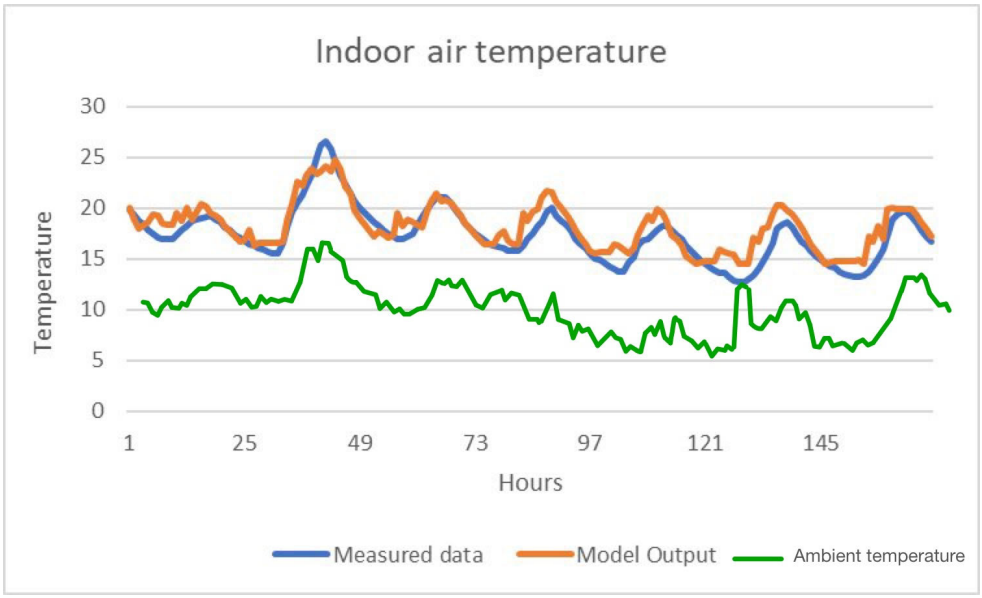

Figure 5.1: Comparison between measured and Model outputs for Indoor air temperature

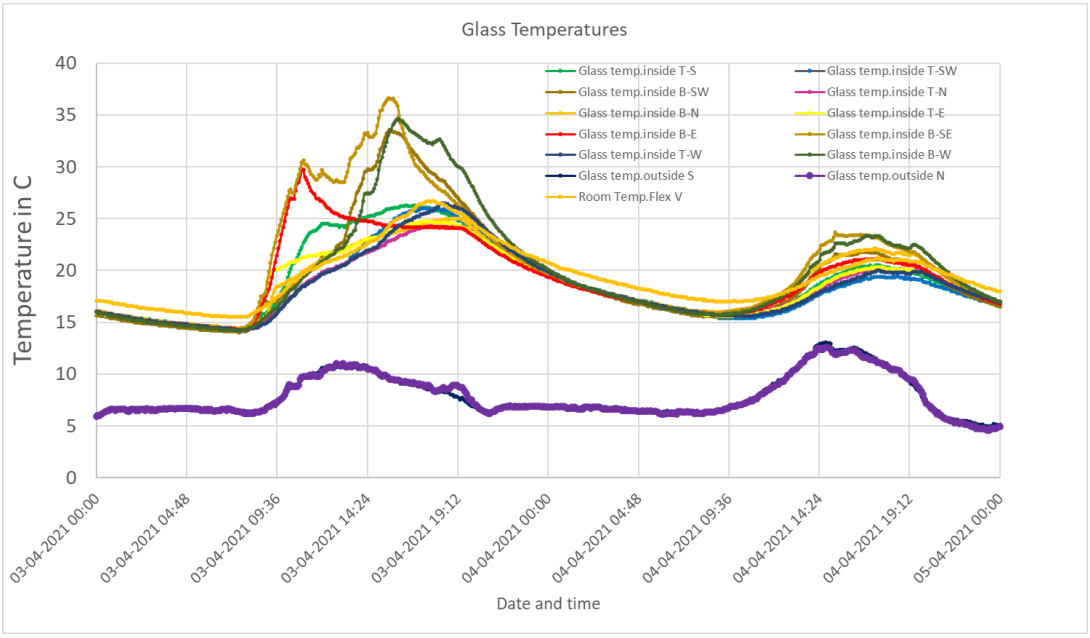

Figure 5.2: Sensor readings of internal and external glazing temperatures

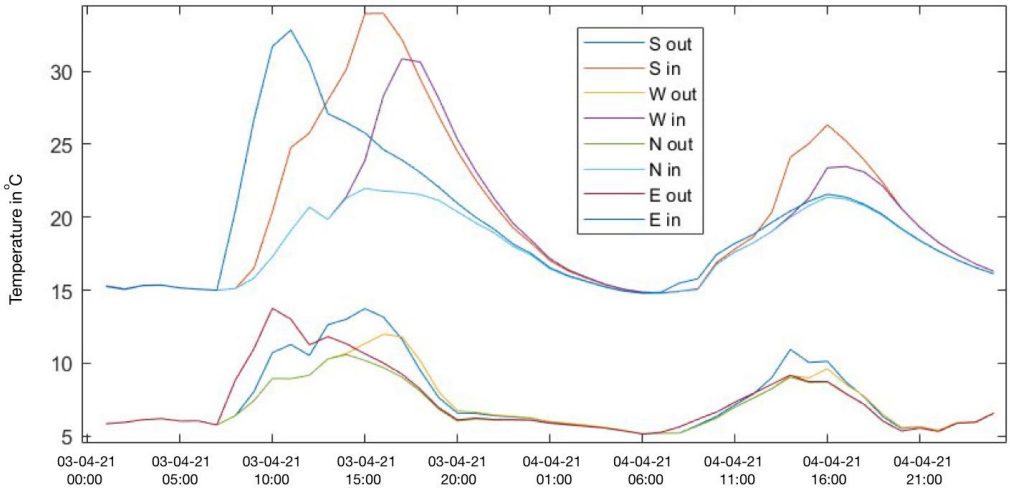

Figure 5.3: Outputs of the model for internal and external glazing temperatures

Raised floor temperatures

The analysis of raised floor temperatures during the first week of April is depicted in Figure 5.4. The comparison indicates a noteworthy level of similarity in the dynamics and magnitudes between the measured data and the output of the model.

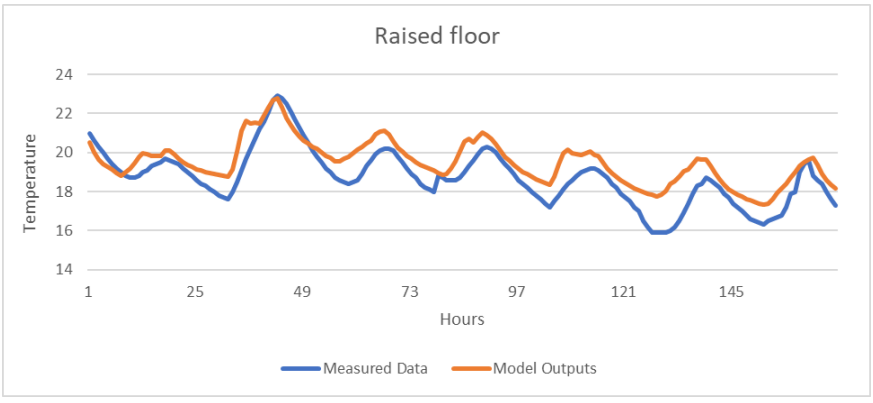

Figure 5.4: Comparison between Measured and Model outputs of Raised floor temperature

Roof temperatures

The comparison of roof temperatures is presented in Figure 5.5. Since temperature sensors are not placed on the external roof to measure its temperature, the roof temperature prediction of the MATLAB model is compared with the prediction of the DFesignBuilder model that has been validated as discussed in Section 3.3. The results show a difference in magnitude on the first day, which could be due to variations in initial conditions and the high thermal mass of the roof. However, from the second day onwards, the magnitudes and thermodynamic behavior of the model and the measured data demonstrate a high degree of similarity.

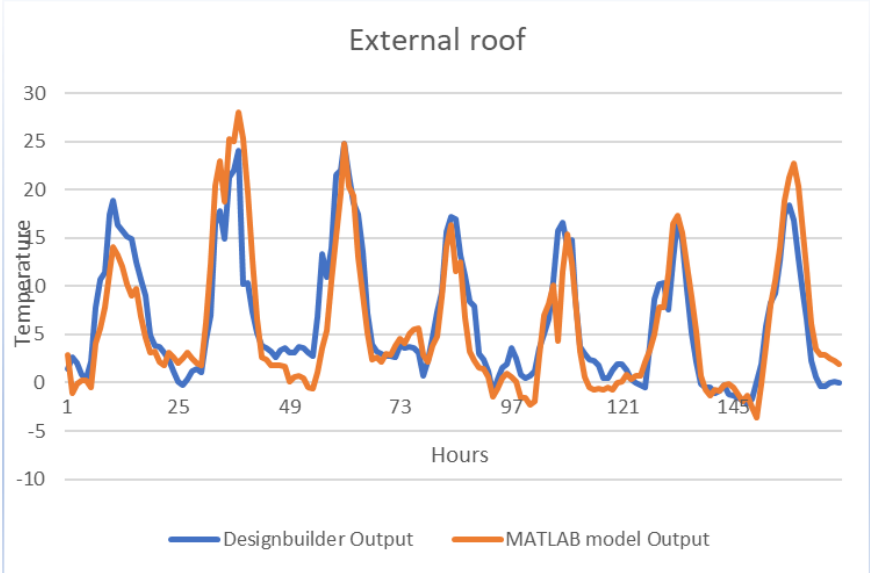

Figure 5.5: Comparison between DesignBuilder and model outputs for Raised floor temperature

Ceiling temperature

The comparison of ceiling temperatures is illustrated in Figure 5.6. The analysis reveals a general similarity in thermodynamic behavior between the measured data and the model. However, the model slightly overestimates the ceiling temperature, suggesting a potential discrepancy in the model's accuracy in estimating the ceiling temperature. The results of the validation are summarized in Table 5.5. It can be seen that though the RMSE error of every component, particularly internal walls, and ceiling have reduced. The Normalized Root mean squared error (NRMSE) is within 0.2 which is within the acceptable limits. The real reduction is found in the increase in Variance Accounted For (VAF) which gives a measure of

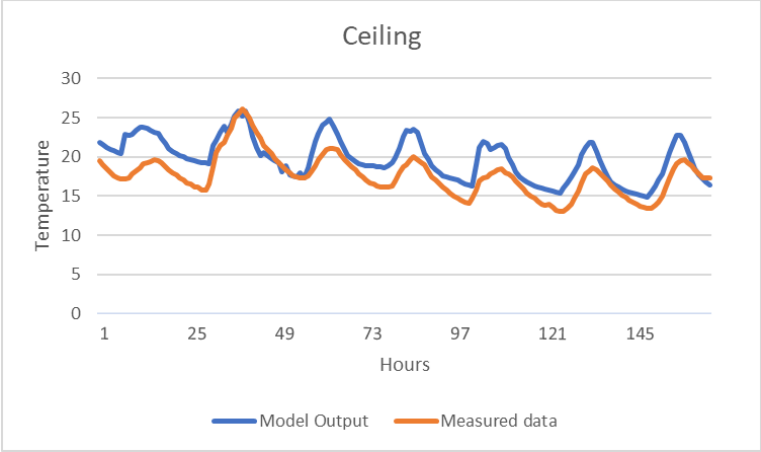

Figure 5.6: Comparison between measured data and Model outputs for Ceiling temperature

the variance of the measured and predicted temperature. Thus, an increase in VAF indicated a closer similarity in the system thermodynamics.

State	RMSE [K]	NRMSE	VAF
T_z	1.38	0.1	82.2
T_c	2.57	0.20	59.5
$T_{ext.walls}$	1.81	0.16	75.6
$T_{int.walls}$	3.31	0.23	28.1
T_{rf}	0.98	0.14	80.9
T_r	2.42	0.09	87.8

Table 5.5: Results of Validation during the first week of April 2021

5.3 Conclusions

Following the development of the model, an initial validation process was conducted, which resulted in significant discrepancies between the measured and predicted temperature values. Consequently, the model underwent a calibration phase, wherein parameter values were optimized through the aforementioned processes. Subsequent to the optimization, a second validation was performed, revealing only a marginal improvement in the accuracy of the system. Henceforth, throughout the remaining duration of this research, the optimized parameter values will be utilized.

6 Design of MPC system

A comprehensive overview of both conventional and intelligent control systems as well as the fundamentals of the MPC strategy is given in Appendix E. Additionally, the core principles of MPC strategies and a literature review on the application of MPC in HVAC control and indoor temperature regulation is provided in Section E.3.

6.1 Non-linear building model

The modeling strategies previously discussed resulted in a nonlinear model of the Co-creation center building, which serves as a simulation testbed for developing a suitable controller. The model aims to accurately represent the building's thermodynamics, and 24 discrete balances are used to achieve this, with each balance representing one state. The building's dynamic systems use an Euler backward scheme for time stepping. To solve the system function, a nonlinear solver called $fsolve$ with the Levenberg-Marquardt algorithm is utilized. The solver iteratively updates the states until the desired benchmark is achieved for each state. If the change in state values is too high, the function is re-solved with the updated states using the same timestep and parameters. This iterative process is repeated until the desired benchmark is reached for all states, after which the next simulation step is executed.

6.2 Matrix formulation

To reduce the computational burden of solving the model, it has been transformed from a function into a matrix representation using a nonlinear state-space model. This resulted in a model with 24 states, 6 inputs, 1 output, and 1 disturbance variable that accounts for the number of occupants at a given time (as illustrated in Figure 3.3. The continuous-time model was then discretized with a time step of Δt, resulting in a nonlinear discrete-time state-space model.

$$x_{k+1} = \mathcal{A}(x_k, p_k)x_k + \mathcal{B}(x_k, p_k)u_k + d_k \tag{6.1}$$

$$y_k = \mathcal{C}(x_k, p_k)x_k + \mathcal{D}(x_k, p_k)u_k \tag{6.2}$$

where:

- x_k : Indoor temperature at time k
- u_k : Control input vector at time k
- p_k : Timestep dependent parameter at time k
- y_k : Measured or observed temperature at time k
- d_k : Disturbances to the model(external weather and occupancy)
- $\mathcal{A}$: State matrix modeling the internal thermal dynamics of the building
- $\mathcal{B}$: Input matrix representing the influence of the control inputs on the temperature.
- $\mathcal{C}$: Output matrix mapping the internal temperature to the measured outputs.
- $\mathcal{D}$: Feedthrough matrix representing the influence of control inputs on the measured outputs.

The state-space representation was chosen for its potential to reduce computational costs compared to the original function representation. This is due to the fact that numerical solvers in MATLAB are optimized for matrix operations. As a result of this transformation, the computation time was reduced by approximately 10%.

6.3 MPC Problem setup

The principal aim of the control system is to reduce primary energy usage while ensuring the occupants' comfort through efficient management of both active and passive energy sources. Therefore, the key challenge of the control system is to generate optimal control signals for all actuators while minimizing computational expenses. Thus, the control system design involves balancing the control system's performance with its computational cost.

6.3.1 Controlled inputs

The complexity of a control system is significantly influenced by the number of controlled inputs, as these are the parameters that need to be optimized for minimizing the objective function. In this case, the control system is required to have six control signals, which adds to the overall complexity of the system. These are :

- T_{hp} : Temperature of airstream after passing through the heatpump
- $\dot{m}$: Mass flow rate of fresh air
- x_h : Position of solar blinds
- x_{sw} : Aperture fraction of sky windows
- x_{pcm} : Fraction of airstream exchanging heat with PCM battery
- x_{rec} : Fraction of heat recuperation

Consequently, the solver is responsible for solving the optimization function by optimizing the six control signals. To ensure that the control signals have realistic and attainable values, hard bounds are established, which restrict the solver from setting the control signal values outside the specified range. The limits are given in Table 6.1.

Parameter	Lower limit	Upper limit
T_{hp}	10	35
$\dot{m}$	0.1	1
x_h	0	1
x_{sw}	0	1
x_{pcm}	0	1
x_{rec}	0	1

Table 6.1: Lower and Upper limit of controlled inputs

6.3.2 Objective function

The primary objective of the control system is to minimize the energy that needs to be supplied by the heatpump to maintain the temperature of the room. In other words, this is the heating/cooling load of the building. Therefore, the optimization function utilized in the control system design solely focuses on minimizing heating/cooling energy that needs to be supplied. However, several studies have proposed multi-objective optimization approaches to incorporate both energy and comfort terms into the optimization problem. Nevertheless, results indicate that using multi-objective optimization leads to increased computation costs and greater difficulty in achieving convexity. Furthermore, such an approach does not ensure the fulfillment of comfort criteria. For these reasons, the current design uses only the energy term in the optimization:

$$Q = \dot{m} c_p |(T_{hp} - T_{mix})| \tag{6.3}$$

where the terms are described as shown in Figure 3.3.

6.3.3 Constraints

To guarantee that the control system preserves indoor comfort, the comfort criteria are integrated into the system as a non-linear constraint. The comfort criteria for the occupied hours are obtained from the adaptive comfort model, whereas the criteria for unoccupied hours are less stringent. The operative temperature for the occupied hours depends on the $T_{e,ref}$ as discussed in Section 2.1.According to classification criteria provided Peeters' [12], the Co-Creation Center belongs to criteria BETA and based on Figure 2.1, the operative temperature can be calculated as:

$$T_{operative} = 21.45 + 0.11 * T_{e,ref} \tag{6.4}$$

and the desired temperature bounds are:

$$\begin{cases} T_{operative,hour} \pm 2^oC & \text{for hour } >8 \text{ or hour } <16 \\ 24 \pm 6^oC & \text{otherwise} \end{cases} \tag{6.5}$$

the given error term is:

$$e_i = |T_{operative,i} - T_{zone,i}| \qquad \text{for i} \in n_p \tag{6.6}$$

and the constraint is:

$$\text{and} \qquad e_i < 2 \tag{6.7}$$

When the space is unoccupied, the indoor temperature is maintained within 18-30^{o}C for the following reasons. Firstly, it prevents the building from experiencing extreme temperature variations, which can lead to structural damage and cause equipment and materials to degrade over time. Secondly, it ensures that the indoor space is at an optimal temperature when the occupants return, which improves their comfort and productivity. Additionally, maintaining a consistent indoor temperature can help to reduce energy consumption and associated costs by preventing the heating or cooling system from having to work at a higher capacity to adjust the indoor temperature to the desired level.

6.3.4 Disturbance data

The number of people in a building can affect the indoor temperature, and they are considered as sources of heat that cannot be controlled. Therefore, having knowledge about occupancy can help in improving the control performance for thermal comfort. An occupancy schedule is externally fed by the user and can be fed to the MPC controller. A representative occupancy schedule is depicted in Figure 6.1.

The predictions of the environmental data are done by two different software. The forecasts

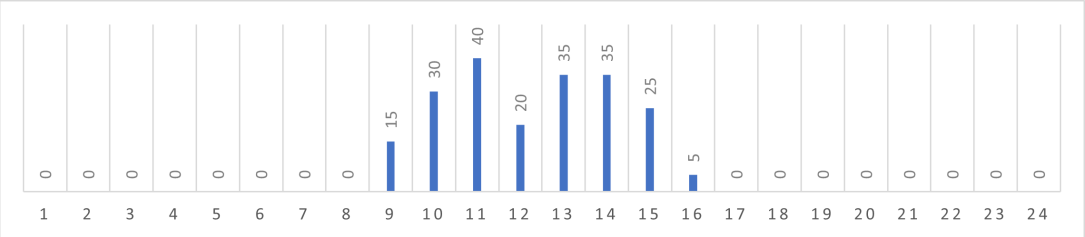

Figure 6.1: occupancy schedule over a day

of solar irradiation and temperatures are done through Solcast® (www.solcast.com) which provides the Global Horizontal Irradiance (GHI) with a time step of 30 minutes and with a very high accuracy [27]. The Solcast tool is based on Geostationary satellite images that

Algorithm 3 Oriented solar irradiance parameters

Input :$Day, t, \beta_c, \gamma_c, I_{bn}, I_d, \rho_r$
Output: $I_o, I_{o,b}, I_{o,r}, I_{o,d}, \theta_z, \gamma_{azi}$

procedure
lat = 4.378 ▷ Latitude
long = 51.996 ▷ Longitude
% Calculations for sun's elevation, zenith, azimuth, and oriented normal angles

$B \leftarrow \frac{360}{365}(Day - 81)$
$EoT \leftarrow 9.87\ sin(2B) - 7.53\ cos(B) - 1.5\ sin(B)$
$TC \leftarrow EoT - 4(15t - long)$
$\omega \leftarrow 15(t + \frac{TC}{60} - 12)$
$\delta \leftarrow sin^{-1}(sin(-23.45)cos(\frac{360}{365}(Day + 10)))$
$\theta_e \leftarrow sin^{-1}(cos(lat)cos(\delta)cos(\omega) + sin(lat)sin(\delta))$
$\theta_z \leftarrow 90 - \theta_e$
$\theta_n \leftarrow cos^{-1}(sin(\delta)sin(lat)cos(\beta_c) - cos(lat)sin(\delta)sin(\beta_c)cos(\gamma_c) + cos(\delta)cos(lat)..$
$cos(\beta_c)cos(\omega) + cos(\delta)sin(lat)sin(\beta_c)cos(\gamma_c)cos(\omega) + cos(\delta)sin(\beta_c)sin(\gamma_c))$
% Calculations for solar irradiance parameters
$a \leftarrow max(0, cos(\theta_n))$
$b \leftarrow max(cos(85), cos(\theta_z))$
$[F_1, F_2] \leftarrow$ **Perez Model**$(\theta_z, I_d, I_{bn}, Day)$
$I_{o,b} \leftarrow I_{bn}cos(\theta_n)$
$I_{o,r} \leftarrow \frac{\rho r}{2}(I_d + I_{bn}cos(\theta_z))(1 - cos(\beta_c))$
$I_{o,d} \leftarrow I_d(0.5(1 - F_1)(1 + cos(\beta_c)) + F_1\frac{a}{b} + F_2 sin(\beta_c))$
$I_o \leftarrow I_{o,b} + I_{o,r} + I_{o,d}$
return $I_o, I_{o,b}, I_{o,r}, I_{o,d}$

facilitate solar surface irradiance retrieval with the highest spatial and temporal resolution [27]. The data is then processed to obtain DHI and DNI through solar irradiance splitting algorithms as explained in Section 5.2. The wind forecast is obtained from Windfinder ® (nl.windfinder.com). Parameters such as solar-oriented irradiance and unshaded floor area are calculated using algorithms defined in Algorithm 3 and Algorithm 4, respectively. Research was conducted to investigate the potential impact of natural shading by trees on indoor operative temperature. However, the findings indicated that the inclusion of trees resulted in only a minor alteration in indoor operative temperature, with a maximum variation of approximately 0.2 ^{o}C. Consequently, it was determined that considering the effect of trees would not significantly contribute to the complexity of the model and, therefore, this aspect was later disregarded.

6.3.5 Prediction horizon

The disturbance dataset employed in this study was sampled at hourly intervals and subsequently interpolated to a more refined timestep of 30 minutes. The performance of the

Algorithm 4 Unshaded floor area parameters

Input : $\theta_z, \gamma_{azi}, X_z, Y_z, Z_z$
Output : A_u
procedure
OH =1.86 ▷ The overhang of roof an all sides is 1.86 m
$H = Z_z - OH$ tan(90-θ_z)
$\gamma_{east} = 90$
$\gamma_{south} = 180$
$\gamma_{west} = 270$
$\gamma_{north} = 360$
if $0 > \gamma_{azi} < 180$ **then**
    $x_e \leftarrow H\frac{cos(|\gamma_{azi}-\gamma_{east}|)}{tan(90-\theta_z)}$
    $x_e(x_e > X_z) = X_z$
if $90 > \gamma_{azi} < 270$ **then**
    $x_s \leftarrow H\frac{cos(|\gamma_{azi}-\gamma_{south}|)}{tan(90-\theta_z)}$
    $x_s(x_s > Y_z) = Y_z$
if $180 > \gamma_{azi} < 360$ **then**
    $x_w \leftarrow H\frac{cos(|\gamma_{azi}-\gamma_{west}|)}{tan(90-\theta_z)}$
    $x_w(x_w > X_z) = X_z$
if $\gamma_{azi} < 90 || \gamma_{azi} > 270$ **then**
    $x_n \leftarrow H\frac{cos(|\gamma_{azi}-\gamma_{north}|)}{tan(90-\theta_z)}$
    $x_n(x_n > Y_z) = Y_z$
if $\gamma_{azi} < 90$ **then**
    $A_u \leftarrow x_e Y_z + x_s X_z + x_n X_z - x_e x_s - x_e x_n$
else
    $A_u \leftarrow x_w Y_z + x_s X_z + x_n X_z - x_w x_s - x_w x_n$
    return A_u =0

MPC algorithm is significantly influenced by the selection of an appropriate prediction horizon. However, determining an optimal Prediction horizon (N_p) is not a singular value, as it relies on the MPC's efficacy in regulating building temperature within predefined limits and minimizing primary energy consumption. Thus, a comprehensive investigation was conducted to identify a suitable prediction horizon, while ensuring that the computational time for a single prediction remains within the allotted timestep of 30 minutes. This investigation spanned a duration of 5 days for each season, effectively capturing the essential characteristics and dynamics of the respective seasons. The subsequent subsections provide a comprehensive presentation of the findings obtained during this period. The performance metrics used are the energy supplied by the heatpump during this 5-day period and the total temperature violations occurring in this period as $\sum_{i=1}^{n} e_i$ where e_i is the temperature constraint as explained in Equation 6.7

6.3.6 Results of varying Prediction horizon

Winter

The period of the simulation was from 01 January 2021 to 05 January 2021 which would be representative of winter. Figure 6.2 depicts the ability of the MPCs with a control timestep of 30 minutes to maintain indoor temperature. From Table 6.2, it can be seen that energy saving is significant till N_p = 16 hours, but there are some minor temperature violations during the course of the week.

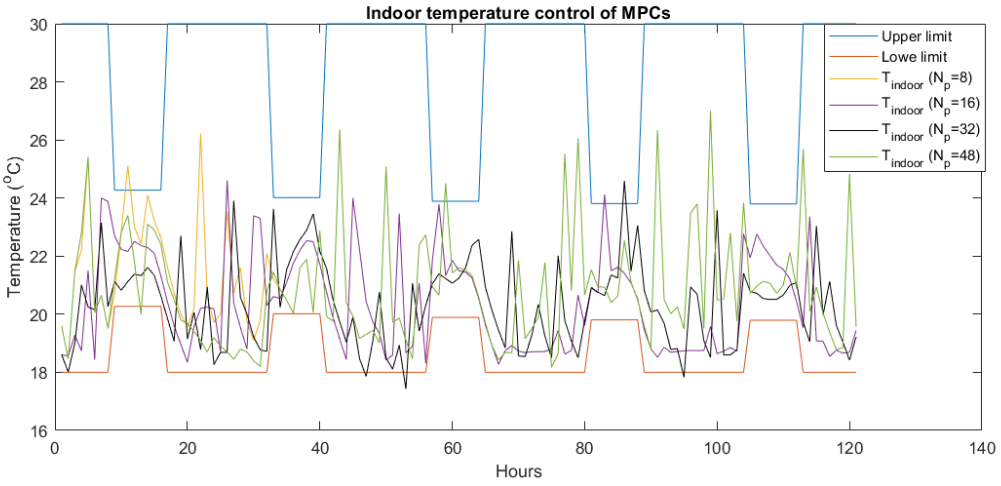

Figure 6.2: Indoor temperature control from 01 January 2021 to 05 January 2021

Prediction horizon (hours)	Computational time (s)	$\sum error$ [^{o}C]	Energy supplied by HP [kWh]
4	40	1.82	148
8	261	0.16	144
16	492	0.68	138
24	1206	0.36	137

Table 6.2: Results of MPC with a control timestep of 30 minutes (winter)

Summer

The period of the simulation was from 20 June 2021 to 25 June 2021 which would be representative of summer.Figure 6.3 depicts the ability of the MPCs with a control timestep of

30 minutes to maintain indoor temperature. From Table 6.3, it can be seen that energy saving is significant tillN_p = 16 hours, but the temperature violations increase for N_p=16 hours, whereas N_p = 24 hours performs better in terms of energy and maintaining indoor comfort.

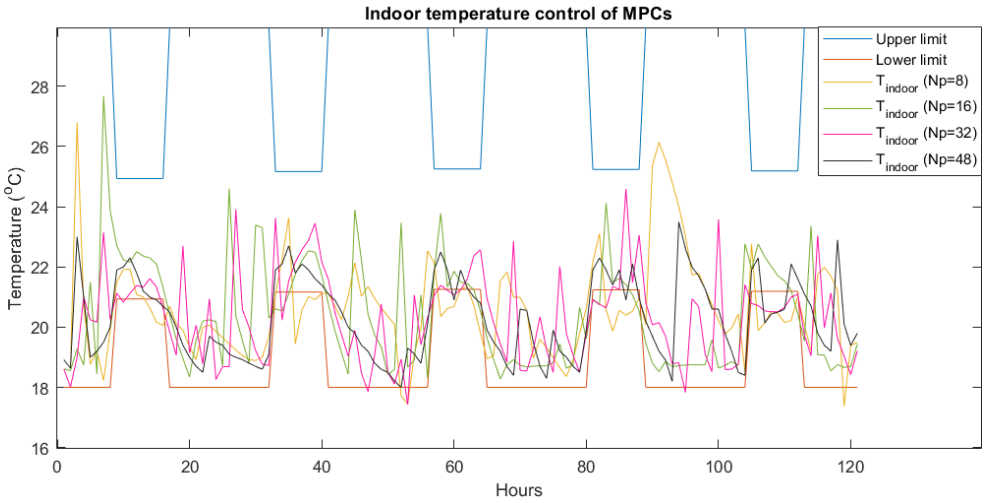

Figure 6.3: Indoor temperature control from 20 June 2021 to 25 June 2021

Prediction horizon (hours)	Computational time (s)	$\sum error$ [^{o}C]	Energy supplied by HP [kWh]
4	39	12.62	23.76
8	168	4.72	21.89
16	361	5.92	10.67
24	1092	4.61	8.58

Table 6.3: Results of MPC with a control timestep of 30 minutes (summer)

Autumn

The period of the simulation was from 01 October 2021 to 05 October 2021 which would be representative of Autumn. Figure 6.4 depicts the ability of the MPCs with a control timestep of 30 minutes to maintain indoor temperature. From Table 6.4, it can be seen that energy saving is significant till N_p = 16 hours and the total temperature violation during the entire week is minimal as well

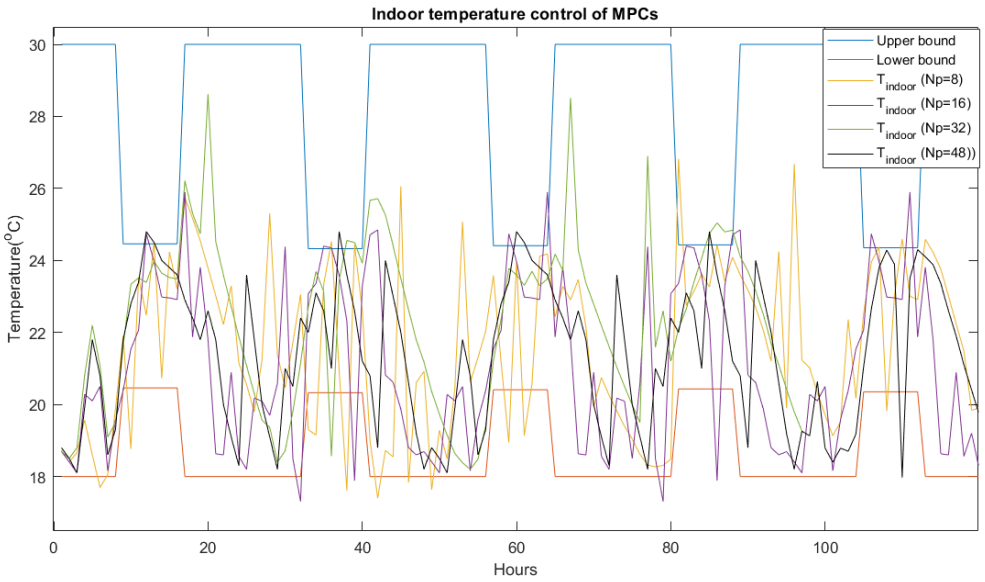

Figure 6.4: Indoor temperature control from 01 October 2021 to 05 October 2021

Prediction horizon (hours)	Computational time (s)	$\sum error$ [^{o}C]	Energy supplied by HP [kWh]
4	42	11.82	108
8	198	8.21	102
16	392	3.42	94
24	982	2.21	93

Table 6.4: Results of MPC with a control timestep of 30 minutes (autumn)

Spring

The period of the simulation was from 01 March 2021 to 06 March 2021 which would be representative of Spring. Figure 6.5 depicts the ability of the MPCs with a control timestep of 30 minutes to maintain indoor temperature. From Table 6.5, it can be seen that energy saving is significant till N_p = 8 hours and the total temperature violations are particularly minimal if N_p is increased to 24 hours.

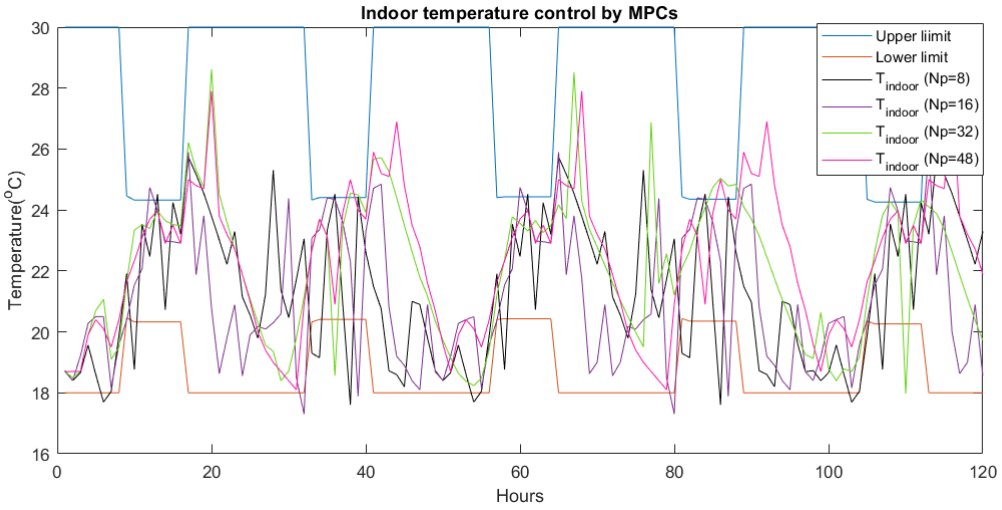

Figure 6.5: Indoor temperature control from 01 March 2021 to 06 March 2021

Prediction horizon (hours)	Computational time (s)	$\sum error$ [^{o}C]	Energy supplied by HP [kWh]
4	51	9.61	74
8	178	6.81	72
16	454	4.81	68
24	1125	0.81	67

Table 6.5: Results of MPC with a control timestep of 30 minutes (spring)

6.3.7 Conclusion

Based on the observations, it is evident that increasing the prediction horizon enhances both the controller's capability to maintain indoor comfort and its ability to minimize the energy demand. Additionally, the tables presented demonstrate a satisfactory convergence of the solution within a 30-minute (1800 seconds) timeframe. Consequently, a prediction horizon of 24 hours is considered appropriate for the remainder of this research.

7 Experimental Validation of MPC

This phase seeks to evaluate the controller's ability to regulate the temperature of the CCC building by controlling the HVAC system

7.1 Experiment setup

To evaluate the accuracy of the developed MPC and its ability to regulate indoor temperature, a set of preliminary experiments was conducted during the second weekend of April 2023, specifically 08-04-2023 and 09-04-2023. The experiment was conducted during the aforementioned dates. The first day of the experiment was a rainy day with ambient temperatures in the range of 8-13^{o}C and the second day was a partly cloudy day with temperatures in the range of 11-14^{o}C.

The experiment involved feeding the MATLAB model with environmental and occupancy data obtained from the weather station and the sensors in the CCC building. The MATLAB program was set to run at a prediction horizon of 24 hours, with one control timestep of 30 minutes.

Since the solar blinds were controlled by an external program and it was not feasible to interfere in the solar blinds control, the fraction of solar blinds was manually fed to the MATLAB model. The control inputs from the MATLAB model other than x_h (as discussed in Section 6.3.1) were then fed into the BEMS for each timestep. This process was repeated for each time step. The data collected from the sensors at the end of each control step was assessed using Priva's online platform to evaluate the performance of the MPC in predicting the temperature of the CCC building.

7.2 Results

The scatter plots depict the correlation between the sensor readings and the corresponding output temperatures (x and y axis in ^{o}C) obtained from the MATLAB model throughout the experimental period. The graph also illustrates the upper and lower boundaries of 0.3^{o}C, which are visually represented by the light blue lines.

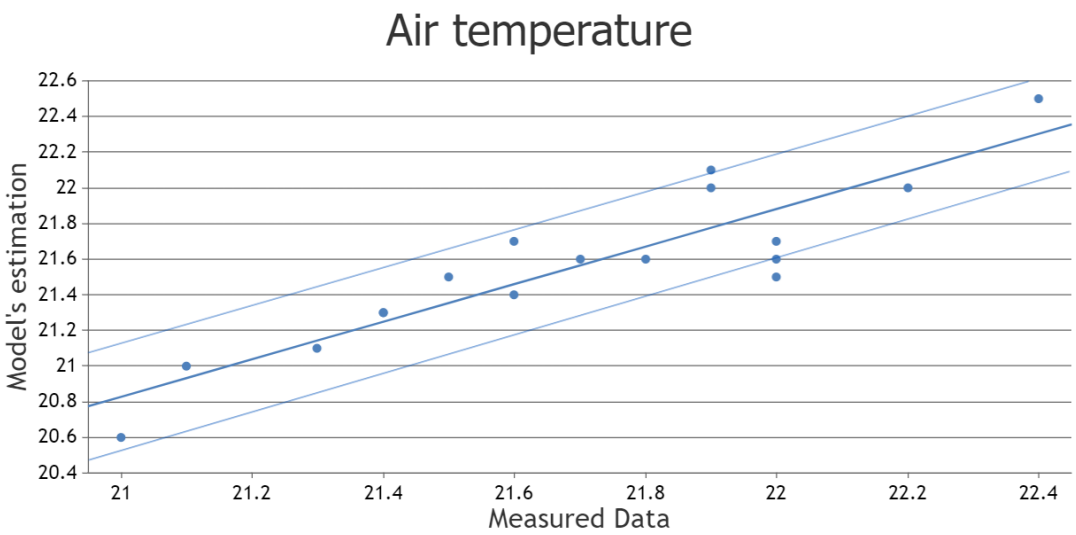

Figure 7.1: Comparison between measured data and prediction of MPC for Air temperature

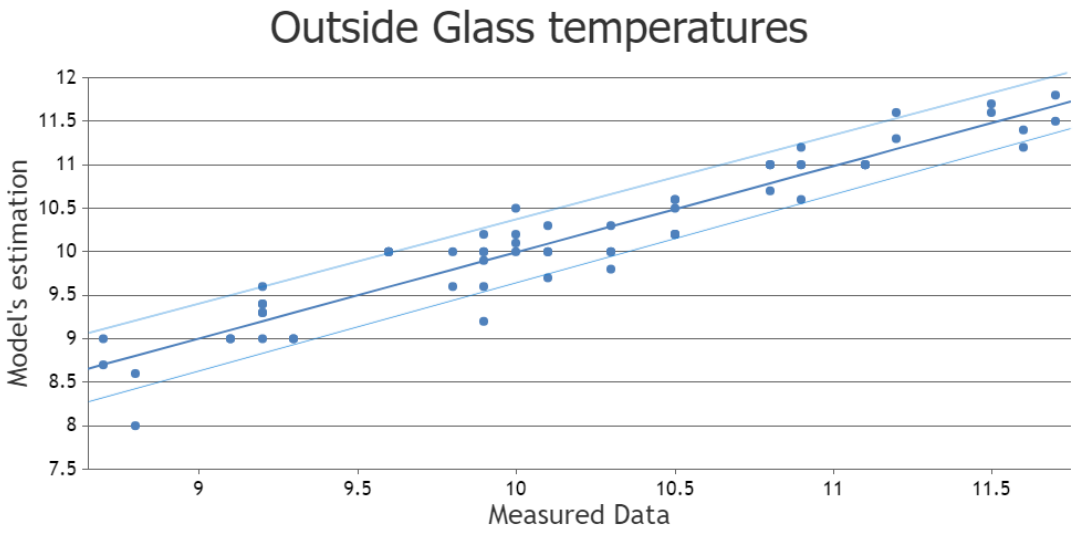

Figure 7.2: Comparison between measured data and prediction of MPC for Exterior Glass temperature

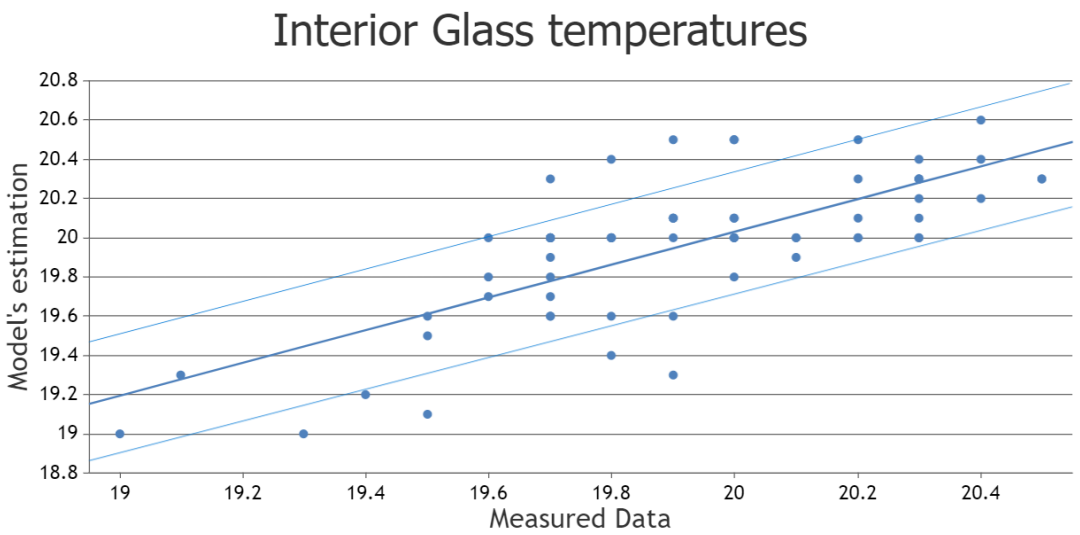

Figure 7.3: Comparison between measured data and prediction of MPC for Interior Glass temperature

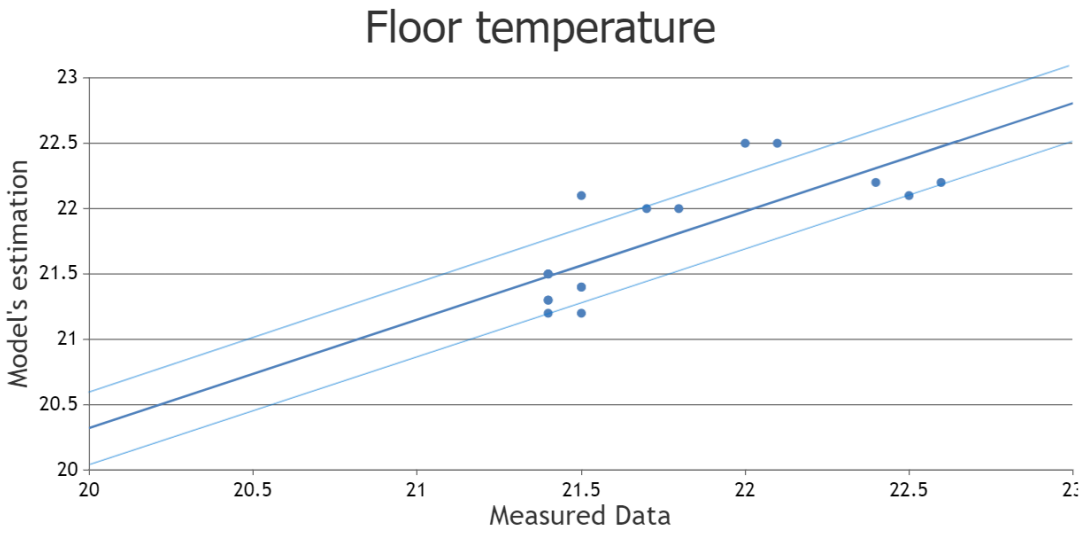

Figure 7.4: Comparison between measured data and prediction of MPC for floor temperature

7.3 Conclusion

The results presented in Table 7.1 indicate that the RMSE error between the actual temperatures and the values predicted by the MATLAB model is within 0.3 K which is a good

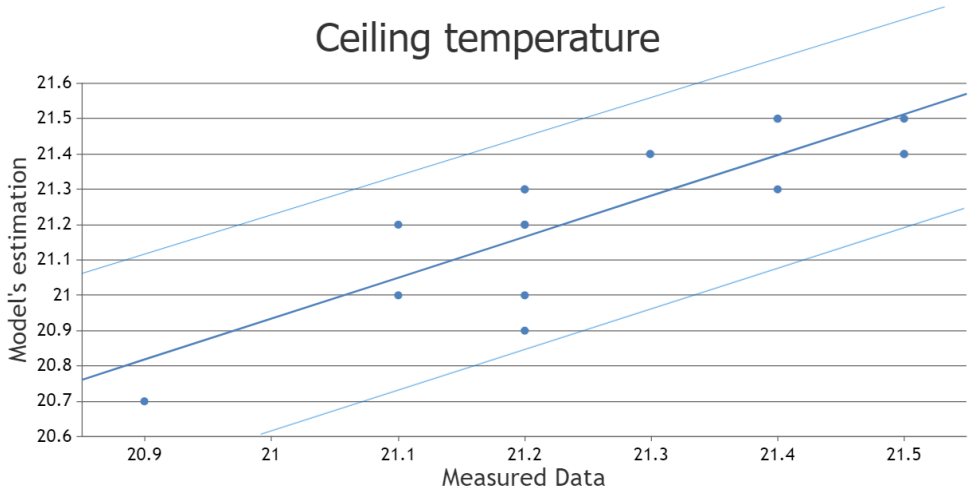

Figure 7.5: Comparison between measured data and prediction of MPC for Ceiling temperature

State	T_z	T_c	$T_{interiorglass}$	$T_{outsideglass}$	T_{floor}
RMSE [K]	0.23	0.12	0.26	0.23	0.29

Table 7.1: Results of experiments during the first week of April 2023

level of accuracy when it comes to building indoor temperature prediction [28]. Therefore, it can be concluded that the developed model provides an accurate representation of the thermal behavior of the building and has the potential to regulate the indoor comfort of the building.

8 Comparitive study: Energy savings potential

This experiment investigates the efficacy of the developed MPC system in conserving energy without compromising indoor comfort levels in comparison to the existing Rule-based controller (as discussed in Section 3.2).

8.1 Experimental setup

The study was conducted for a week in spring during the second week of April 2023, specifically from 10th April 2023 to 14th April 2023. Since both the controllers cannot be run simultaneously, the RBC was run and MPC was simulated using identical data. During this period, the temperature bounds were manually set to match the temperature bounds of the MPC program. Thus, any advantages of using a more flexible temperature bound would be diminished and the comparison can be fair. This was a period of occupancy and the Rule-based controller was in operation during the period. During the comparative study, identical weather and occupancy data were provided to the MPC to assess the performance of MPC in terms of total energy consumption and the number of comfort violations. Hence, it is a simulation-based study and the objective was to evaluate the energy-saving potential of the MPC and compare it with the existing Rule-based Controller (RBC), while ensuring indoor comfort.

8.2 Results

The results of the comparison indicate that the MPC effectively achieves thermal comfort. Analysis of the blinds' position (as shown in Figure 8.3) reveals that the blinds are predominantly open during the day to allow passive heating, and they remain open during most parts of the night as the heat balance is not affected by the blinds' position. Furthermore, the graph depicting the loading and utilization of PCM (Figure 8.4) illustrates that the PCM is charged during the night and the stored energy is utilized during the early hours of occupancy. Additionally, the utilization of heat recovery is evident in almost all time periods, except for a few instances when the heat pump is active (Figure 8.5).

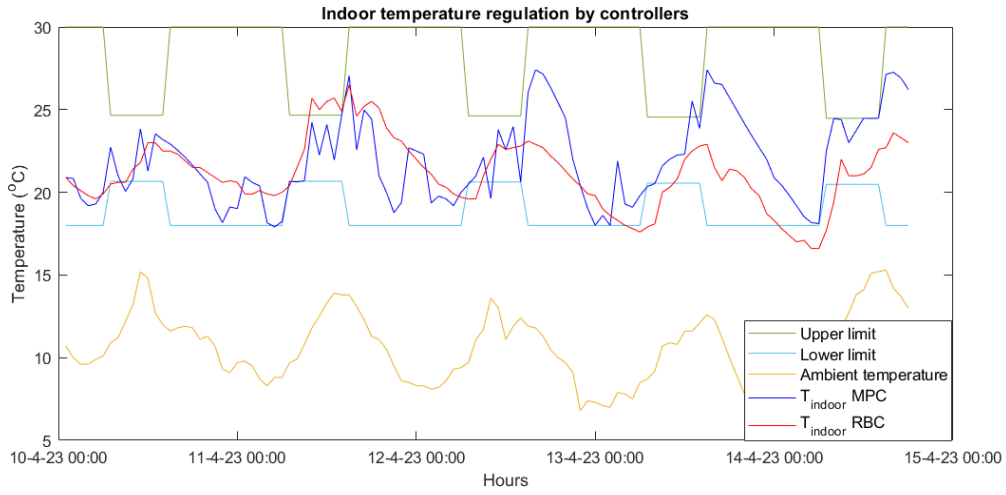

Figure 8.1: Comparison between indoor temperature regulation by controllers

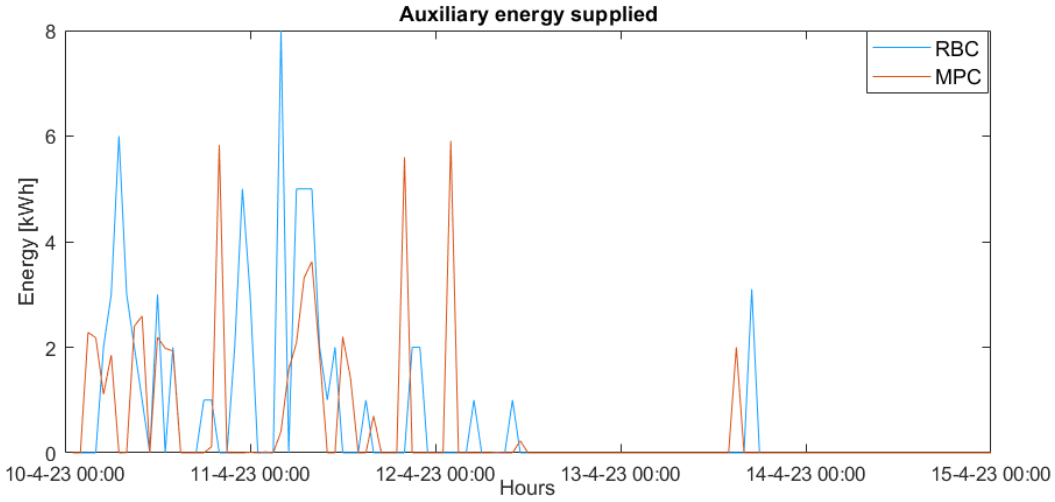

Figure 8.2: Comparison between energy supplied by Heatpump

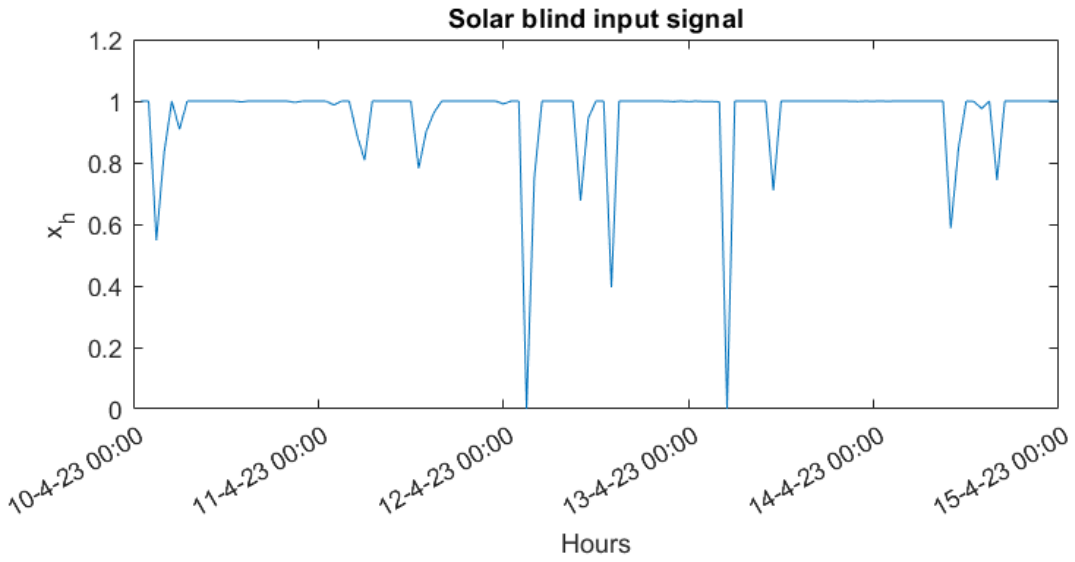

Figure 8.3: Position of the blinds (x_h =1 is completely open and x_h=0 is completely closed)

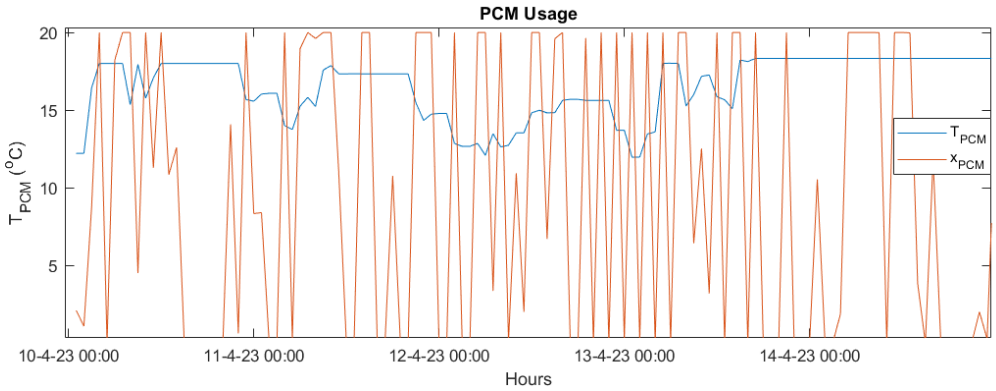

Figure 8.4: Usage of PCM

To maintain these temperature limits using the RBC, an energy supply of 69 kWh was required. On the other hand, the developed MPC consumed approximately 53 kWh, resulting in a 22% reduction in energy consumption compared to the RBC. The reduction in energy supplied by heatpump can be attributed to the usage of passive energy sources throughout the day. PCM is only used up to heat up the building during the inactive periods when the lower limit of operative temperature is 18^{o}C, whereas heat recovery is used in most instances. The difference in energy consumption is also because of the fact that the RBC does not pre-heat the building during the early unoccupied hours of the day. In addition, it is observed from Figure 8.1 that the MPC pre-heats the building passively using PCM on 13-4 around 17:00 anticipating that it will get cooler as the day progresses. But the rule-

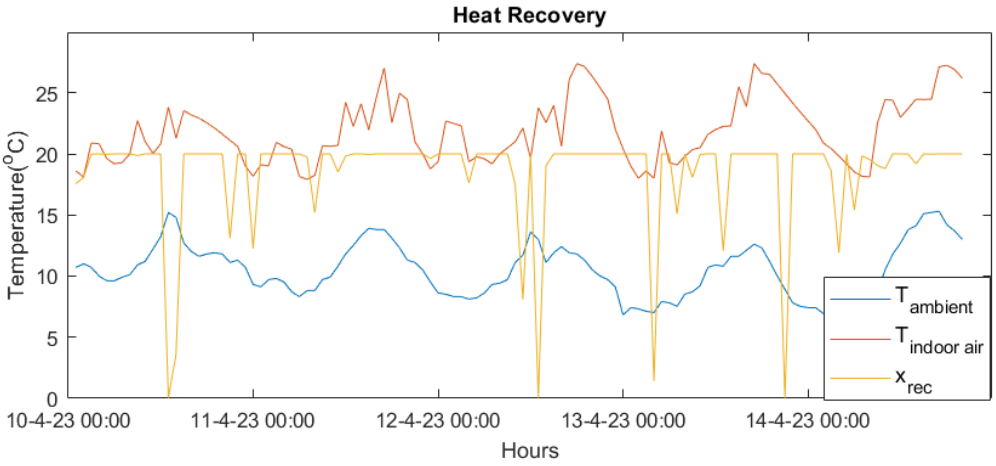

Figure 8.5: Usage of Heat recovery

based controller fails to recognize this. Another instance is during 11-4 around 17:00 when the MPC heats up the building knowing that the day will get colder and it will cost more energy to heat up the building during the night.

Assessment Criteria	RBC	MPC
Energy supplied BY heatpump [kWh]	69	53.4
Total temperature violations $\sum e$ [K]	3.89	3.21

Table 8.1: Performance comparison of controllers during 5-day period

8.3 Conclusions

In summary, it is evident from Table 8.1 that the developed MPC demonstrated its effectiveness in maintaining thermal comfort while minimizing energy consumption. The MPC outperformed the RBC, achieving significant energy savings during the experimental period. Furthermore, the MPC reduces the peak heating/cooling load and hence the capacity of the heat pump can be potentially reduced if this simulation is performed over a typical meteorological year.

9 Energy flexibility potential

9.1 Introduction

Energy flexibility refers to the capacity of buildings to adapt their energy consumption in accordance with the requirements set by energy suppliers. Certain hours of the year witness significantly high energy demands, placing considerable strain on the energy grid. To meet this heightened demand, costly electricity sources are employed, resulting in increased electricity expenses. Conversely, during periods of lower demand, renewable energy sources are utilized for electricity generation, leading to generally lower electricity costs. In some cases, electricity prices may even turn negative, providing incentives for electricity utilization during periods of extremely low demand. Intelligent BEMS capitalize on this opportunity by optimizing electricity usage, thereby achieving two key advantages: mitigating stress on the electricity grid and reducing operational/electricity expenses for the building.

9.2 Modifications to the system

To harness the energy flexibility of a building through MPC, a subtle adjustment was made to the objective function. Rather than minimizing the energy supplied by heatpump, the focus shifted to minimizing the energy cost. Hourly energy cost data from PJM Interconnection, a regional transmission organization in the US, was incorporated into the MPC problem formulation by linearly interpolating it in timesteps of 30 minutes. It should be noted that while the dataset is employed in the problem setup, in practical implementation, an energy cost forecast would be utilized. Consequently, the modified objective function prioritizes the minimization of energy expenses as:

$$Q = Cost_{timestep} * \dot{m}c_p|(T_{hp} - T_{mix})| \tag{9.1}$$

The energy flexibility potential of MPC is studied by considering two cases, one in summer and one in winter.

9.3 Results

9.3.1 Winter

The simulation period is from 01-01-2021 to 03-01-2021 which is representative of Winter. Simulating a period of three days would give deep insights into the difference in control strategy as compared to the original objective function. Figure 9.1 illustrates that the developed MPC optimizes energy usage by consuming more energy when it is available at a lower cost. This approach reduces the strain on the grid and leads to lower energy costs. Despite this strategy, the MPC effectively maintains indoor comfort, as demonstrated in Figure 9.2. The flexibility of the building is leveraged by thermally charging the PCM during the night when energy costs are lower. This utilization of PCM to increase building flexibility is evident from Figure 9.3. It is evident that the PCM is heat-loaded during the night when inexpensive energy is available and the heat energy stored in PCM is utilized in heating the building in the early parts of the occupied periods of the subsequent day.

Furthermore, Table 9.1 provides support for the effectiveness of the MPC. It reveals that the MPC not only requires 45% less energy but also results in a 54% reduction in electricity costs compared to other methods assuming a constant Coefficient of Performance (COP) of the heatpump.

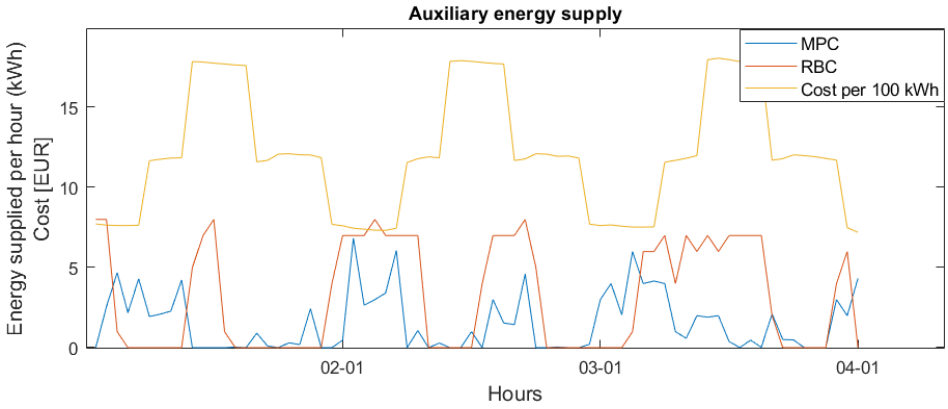

Figure 9.1: Energy supplied by heatpump from 01-01-2021 to 03-01-2021

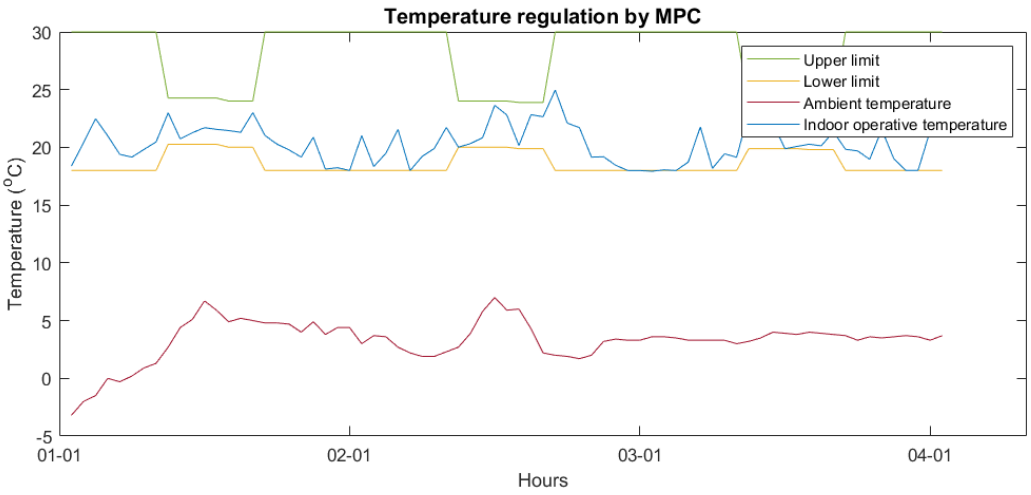

Figure 9.2: Temperature regulation by MPC from 01-01-2021 to 03-01-2021

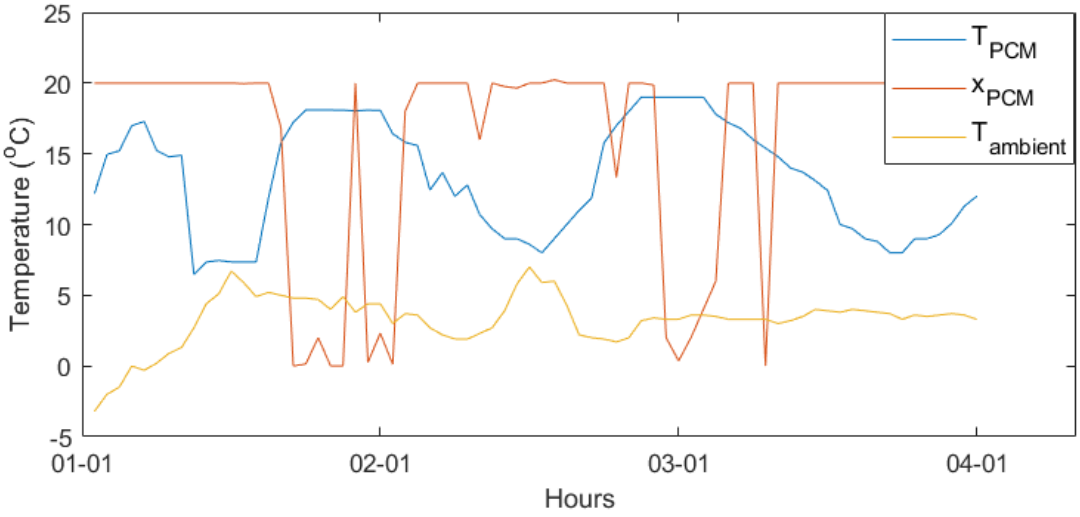

Figure 9.3: Usage of PCM to increase the energy flexibility of building

9.3.2 Summer

The simulation period is from 20-06-2021 to 22-06-2021 which is representative of Summer. The developed MPC utilizes energy when available at a lower cost, resulting in reduced pressure on the grid and lower energy costs as shown in Figure 9.4. Importantly, the MPC achieves this while maintaining indoor comfort, as shown in Figure 9.5. Figure 9.6 illustrates

Assessment Criteria	Rule-Based Controller	MPC
Energy supplied by heatpump [kWh]	216	117
Estimated cost of electricity [EUR]	27.9	12.7

Table 9.1: Energy flexibility of MPC

the utilization of passive strategies, such as the use of sky windows for natural ventilation during the day. Furthermore, Figure 9.7 illustrates that the blinds are closed during the day to prevent overheating of building during the day. It is noteworthy from Figure 9.8that the temperature of the airstream after passing through PCM (T_{mix}) is cooler than the temperature of the airstream entering PCM (T_h), which indicates that PCM is passively used in cooling during the day. Also, the PCM is cold-loaded during the night and this energy is used to cool the building the next day.

In addition,Table 9.2 provides quantitative insights into the performance of the MPC algorithm. It reveals that the MPC achieves a reduction of approximately 48% in energy supplied and a significant 42% reduction in electricity costs compared to other approaches assuming a constant COP of the heatpump.

Assessment Criteria	Rule-Based Controller	MPC
Energy supplied by heatpump [kWh]	42	21.8
Estimated cost of electricity [EUR]	5.98	3.45

Table 9.2: Energy flexibility of MPC

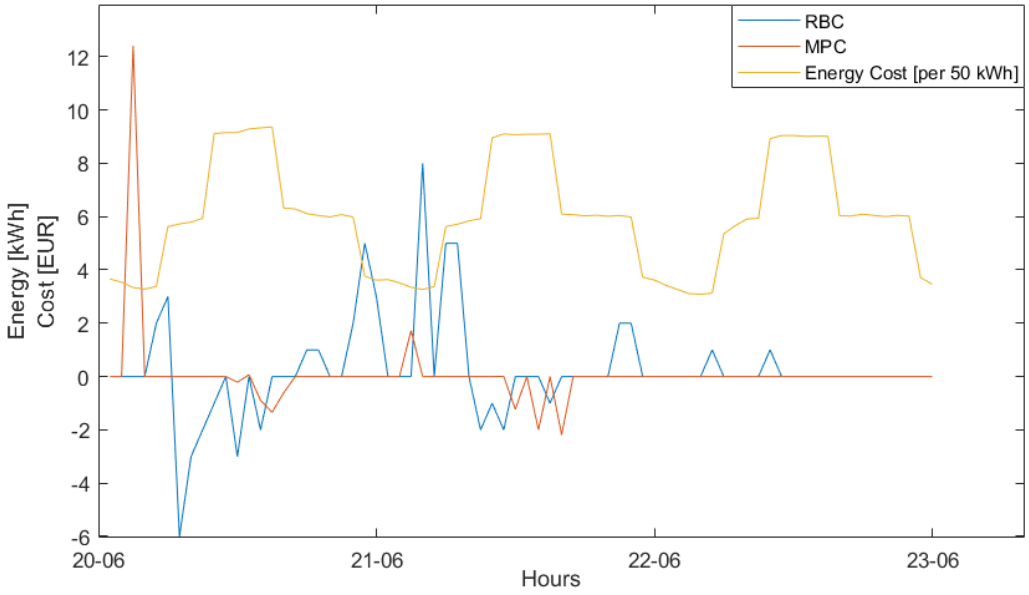

Figure 9.4: Energy supplied by heatpump from 20-06-2021 to 22-06-2021

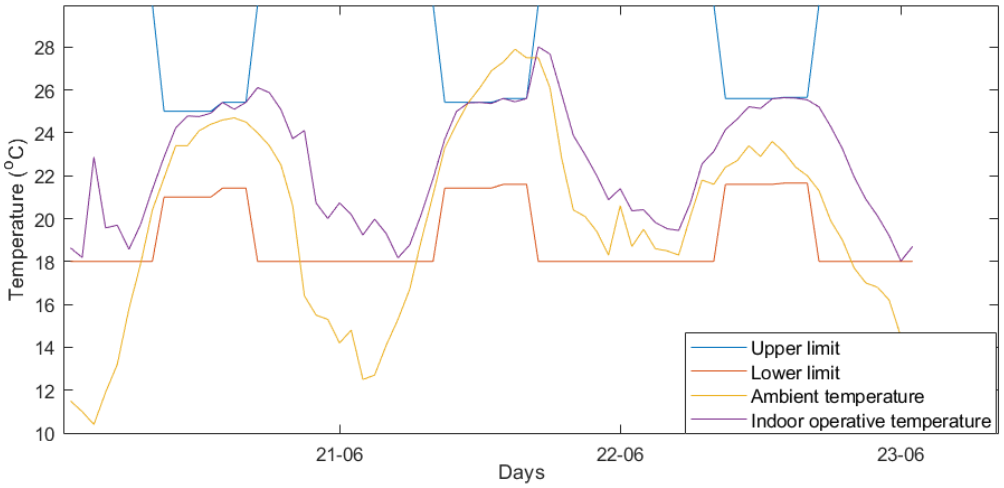

Figure 9.5: Temperature regulation by MPC from 20-06-2021 to 22-06-2021

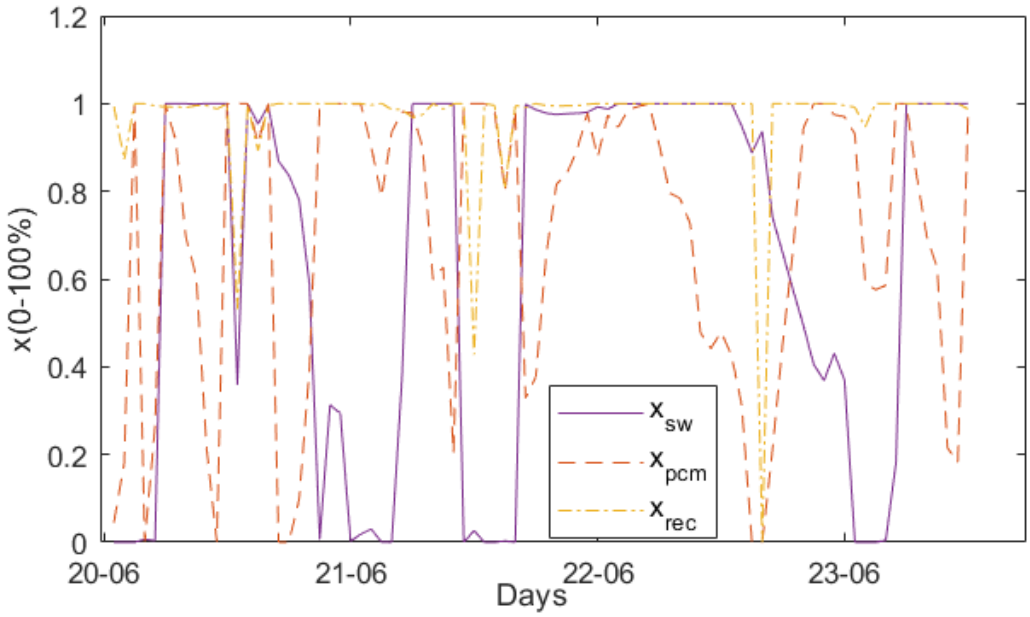

Figure 9.6: Usage of passive systems to increase the energy flexibility of building

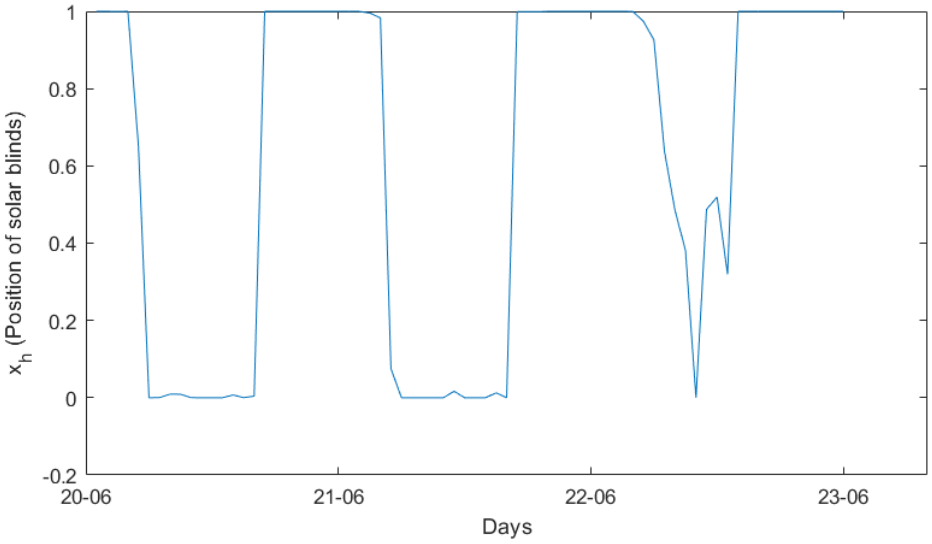

Figure 9.7: Deployment of solar blinds

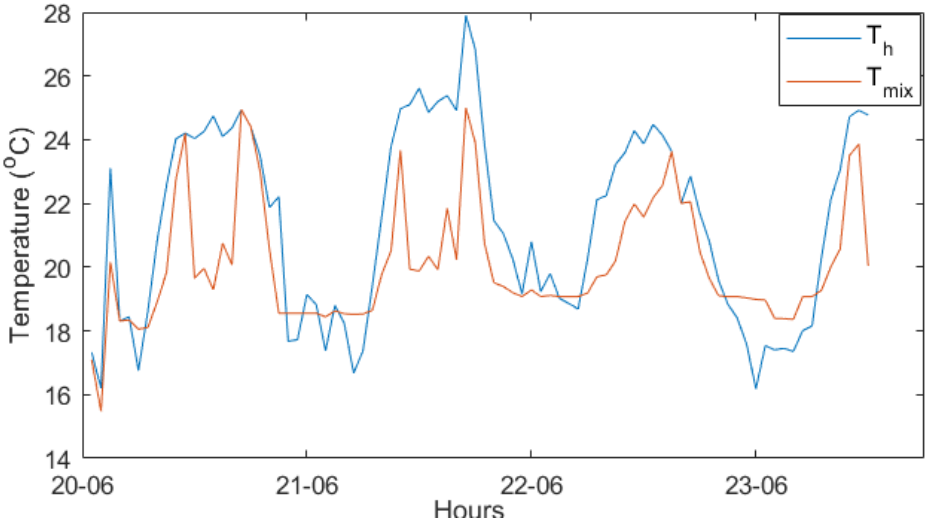

Figure 9.8: Usage of PCM

Season	Regular MPC	Modified MPC
Energy supplied by heatpump in summer [kWh]	7.2	21.8
Energy supplied by heatpump in winter [kWh]	98	117

Table 9.3: Energy flexibility of MPC

9.4 Conclusions

The investigation focused on evaluating the energy flexibility potential of the CCC through the utilization of MPC over a representative period of 3 days in both the summer and winter seasons. The findings reveal a noteworthy reduction in energy consumption and energy cost when employing the modified cost function. However, it is intriguing to observe the energy-saving benefits of the modified optimization function in contrast to the optimization function employed in previous chapters. Table 9.3 demonstrates that the modified optimized function necessitates a higher supply of heating/cooling energy for the same sample period during both the summer (January 1, 2021, to January 3, 2021) and winter (June 20, 2021, to June 22, 2021), as discussed in Chapter 6. While the modified MPC approach offers cost savings, it requires a greater amount of heating/cooling energy compared to the previous optimization function.

10 Optimization to PCM configuration

The set of simulations focuses on the possibility of varying the temperature range of the PCM battery to increase the energy savings potential of the building. This simulation-based study will compare each scenario's performance for a sample period of 20 days in each of the four seasons which could give an idea about the average energy consumption of each season.

10.1 Winter

The period of study is from 01 January 2021 to 20 January 2021. It can be seen from Figure 10.1 that both the options are able to maintain the indoor operative temperatures within the permissible limits except few exceptions in unoccupied hours. Using a PCM with 18-21^{o}C requires less heating energy as this option would provide more latent heat option at a lower temperature. Furthermore, Figure 10.2 and Figure 10.3 show that the lower temperature option clearly has more temperature between the inlet and exit air temperatures and the lower temperature option outperforms as depicted in Table 10.1

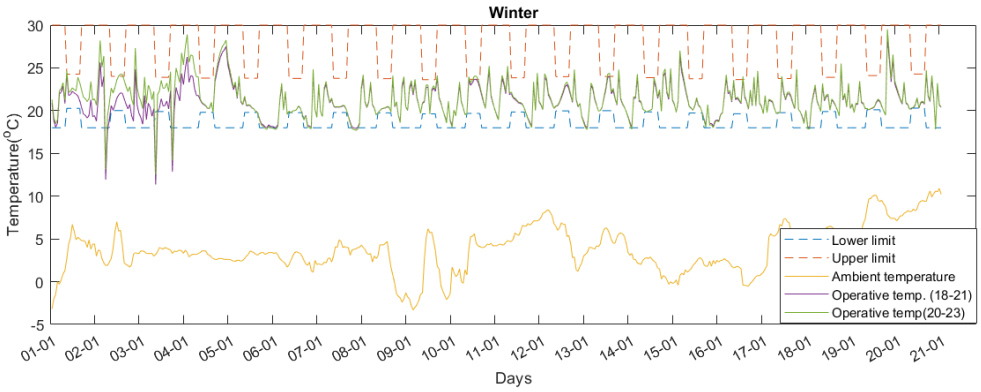

Figure 10.1: Comparison of temperature regulation by using different PCMs from 01 January 2021 to 20 January 2021

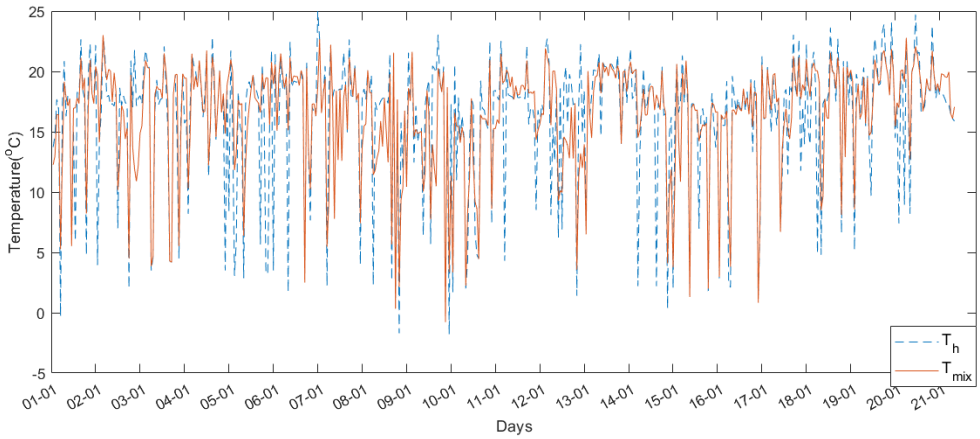

Figure 10.2: Utilization of PCM (20-23^{o}C)

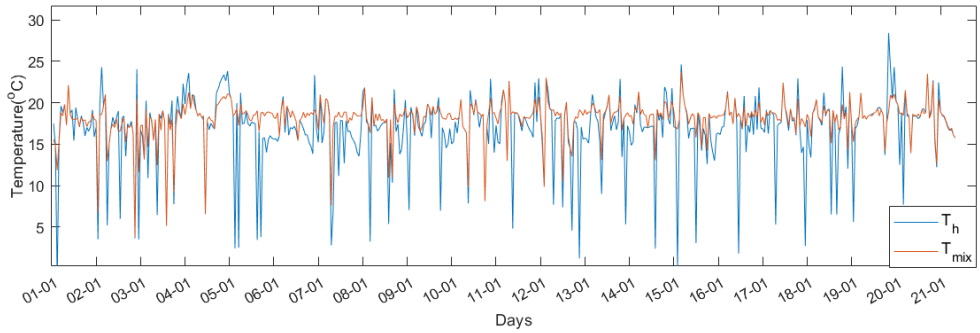

Figure 10.3: Utilization of PCM (18-21^{o}C)

Assessment Criteria	18-21^{o}C	20-23^{o}C
Energy supplied by Heatpump [kWh]	1140	1846

Table 10.1: Energy supplied by Heatpump

10.2 Summer

The period of study is from 20 June 2021 to 9 July 2021. It can be seen from Figure 10.4 that both options are able to maintain the indoor operative temperatures within the permissible limit. While using 20-23^{o}C, the heating/cooling load is lesser as more energy could be stored as latent heat in a higher temperature range. Furthermore, Figure 10.5 and Figure 10.6 show that the difference between the inlet and exit air temperatures is similar for both the options, but the higher temperature option outperforms as depicted in Table 10.2. Thus, in summer,

using 20-23^{o}C is the better option.

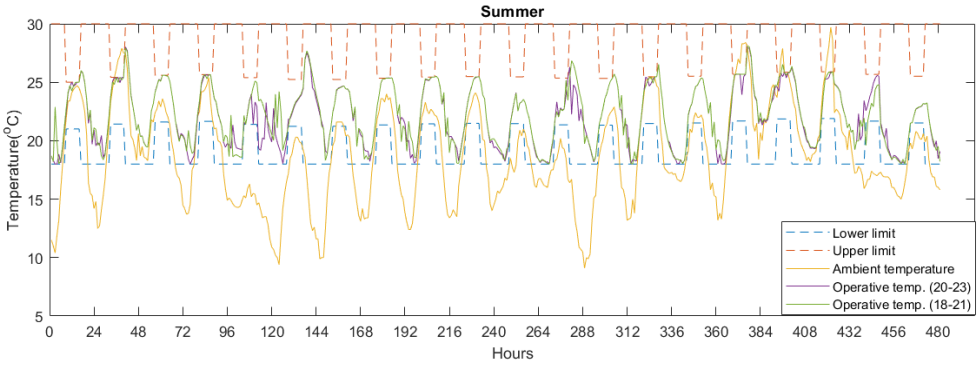

Figure 10.4: Comparison of temperature regulation by using different PCMs from 20 June 2021 to 9 July 2021

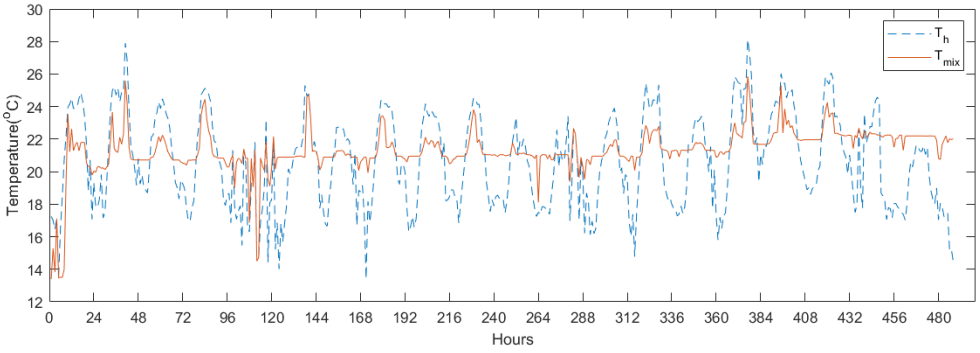

Figure 10.5: Utilization of PCM (20-23^{o}C) from 20 June 2021 to 9 July 2021

Assessment Criteria	18-21^{o}C	20-23^{o}C
Energy supplied by Heatpump [kWh]	152	96

Table 10.2: Energy supplied by Heatpump

10.3 Autumn

The period of study is from 01 October 2021 to 20 October 2021. It can be seen from Figure 10.4 that both options are able to maintain the indoor operative temperatures within the

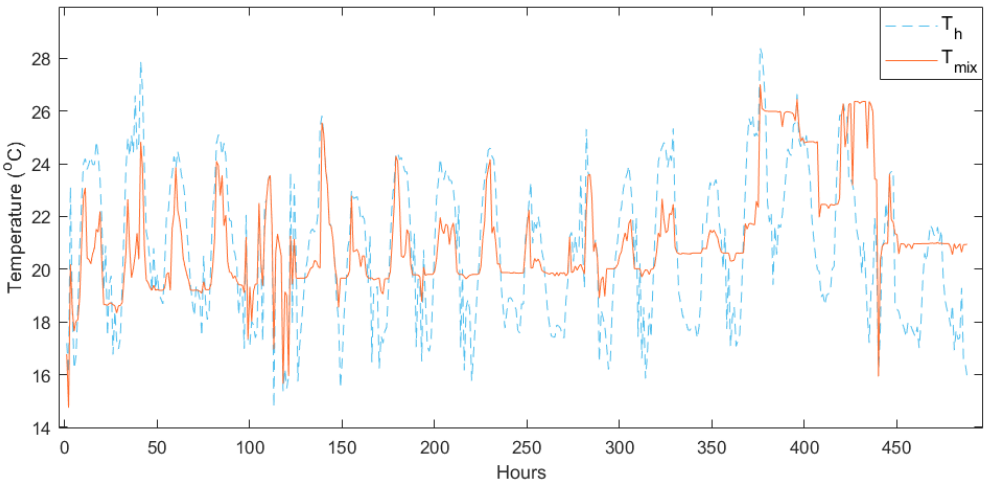

Figure 10.6: Utilization of PCM (18-21^{o}C) from 20 June 2021 to 9 July 2021

permissible limit. While using 20-23^{o}C, the heating energy required is lesser as more energy could be stored as latent heat in a higher temperature range (as shown in Table 10.3). Thus, in autumn, using 20-23^{o}C is the better option.

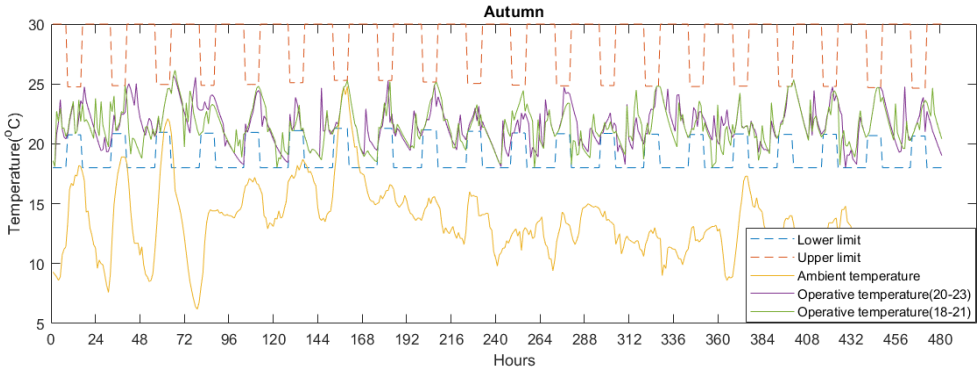

Figure 10.7: Comparison of temperature regulation by using different PCMs from 01 October 2021 to 20 October 2021

Assessment Criteria	18-21^{o}C	20-23^{o}C
Energy supplied by Heatpump [kWh]	418	364

Table 10.3: Energy supplied by Heatpump

10.4 Spring

The period of study is from 01 March 2021 to 20 March 2021. It can be seen from Figure 10.4 that indoor operative temperature is maintained within the permissible limit except while using 18-21^{o}C but while using 20-23^{o}C, there are considerable instances of temperature violations. While using 18-21^{o}C, the heating energy required is lesser as more energy could be stored as latent heat in a lower temperature range (as shown in Table 10.4). Thus, in spring, using 18-21^{o}C is the better option.

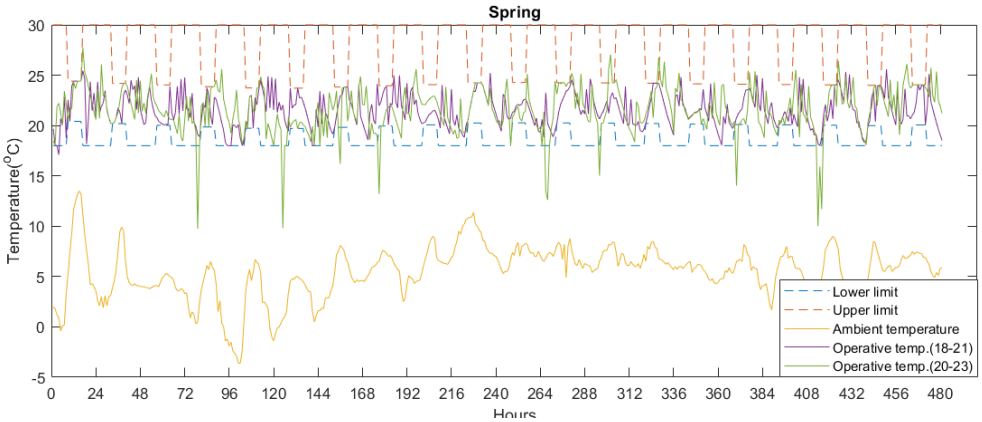

Figure 10.8: Comparison of temperature regulation by using different PCMs from 01 March 2021 to 20 March 2021

Assessment Criteria	18-21^{o}C	20-23^{o}C
Energy supplied by Heatpump [kWh]	878	1364

Table 10.4: Energy supplied by Heatpump

10.5 Conclusions

It is evident that employing PCMs within the temperature range of 18-21^{o}C yields greater effectiveness during the spring and winter seasons, whereas an alternative option proves more effective during the summer and autumn seasons. Consequently, it would be intriguing to investigate the feasibility of employing a hybrid combination of two distinct PCM options, with the aim of surpassing the performance of the previously considered separate options.

10.6 Modifications to PCM battery

From the previous study, it is clear that a single temperature range of PCM is not the most efficient option for every season. Thus, it is interesting to see if splitting up of PCM battery into two equal modules having different phase transition temperature ranges could reduce the overall heating/cooling load compared to the two options explored before. The modification requires another term for a fraction of PCM usage. The newer schematic is represented by a figure shown below in Figure 10.9. The heat transfer between air and PCM is modeled as described in Section 4 The temperature of air stream after passing through

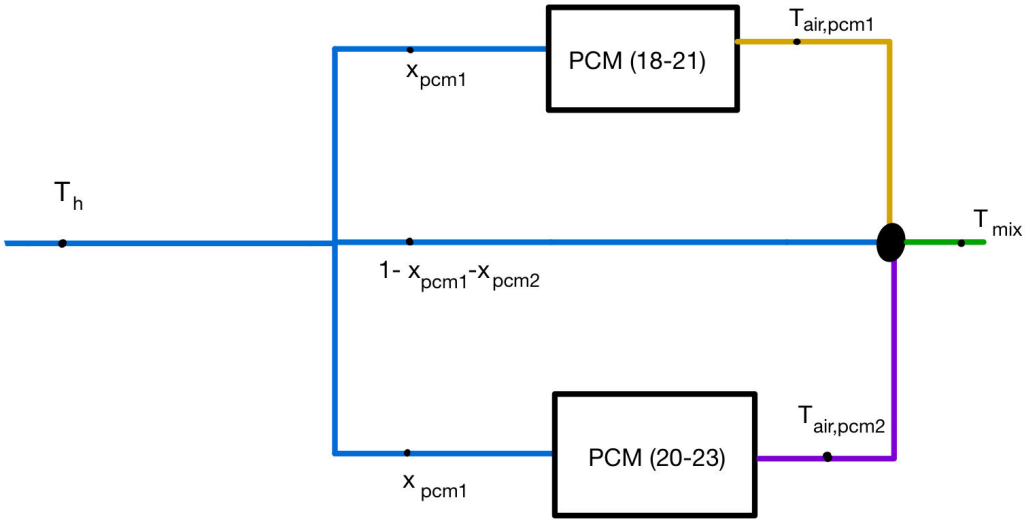

Figure 10.9: Modification to PCM battery

PCM is expressed as:

$$T_{mix} = x_{pcm1}T_{air,pcm1} + x_{pcm2}T_{air,pcm2} + (1 - x_{pcm1} - x_{pcm2})T_h \tag{10.1}$$

The optimization parameter x_{pcm} is replaced by x_{pcm1} and x_{pcm2} where x_{pcm1} represents the fraction of airstream through PCM battery of phase transition temperature between 20-23^{o}C and x_{pcm2} representing the fraction through the other one (18-21^{o}C) and the following sections present the difference in the performance of this approach. In order to closely observe the difference made by this approach, a sample period of three days is studied for a season, even though the comparison in energy has been made for the same duration of 20 days for each season.

10.6.1 Summer

The period of study is from 20 June 2021 to 9 July 2021. It can be seen from Figure 10.10 that both options are used as a passive energy storage option, but the PCM with higher phase transition temperature is predominantly used while the lower temperature option is mostly used during the night for storing energy at a lower temperature.

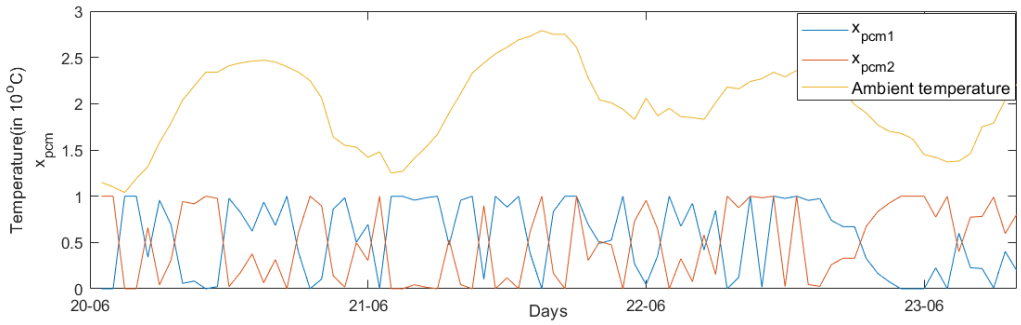

Figure 10.10: Utilization of PCM in summer

10.6.2 Winter

The period of study is from 01 January 2021 to 20 January 2021. It can be seen from Figure 10.11 that both options are used as a passive energy storage option, but the PCM with lower phase transition temperature is the predominantly utilized option

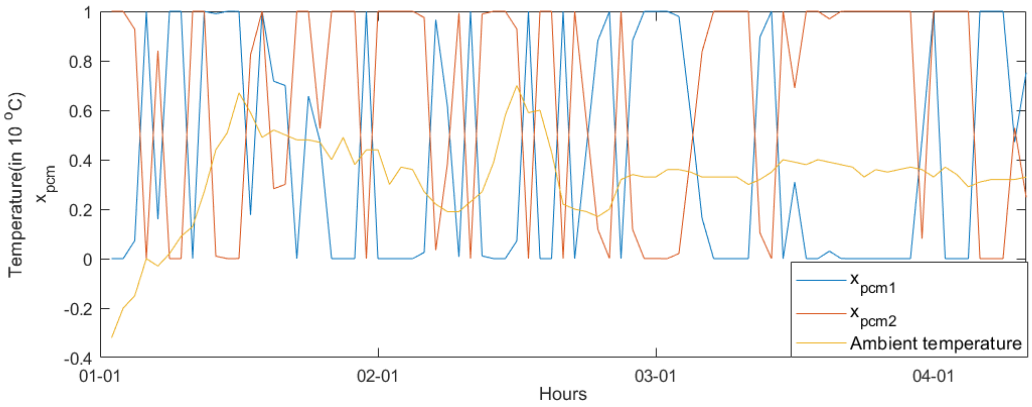

Figure 10.11: Utilization of PCM in winter

10.6.3 Autumn

The period of study is from 01 October 2021 to 20 October 2021. It can be seen from Figure 10.12 that both options are used as a passive energy storage option, but the PCM with higher phase transition temperature is the predominantly utilized option

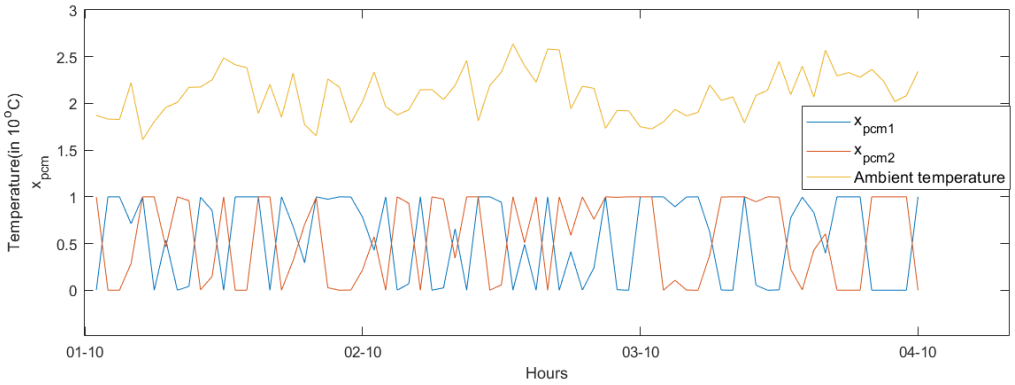

Figure 10.12: Utilization of PCM in Autumn

10.6.4 Spring

The period of study is from 01 March 2021 to 20 March 2021. It can be seen from Figure 10.13 that both options are used as a passive energy storage option, but the PCM with lower phase transition temperature is the predominantly utilized option

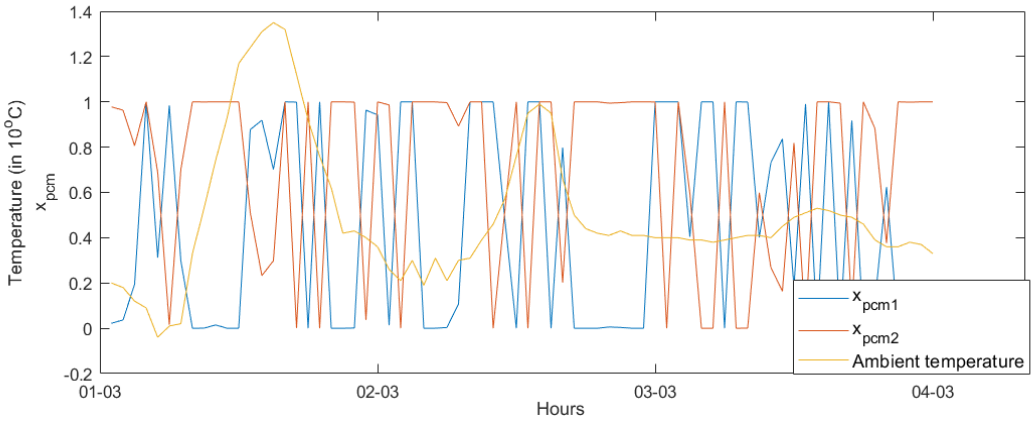

Figure 10.13: Utilization of PCM in Spring

10.6.5 Results of the Hybrid system

The tabulated results in Table 10.5 demonstrate the superior performance of the hybrid combination over the lower temperature PCM during Summer and Autumn, as well as its outperformance compared to the higher temperature PCM during Winter and Spring. Nevertheless, it is noteworthy that the energy savings achieved by the lower temperature PCM during Winter and Spring outweigh its comparatively weaker performance during the other two seasons. Consequently, despite the hybrid option exhibiting favorable performance characteristics overall, the logical choice still favors the utilization of the lower-temperature PCM due to its energy savings during the Winter and Spring seasons.

Season	18-21^{o}C	20-23^{o}C	Hybrid system
Summer	152	96	112
Winter	1140	1846	1267
Spring	878	1364	924
Autumn	418	364	378
Total	2588	3670	2681

Table 10.5: Energy supplied by Heatpump [kWh]

11 Alternative thermal comfort model

The control of indoor thermal comfort is based on the beta temperature limits [12]. But this chapter discusses the possibility of using more flexible temperature limits using the alpha model as discussed in Section 2.1

11.1 Modifications to the model

This model makes a difference as it has higher upper limits for indoor operative temperature when the running mean outdoor temperature is more than 11^{o}C. The model is varied as shown below:

$$T_{operative} = 21.45 + 0.11 * T_{e,ref} \tag{11.1}$$

and the desired temperature limits for occupied hours are:

$$T_{operativelimits} \in \begin{cases} \text{Lower limit} & T_{operative,hour} - 2^oC \\ \text{Upper limit} & T_{operative,hour} + 0.21 * (T_{e,ref} - 11) + 2^oC \end{cases} \tag{11.2}$$

whereas for the original model, the operative limits are $T_{operative}$ $\pm 2^o$C

11.2 Results

The MPC program runs on the aforementioned comfort models from 20-06-2021 to 25-06-2021, which is representative of Summer and gives an insight into the difference in performance if the ambient temperature exceeds the indoor operative temperature. Analysis of the Figure 11.1 reveals that the alpha model allows for higher upper limits in the indoor operative temperature, resulting in generally elevated indoor temperatures compared to the beta model. The cooling energy consumption of the building is minimized as a significant portion of temperature control is achieved through passive means. Notably, during the second day of simulation when the outdoor temperature surpasses the indoor operative temperature, it was observed that utilizing the alpha model results in reduced cooling load, as higher indoor operative temperatures are deemed acceptable. As detailed in the Section 10.2, temperature control primarily relies on PCM loading during the night and natural ventilation facilitated by sky windows. Consequently, the implementation of the beta model necessitates less energy input from the heat pump, consequently reducing the cooling energy requirement for maintaining thermal comfort. Further analysis of the energy demand over the 5-day simulation period can be found in Table 11.1.

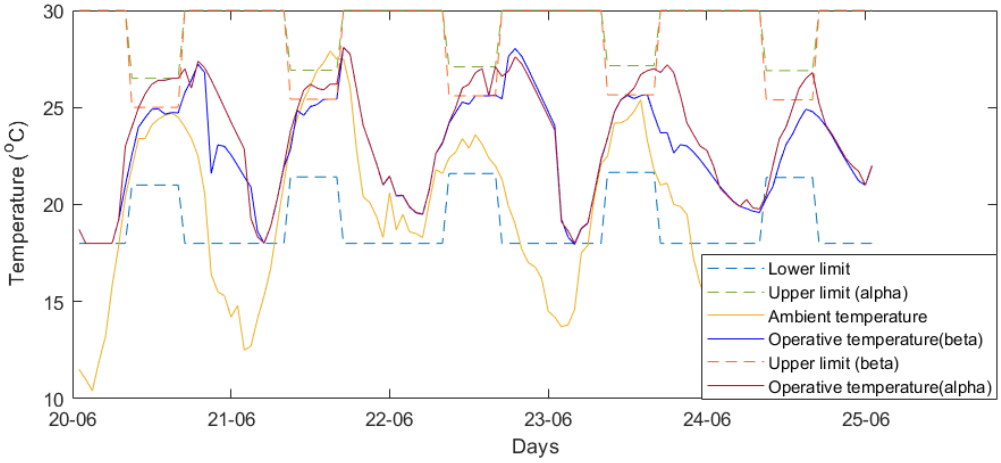

Figure 11.1: Indoor temperature regulation by various indoor comfort models from 20-06-2021 to 25-06-2021

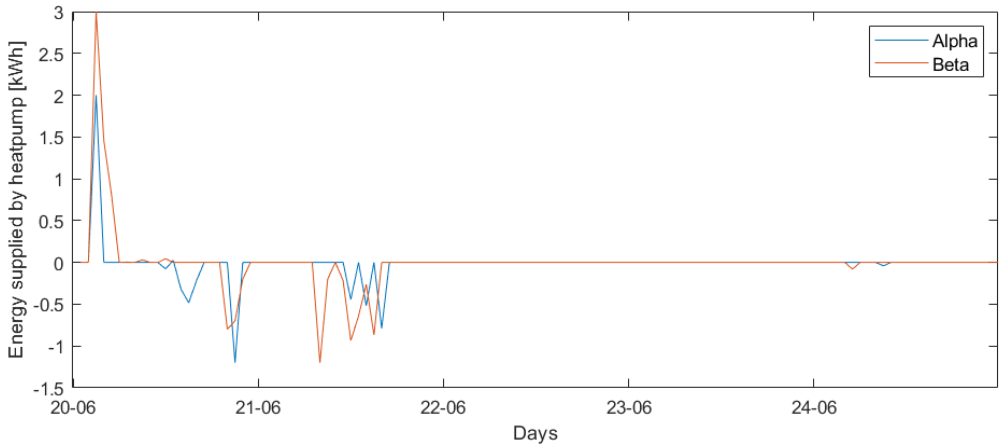

Figure 11.2: Comparison of Energy supplied by heatpump from 20-06-2021 to 25-06-2021

Assessment Criteria	Beta	Alpha
Energy supplied by Heatpump [kWh]	8.5	7.2
$\sum$ error [^{o}C]	4.61	4.82

Table 11.1: Performance comparison of MPC on different thermal comfort models from 20-06-2021 to 25-06-2021

11.3 Conclusions

Considering the Co-creation center as a building type BETA, as defined by Van der Linden [12].In their criteria, an alternative approach that impacts the upper limit for operating temperature, particularly in summer conditions is presented. Consequently, this approach marginally decreases the cooling load, especially on the second day of simulation when the ambient temperature exceeds the indoor operating temperature.

12 Conclusions and Future Work

12.1 Conclusions

This research aimed to address the gap in the optimal integration of active and passive energy sources to minimize energy consumption while maintaining indoor thermal comfort. The thesis proposed a model predictive control algorithm with low computational costs and good control performance that could harvest the optimal amount of passive energy from the building. This research answers the following sub-questions as :

1. How well does the developed building model compare to the thermal behavior in an actual building?

The Co-Creation center building was modeled using the Grey-box modeling approach in a previous study by Ceha et.al [22], starting with a physics-based model and in the present study, the model has been calibrated with test data. To ensure the accuracy of the model, it was then validated with data measured over one week in April 2021. However, concerns arose about the specificity of the model since it was tuned using the same data. To address this issue, experiments were conducted to regulate the building's temperature using the model, which showed that the temperature predictions of the model were within 0.3 K of the measured values. This result confirmed the model's ability to provide a good representation of the building's thermal behavior and demonstrated the effectiveness of the developed controller in regulating the building's temperature.

2. How can a building's model be both accurate and not overly complex for model-based control?

In addition to assessing the control performance of the developed Model Predictive Control (MPC), this research also investigated the computational cost of the optimization function. The results indicate that the optimization function can be solved successfully within a control timestep of 30 minutes. This finding led to the consideration of linearization strategies in the initial stages of the research. However, it was later determined that the existing nonlinear model accurately represents the building and converges well within the chosen control timestep, rendering linearization unnecessary. Thus, the developed MPC can regulate the indoor temperature of the building with high accuracy and low computational cost.

3. How does the created model predictive control strategy effectively combine passive and active energy sources while still ensuring thermal comfort?

The case studies indicate that the utilization of MPC is more prominent with the incorporation of passive energy sources, particularly when the prediction horizon is extended.

This approach can be optimally exploited with precise forecasts of future energy consumption. Moreover, the reduction in the usage of primary energy sources reinforces the notion that more energy is acquired from passive sources.

4. Is it possible to decrease energy consumption in a building by using this strategy compared to a rule-based controller in a real-case scenario?

ased on the comparison made during the second week of April, it has been found that the application of MPC results in a potential reduction of up to 17% in the utilization of heating/cooling energy from the heatpump. Hence, the MPC system can be utilized for the effective harnessing of passive energy sources. Furthermore, the MPC system not only minimizes the energy consumption of the building but also enhances its energy flexibility. By accurately forecasting future energy requirements, the building's energy demands can be made more flexible through the utilization of pre-cooling and pre-heating mechanisms. This approach not only decreases overall energy consumption but also improves the utilization of readily available energy, thereby alleviating the stress on the electricity grid.

12.2 Limitations of this research

No glare control

The control strategy employed in the developed MPC system for the blinds is solely based on energy considerations. Specifically, the blinds are opened when heating is required and when solar irradiance is present. Conversely, if the building requires cooling, the blinds are completely closed. However, this approach overlooks the specific conditions of spring and autumn when ample sunlight is available, but cooling is predominantly needed. As a result, the blinds would remain open regardless of the need to prevent direct glare. This can potentially cause visual discomfort for the occupants.

No active fresh air control

In accordance with ASHRAE standards 62.1-2019, a minimum fresh air supply of 2.5-5.1 l/s per person is recommended. Assuming full occupancy within the Co-creation center, the fresh air supply should be maintained at a minimum of 0.19 Kg/s. To ensure this, an average lower limit of 0.1 Kg/s for the mass flow rate of fresh air is maintained. However, it is important to note that this approach does not consider the actual occupancy levels and can result in ventilation losses, as detailed in Appendix A.

Frequent actuation of actuators

The MPC program operates based on the principle of minimizing the optimization function to find a global minimum. However, this approach does not take into account the previous

states of the actuators. Consequently, it can result in frequent opening and closing of valves, as well as repeated loading and unloading of the PCM battery. Such frequent and abrupt operations can potentially have detrimental effects on the lifecycle of the actuators and the PCM battery.

Constant COP of Heatpump

The current objective function of the MPC focuses on minimizing the energy supplied by the heat pump. However, incorporating the heat pump model and utilizing its electricity consumption as the objective function would provide a more realistic assessment of performance, particularly in terms of energy savings and energy flexibility potential. This approach would enable a comprehensive comparison that considers the actual energy consumption of the heat pump, thereby enhancing the accuracy of evaluating energy efficiency and potential improvements.

12.3 Recommendations for future work

The primary objective of this thesis was to develop an efficient MPC strategy for optimally integrating various passive energy sources. The proposed methodology has been successfully implemented, which validates the effectiveness of the developed MPC approach. However, as with any research work, there is always room for further improvements and investigations. Therefore, this article recommends potential avenues for future research in this area.

Installation of Solar irradiance sensors

Presently, the Co-Creation center utilizes a solitary sensor to measure the Global irradiance, and the DNI and DHI components are estimated through analytical models. However, these models make several underlying assumptions, including a constant distribution of diffuse radiation throughout the day and year, and uniform terrain. In order to improve the accuracy of the measurements, it is recommended to install DNI and DHI sensors, which can directly measure each of these components.

Modeling of Indoor Air quality

The model can be enhanced by incorporating the modeling of CO_2 concentration of the air, which would help in maintaining fresh and pollutant-free air. Additionally, the model should consider maintaining the relative humidity of the air to prevent the growth of mold and other unwanted elements.

Interfacing of developed MPC with BEMS

In the testing phase, the results obtained from the MPC algorithm were entered manually into the BEMS for the operation of energy systems. However, this approach could lead to potential issues such as delays and human errors during the control process. To address this limitation, future work should focus on integrating the BEMS with the controllers in an efficient manner to enable more viable testing and validation activities.

Inclusion of Visual Comfort

The present blind control system does not consider the impact of direct sunlight glare, which could result in visual discomfort for occupants. Therefore, there is a need to enhance the model by incorporating improved blind control mechanisms to mitigate the effects of direct glare.

A Basics of heat transfer

A.1 Introduction

An in-depth understanding of the energy consumption of buildings is essential for identifying ways to reduce consumption and make it more sustainable. Energy demand can be divided into two categories: building-related energy demand and user-related energy demand.

User-related energy demand, which primarily comes from electrical appliances, cannot be directly influenced by the building's design. Building-related energy demand, on the other hand, is the thermal energy required to maintain comfort criteria such as temperature and humidity. This demand is influenced by various factors such as the occupants' comfort preferences, building design, occupancy characteristics, weather, and the heat generated by electrical appliances within the building.

The energy balance of a building can be represented by the sum of the heat generated by internal sources, the heat transferred from the external environment, and the energy stored in the building's components or air-filled zones. The first law of thermodynamics states that:

$$\frac{dE}{dt} = \dot{Q} - \cancelto{0}{\dot{W}} = \rho V c_p \frac{dT}{dt} \tag{A.1}$$

where E denotes internal energy, $\dot{Q}$ is the heat flowing into the system and W is the work done by the system, ρ is the density, V is the volume, T is the temperature and c_p is the specific heat capacity of the considered component.

To accurately predict the energy consumption of a building, it is crucial to take into account all the energy flowing into and out of the indoor environment. The energy flow is dependent on the energy transmitted into the building $\dot{Q}_{trans}$, the energy transferred via ventilation $\dot{Q}_{vent}$, the energy transferred via infiltration $\dot{Q}_{inf}$, the energy gained from *internal loads* $\dot{Q}_{int}$ and the solar energy gain $\dot{Q}_{sol}$.

$$\rho V c_p \frac{dT}{dt} = \dot{Q}_{trans} + \dot{Q}_{vent} + \dot{Q}_{inf} + \dot{Q}_{int} + \dot{Q}_{sol} \tag{A.2}$$

If the total energy flow is negative, it means the building needs extra heating energy to maintain a comfortable temperature. Conversely, if the energy flow is positive, the building needs to be cooled to keep it at a suitable temperature.

A.1.1 Energy flow through transmission

Because of the temperature difference between indoor and outdoor air, heat will transfer through the building's components such as the roof, walls, floor, and windows. The heat transfer through a wall of surface area A is determined using the equation:

$$\dot{Q}_{trans} = UA(T_o - T_i) \tag{A.3}$$

$$with\ U = \frac{1}{\frac{1}{\alpha_i} + R_c + \frac{1}{\alpha_o}} \quad [Wm^{-2}K^{-1}] \tag{A.4}$$

where U is the overall heat transfer coefficient in W/m^2K, A is the overall cross-sectional area of the wall, R_c is the thermal resistance of the wall in $W^{-1}m^2K$, T_i is the indoor temperature and T_o is the outdoor temperature . α_i and α_o are the convective heat transfer coefficient for indoor and outdoor air respectively.

Determining the heat transfer coefficients is a complex task. As per Obyn et.al [29], the convective heat transfer coefficient can be experimentally computed by measuring the convective heat flux density and the temperature of the surface as well as the corresponding fluid medium. However, measuring the heat flux density is a difficult process, thus the coefficient is usually represented by a function of the dimensionless Nusselt number (Nu).The Nusselt number is a measure of the efficiency of heat transfer between a fluid and a solid surface, as outlined in the following equation:

$$h = \frac{Nu.k}{l} \tag{A.5}$$

where k is the thermal conductivity of the fluid or gas, h is the convective heat transfer coefficient between the two mediums in consideration and l denotes the *characteristic length* along the direction of motion of the fluid/gas.

The Nusselt number plays a critical role in estimating the convective heat flux, but there is no universally accepted method for calculating it. Obyn et al. [29] reviewed around 90 different convection coefficient correlations from over 25 sources. These correlations were specifically chosen for models of vertical and horizontal surfaces in buildings. The estimation methods were broadly classified into four categories:

- **Constant Value**: Nusselt number can be assumed to be constant over a working range or constant over divided working spaces defined by if-else statements
- **Function of temperature differences**: Nu depends on temperature differences. In this case, the airflow is assumed to be laminar
- **Function of airflow**: Nu depends on Reynolds number that can be derived from air change rate. In this case, airflow is assumed to be fully turbulent
- **Function of multiple factors**: Nu depends on temperature temperature difference as well as the flow velocity. The flow is assumed to be partly turbulent in this case.

To achieve greater precision in estimating the Nusselt number, which is crucial for the analysis of heat transfer, this thesis adopts a method that considers multiple factors. This approach is chosen over other methods because of its potential to enhance accuracy [29], and it will be used throughout the remainder of this study.

A.1.2 Energy flow through ventilation

The introduction of outdoor air into the building occurs through various means, including natural openings such as windows and doorways, or through specialized systems specifically designed for this purpose. Ventilation systems are basically divided into four types:

- Natural ventilation through grill and window
- Mechanical supply ventilation: A mechanical ventilator is used on the supply side.
- Mechanical exhaust ventilation: A mechanical ventilator is used on the exhaust side.
- Mechanical supply ventilation and mechanical exhaust ventilation with heat recovery. It is also called Balanced ventilation

The utilization of advanced ventilation systems is crucial in maintaining appropriate indoor air quality, as well as curbing the transmission of viral infections such as SARS-COVID-19. These systems monitor the concentration of carbon dioxide in the indoor air and introduce fresh air when levels exceed 800 parts per million to reduce the transmissivity of viral infections [30]. This infusion of fresh air not only supplies the necessary oxygen for respiration but also dilutes pollutants and lowers the humidity levels present due to human respiration and perspiration. In instances where mechanical ventilation is employed on both the supply and exhaust sides, it is advisable to incorporate heat recovery between the air handling units. For example, during the heating season, outdoor air can be preheated with the relatively warmer exhaust air. Conversely, during the cooling season, outdoor air can be precooled by the relatively cooler exhaust air.

The heat loss through a mechanical supply and exhaust ventilation system with heat recovery is dependent on the efficiency of heat recovery η which is usually in the range of 0.8-0.9[31]

The heat exchanged in the ventilation system per unit of time is given by:

$$\dot{Q}_{vent} = \eta \dot{m}_{vent} C_p (T_o - T_i) \quad [W] \tag{A.6}$$

where T_o is the outdoor air temperature, T_i is the indoor air temperature , C_p is the specific heat capacity of air in [J/Kg.K], $\dot{m}_{vent}$ is the mass flow rate of air in [Kg/s] and η is the efficiency of heat recovery.

A.1.3 Energy flow through infiltration

The infiltration of exterior air can occur through various means, such as cracks in the building structure or narrow gaps in windows. In contemporary dwellings, which are often highly air-tight, the infiltration of air is usually minimal, therefore necessitating the implementation of sufficient ventilation systems to maintain indoor air quality. The heat transfer resulting from infiltration can be quantified using the following equation:

$$\dot{Q}_{inf} = \dot{m}_{inf} C_p (T_o - T_i) \quad [W] \tag{A.7}$$

where $\dot{m}_{inf}$ is the mass of infiltrated air in [Kg/s] ,C_p is the specific heat capacity of air in [J/Kg.K], T_o is the outdoor air temperature and T_i is the indoor air temperature.

Infiltration in the building occurs mainly due to pressure differences between the indoor and outdoor environments, resulting from wind-induced airflow or stack effect caused by temperature differences. However, since the building is a recent construction, the heat transfer caused by infiltration can be disregarded for the rest of this study.

A.1.4 Internal heat gains

The interior of a building contains a variety of sources of energy, including electrical appliances such as computers and televisions, lighting fixtures, and the presence of people. The combined heating load generated by these factors is commonly referred to as the internal heat load.

Occupants

The human body generates heat as a byproduct of metabolism, which is dissipated to the surrounding environment in order to maintain a stable internal body temperature. This heat is dissipated through various means, including respiration, convection from the skin to the air, and sweating. The amount of heat transferred is influenced by a variety of factors, including the individual's activity level, the level of clothing worn, as well as environmental factors such as the humidity and temperature of the indoor air [32]

The internal heat gain from people is calculated using typical metabolic heat generation data given in Table A.1.

$$\dot{Q}_{people} = n_{people} * \dot{Q}_M \quad [W] \tag{A.8}$$

where is the typical heat gain caused by people pursuing various activities.

Resting/Sitting	Writing/Typing	Standing/Filing	Walking	Aerobics/Dancing
100	117	144	180	360

Table A.1: Typical heat gains ($\dot{Q}_M$) by people in [W] [1]

Electrical Lighting

The instantaneous electrical lighting power consumed by a building is dependent on the total electrical lighting installed and the type of lamps used. Additionally, the operation of the building also plays a role in determining the electrical lighting power. Common types of lighting used in buildings and their average luminous efficiency range in lumen per watt (1 lum= 1 lux/m^2) is presented in Table A.2. Standards have been established by American Society of Heating, Refrigerating and Air-Conditioning Engineers (ASHRAE) [33] for the maximum allowable electrical lighting power per square meter of floor area as shown in Table A.3 (P_{light} in ([W/m^2]) and since the CCC is a conference room, P_{light} can be assumed to be around 12 [W/m^2].

However, only a fraction of the power supplied to the lighting equipment is converted to light, with the majority being converted to heat through convection and radiation. The light that is produced is absorbed by surfaces within the room and also contributes to the heating of the room. Therefore, a significant portion of the electricity consumed for lighting is released into the indoor environment as heat. Exceptions to this include when the luminaries are connected to ventilation ducts and the exhaust air is expelled through the lighting fixtures, which allows for a large portion of the heat to be removed by the exhaust air. This concept can be applied in building systems with low heating demand and high cooling demand. In general, the internal heat gains from artificial lighting can be calculated using the following equation.

$$P_{int,lighting} = \zeta_{light} A_{floor} P_{light} \qquad [W] \tag{A.9}$$

where A_{floor} is the building floor area, P_{light} is the electric power of the lighting in W/m^2 and ζ_{light} is the fraction of installed power released to the room. ζ_{light}= 0.2-0.6 for ventilated and ζ_{light} = 1 for non-ventilated luminaires.

Incandescent	CFL	LED	Fluorescent tubes (Argon)	Fluorescent tubes (Sodium)
10-13	35-60	45-60	55-90	100-130

Table A.2: Luminous efficacy range of light bulbs ($\dot{Q}_M$) in [lum/W] [2]

Other Electrical appliances

Heat gain from appliances refers to the thermal energy produced by electrical devices and equipment within a building. This includes but is not limited to, electronic devices such

Residential	Office	Retail	School	Theatre
10	12	18	14	28

Table A.3: Maximum allowable lighting power per floor area P_{light} [W/m^2]

as computers, televisions, and printers. The heat generated by these appliances can significantly contribute to the overall internal heat load, particularly in structures with a high density of occupants or electronic equipment.

Total Internal Energy gains to the model

The Co-creation Center has LED lights that remain switched on when the room is occupied, and it is predominantly used as a conference room, implying a constant activity level. Although the occupants wear different clothes depending on the season, the variations in thermal resistances are disregarded during modeling. The internal heat gains of the building are evaluated using a range of values presented in Table A.3 and Table A.1.

$$\dot{Q}_{int.gains} = n_{people} * \dot{Q}_M + \zeta_{light} P_{light} A_{floor} \; ; \quad [W] \tag{A.10}$$

$$\Rightarrow \dot{Q}_{int.gains} = n_{people} * 117 + 0.4 * 12 * 303.75 \quad [W] \tag{A.11}$$

A.1.5 Energy flow through solar radiation

Modeling solar radiation is a complex task as it is subject to constant variation due to a number of factors such as the position of the sun, the geographical location of the building, and its geometric properties. The amount of solar radiation absorbed also depends on the dimensions and thermophysical properties of the component. The correlation between solar irradiance and absorbed heat energy is expressed as:

$$\dot{Q}_{in} = I_o A . \xi^n \alpha_{glazing} \quad [W] \tag{A.12}$$

where $\dot{Q}_{in}$ is the rate of absorbed solar radiation energy depends on the total incident radiation per unit area (I_o), the effective optical transparency (ξ), the absorptance of the glazing ($\alpha_{glazing}$), and n is the number of glazings in series before the considered component and A is the surface area of the glazing. Furthermore, the total incident solar radiation (I_o) consists of three components: direct beam, reflected, and diffuse radiation, which are discussed in further detail in this section

$$I_o = I_{o,b} + I_{o.r} + I_{o,d} \tag{A.13}$$

Direct beam radiation

The oriented direct beam radiation $I_{o.b}$ is the direct beam radiation received on the object's surface. Contemporary irradiation sensors measure two types of direct beam radiation:

- Direct beam radiation perpendicular to Earth's horizon (I_{bh})
- Direct beam radiation perpendicular to tracking surface (I_{bn})

I_{bh} is measured by stationary upward-facing sensors, whereas the value of I_{bn} is obtained by modern sensors orienting themselves with the Sun's position in the sky. The total direct beam radiation can be obtained as [34], [35] :

$$I_{o,b} = I_{bh}\frac{cos(\theta_n)}{cos(\theta_z)} = I_{bn}cos(\theta_n) \tag{A.14}$$

where θ_n is the angle between the object's surface normal and solar beam direction and θ_z is the zenith angle.

Reflected radiation

The oriented reflected radiation ($I_{o,r}$) represents the quantity of incident radiation that has been reflected from surfaces in the vicinity, such as the Earth's surface and surrounding objects, such as trees and buildings. The horizontal component of solar radiation is determined by the direct beam radiation perpendicular to the horizon (I_{bh}) and the diffused radiation (I_d), as measured by irradiation sensors. Assuming a total isotropic reflection and diffuse reflectance value of ρ_r for all irradiance, $I_{o.r}$ can be estimated using [34], [35]:

$$I_{o,r} = (I_d + I_{bh})\rho_r\frac{1 - cos(\beta)}{2} \tag{A.15}$$

where β is the angle between the tilted surface and the earth's horizon. The ground reflectance ρ_g is expressed in albedo. albedo is defined here as the ratio between the ground-reflected radiation and the global radiation incident on the ground. Albedo is a quantitative measure of the reflectivity of a surface. It is defined as the ratio of the amount of shortwave radiation reflected by a surface to the amount of shortwave radiation incident upon it. This ratio is typically represented as a decimal value between 0 and 1. High albedo surfaces (such as snow or ice) reflect most of the incident solar radiation, while low albedo surfaces (such as dark-colored soil or vegetation) absorb most of the incident solar radiation [36]. Typical diffuse reflectance values were discussed in [35] and is given in Table A.4 The study con-

Humid climates	Dry climates	Snow covered grounds
0.2	0.5	0.9

Table A.4: Typical ρ_g values in [Albedo]

ducted by Ineichen et.al [36] demonstrates that utilizing a localized constant albedo value

for a specific site can provide more precise results in comparison to utilizing complex models. The research suggests that a constant albedo value, specific to the site in question, can be used as an alternative to sophisticated models that require extensive input data.

Diffused radiation

The oriented diffused radiation $I_{o,d}$ is the amount of received solar radiation that has changed direction due to atmospheric scattering. The extent of scattering is dependent on a wide range of parameters that are difficult to determine, such as cloud cover and atmospheric clarity. The value of $I_{o,d}$ entails three types of radiation:

$$I_{o,d} = I_{d,iso}\frac{1+cos(\beta)}{2} + I_{d,cir}\frac{cos(\theta_n)}{cos(\theta_z)} + I_{d,hor}F_{c-hor} \tag{A.16}$$

where $I_{d,iso}$ is the Isotropic diffuse radiation received, $I_{d,cir}$ is the circumsolar radiation which refers to the onward dispersion of irradiance coming from the sky section surrounding the Sun, and $I_{d,hor}$ is horizon brightening radiation concentrated around the horizon and it depends on the clearness of Sky.

The literature presents several methodologies for modeling the diffuse irradiance term ($I_{d,iso}$). These models that take into account solely $I_{d,iso}$ are classified as Isotropic models, while models that incorporate all the aforementioned terms are referred to as Anisotropic models. The values of $I_{d,iso}$, $I_{d,cir}$ and $I_{d,hor}$ are not individually measurable by sensors, however, the value of I_d can be measured. Therefore, various models have been developed to determine the total incident solar radiation (I_o). The majority of the models concur on the mathematical expression for the direct beam radiation $I_{o,b}$ and the oriented reflected radiation $I_{o,r}$, however, they differ in their expression for the diffuse radiation term ($I_{o,d}$) [3].

A study [3] conducted a statistical analysis on 30 models using the root mean squared error (RMSE) and the coefficient of determination (R^2) as performance metrics and a comparison between the models that performed well and the well-acknowledged models are presented in Table A.5. The study indicates that Anisotropic models have outperformed Isotropic models due to their increased complexity. The Perez model and the Muneer model are particularly promising. As locally trained Artificial Neural Network (ANN) models are highly specific and cannot be applied in other locations, these models will not be considered. A comparison between the Perez and Muneer models[37] and [38] suggests that the Perez model performs better under most sky conditions. Therefore, the Perez model is selected for the remainder of the thesis.

The Perez model

The Perez model is a widely used model for estimating diffuse radiation on a tilted surface. The Perez model is based on Perez's anisotropic sky model [43], which is widely used for the calculation of the diffuse radiation on a tilted surface. Perez's anisotropic sky model

Model Name	Model Type	Complexity	Local data needed	RMSE	R^2
Liu and Jordan [39]	Isotropic	Simple	-	7	6
Koronakis [40]	Isotropic	Simple	-	6	7
Hay and Davies [41]	Anisotropic	Simple	-	5	5
Muneer [42]	Anisotropic	Moderate	-	3	4
Perez [43]	Anisotropic	Moderate	-	4	3
Perez opt.[43][3]	Anisotropic	Complex	$\surd$	2	2
MLP [3]	ANN	Complex	$\surd$	1	1

Table A.5: Comparison of 7 models for oriented diffused radiation [3]

considers the sky's diffuse and circumsolar radiation and the inclination angle of the surface.

The Perez model estimates the diffuse irradiance on a tilted surface by considering the sky's diffuse and circumsolar radiation and the inclination angle of the surface. The Perez model uses the following parameters:

1. The direct normal irradiance (I_{bh})
2. The diffuse horizontal irradiance (I_d)
3. The relative airmass (ρ_{air})
4. The solar zenith angle (θ_z)
5. The tilt angle of the surface (β)
6. The azimuth angle of the surface (γ)
7. Ground reflectance (ρ_g)

The Perez model uses these parameters to estimate the diffuse radiation on a tilted surface. It is a physically based model and it takes into account the effect of the sun's position and atmospheric conditions on the diffuse radiation.

Step 1: Determination of Air mass (m)

$$m = \begin{cases} \frac{1}{cos(\theta_z)}; & \theta_z \geq 0 \text{ and } \theta_z \leq 70 \\ \frac{1}{cos(\theta_z)+0.5057*(96.080-\theta_z)^{-1.634}} & \theta_z > 70 \text{ and } \theta_z \leq 90 \\ 0 & otherwise \end{cases} \tag{A.17}$$

Step 2: Determination of clearness of sky (ϵ_{sky})

$$\epsilon_{sky} = \frac{\frac{I_d + I_{bn}}{I_d} + 5.535 * 10^{-6} * \theta_z^3}{1 + 5.535 * 10^{-6} * \theta_z^3} \tag{A.18}$$

Step 3: Determination of model coefficients
Based on the value of ϵ_{sky}, the empirical coefficients of the model are determined as shown in Table A.6.

Step 4: Calculation of oriented normal radiation(I_{on})

Value of ϵ_{sky}	f_{11}	f_{12}	f_{13}	f_{21}	f_{22}	f_{23}
1-1.065	-0.008	0.588	-0.062	-0.060	0.072	-0.022
1.065 - 1.230	0.130	0.683	-0.151	-0.019	0.066	-0.029
1.230-1.50	0.330	0.487	-0.221	0.055	-0.064	-0.026
1.50-1.95	0.568	0.187	-0.295	0.10	-0.152	-0.014
1.95 - 2.80	0.873	-0.392	-0.362	0.226	-0.462	0.001
2.80-4.50	1.132	-1.237	-0.412	0.288	-0.823	0.056
4.50-6.20	1.060	-1.600	-0.359	0.264	-1.127	0.131
>6.20	0.678	-0.327	-0.250	0.156	-1.377	0.251

Table A.6: Coeffients to the model

$$I_{on} = G_{sc} * (1 + 0.033 * cos(\frac{360 * day}{365})) \tag{A.19}$$

where G_{sc} = 1367 kW/m^2 is the solar constant

Step 5: Calculation of diffuse fraction (Δ)

$$\Delta = \rho_{air} * \frac{I_d}{I_{on}} \tag{A.20}$$

Step 6: Calculation of model parameters

$$F_1 = max(0, (f_{11} + \frac{f_{12} * \Delta + \pi * \theta_z * f_{13}}{180})) \tag{A.21}$$

$$F_2 = f_{21} + f_{22} * \Delta + \frac{\pi * \theta_z * f_{23}}{180} \tag{A.22}$$

$$a = max(0, sin(\theta_z)) \tag{A.23}$$

$$b = max(cos(85), cos(\theta_z)) \tag{A.24}$$

where a,b,F_1 and F_2 are model parameters Step 7 : Estimation of oriented diffuse radiation ($I_{o,d}$)

$$I_{o,d} = I_d * (1 - F_1) * 0.5 * (1 + cos(\beta)) + I_d * F_1 \frac{a}{b} + I_d * F_2 * sin(\beta) \tag{A.25}$$

A.2 Discretization and multi-node modeling of buildings

As the building systems become more complex, owing to the presence of various components such as walls and glazing, the mathematical models used to describe the heat transfer within the building become increasingly intricate. This is due to the non-homogeneity of the building systems, which results in heat accumulation in certain components. To account for this non-homogeneity, and also to account for the thermal inertia of systems with a large mass, it becomes necessary to employ discretization techniques. This allows for the development of dynamic equations that accurately model the thermal behavior of the building. This section focuses on the overall energy balance of an indoor space and the process of converting this balance into a system of differential equations.

Using the laws of thermodynamics and the principles of conservation of energy and mass, the overall energy balance equation can be derived by considering the different ways heat can be gained or lost in a room, such as through conduction, convection, and radiation. These terms can then be mathematically modeled using differential equations to accurately represent the heat transfer phenomena in the indoor space. This process of generating a system of differential equations allows for a more in-depth analysis of the thermal performance of a room and can aid in optimizing the insulation, ventilation and heating and cooling systems for improved energy efficiency.

The finite difference method is a widely used numerical approach for solving differential equations, including those associated with heat transfer phenomena. The method involves discretizing a continuous system, such as a room, into a set of discrete elements, referred to as ”cells”, and approximating the temperature distribution within the room by solving the finite difference equations.

The discretization process is essential in the context of thermal energy balance, as it allows for the representation of the continuous temperature distribution in a room as a set of discrete values at specific points in space. The finite difference method for thermal energy balance entails discretizing the room into small, discrete elements, and approximating the temperature at the center of each cell using finite difference equations. These equations are used to calculate the temperature at the center of each cell based on the temperatures of the surrounding cells and the heat flow into or out of the cell. The most commonly used finite difference equation in thermal energy balance is the explicit finite difference equation, which is based on the principle of conservation of energy. The equation relates the temperature at a point in time and space to the temperatures of the surrounding points at the previous time step and takes into account the heat flow through the walls, roof, floor, windows, and doors of the room, as well as any internal heat gains or losses.

By solving the finite difference equations for each cell in the room, the temperature distribution throughout the room can be determined at any given time. The results of this analysis can be utilized to evaluate the thermal performance of a room and to optimize the insulation, ventilation, heating, and cooling systems in order to improve energy efficiency.

B Indoor building comfort

B.1 Aspects of thermal comfort

Indoor comfort refers to the state of being within a building that allows its occupants to feel comfortable both physically and mentally. Indoor comfort is achieved by controlling and maintaining thermal, acoustic, and visual comfort along with ensuring adequate indoor air quality.

B.1.1 Thermal comfort

Thermal comfort is the perception of warmth or coldness by the thermal receptors located in the skin and hypothalamus, which act as thermal sensors. The human body has the ability to maintain an internal temperature of approximately 37°C ±1°C, regardless of the external temperature. The signals transmitted by cold sensors and warm sensors determine an individual's thermal sensation. Cold sensors, primarily located in the skin, send signals to the thermoregulatory center when the body temperature drops below 34°C. In response, the body initiates warming processes such as shivering, increasing muscle activity, and decreasing blood flow to the skin. Warm sensors, primarily located in the hypothalamus, signal when the body temperature exceeds 37°C. In response, the body initiates cooling processes such as sweating and increasing blood flow to the skin. Thermal comfort is achieved when the heat generated by metabolism is in balance with the heat lost from the body [44]. Factors that influence the heat balance of the human body include skin temperature and metabolism rate, as well as ambient temperature, clothing, and time of day [45].

A rational approach to evaluate thermal comfort considers it to be dependent on the heat balance of the human body. In order to attain thermal comfort, the heat flowing into the body and the heat flowing from the body have to be balanced [46]. The heat balance is affected by external factors such as ambient temperature, humidity, etc, and internal factors such as metabolism rate and clothing [10].

B.1.2 Acoustic comfort

Acoustic comfort pertains to the sound environment within a building. It encompasses a variety of factors such as noise levels, reverberation time, and speech intelligibility. Excessive noise can lead to distractions, discomfort, and even hearing impairment, whereas poor speech intelligibility can impede effective communication among the occupants [47].

B.1.3 Visual comfort

Visual comfort pertains to the lighting levels and color rendering within a building. It encompasses a variety of factors such as the quantity of light, the distribution of light, and the color of light [48]. Adequate lighting levels are necessary for visual tasks, whereas poor lighting can cause eye strain, headaches, and visual discomfort. The color rendering of the light is also significant as it impacts the way colors appear in the space, affecting the visual aesthetics of the building.

B.1.4 Indoor air quality

Indoor air quality (IAQ) encompasses various factors that contribute to the overall well-being of the occupants in a building. Specifically, IAQ pertains to the physical and chemical characteristics of the air inside a building, including factors such as temperature, humidity, ventilation, and the presence of pollutants or irritants. Poor IAQ can lead to various health issues such as headaches, fatigue, and respiratory problems, and can exacerbate existing health conditions. It is thus essential to ensure that the air inside a building is clean, fresh and healthy, which can be achieved by appropriate ventilation, air filtration, and controlling the sources of pollutants.

B.2 Parameters related to thermal comfort

The parameters associated with thermal comfort are briefly categorized as *Personal* and *ambient* parameters. Personal parameters represent the characteristics of the occupant such as Clothing insulation and Metabolic heat rate. Ambient parameters include temperature, air velocity, and relative humidity.

B.2.1 Dry bulb (air) temperature

The *dry bulb* temperature T_{db} refers to the air temperature of indoor air. It is a fundamental parameter in determining thermal comfort within a building. Various models have established recommended ranges of values for air temperature to ensure the thermal comfort of occupants. The dry bulb temperature is an important factor in the design and operation of a building's heating, ventilation and air conditioning systems, as it can affect the thermal comfort and overall well-being of the occupants. [49].

B.2.2 Mean radiant temperature

The *mean radiant* temperature T_{MR} is a measure of the thermal radiation that is exchanged between a human and the surrounding surfaces in a building environment [50] [51] . It is defined as the temperature of a hypothetical black body that emits and absorbs the same amount of thermal radiation as the human and the surrounding surfaces. T_{MR} is estimated by calculating the weighted average of the temperatures of various internal surfaces within a building. This parameter plays a crucial role in determining the thermal comfort of building occupants, as it takes into account not only the air temperature but also the temperatures of the surfaces that surround the occupants.

$$T_{MR} = \frac{\sum_{i=1}^{n}(T_i * S_i)}{\sum_{i=1}^{n} S_i} \tag{B.1}$$

where T_i is the temperature of surface i and S_i is the surface area of surface i.

B.2.3 Operative temperature

The *operative temperature* T_{op} is a measure of thermal comfort that takes into account the combined effect of air temperature, mean radiant temperature, and air velocity. It is defined as the temperature of a hypothetical black enclosure in which an occupant would exchange the same amount of heat by radiation and convection as they do in the actual heterogeneous environment [14]. The operative temperature is derived as a function of the air temperature, mean radiant temperature, and air speed, and it is a widely used metric to evaluate thermal comfort in buildings. It gives a more comprehensive understanding of the thermal environment by considering various thermal factors and their interactions.

$$T_{OP} = \frac{(T_{MR} * h_r + T_{db} * h_c)}{(h_r + h_c)} \tag{B.2}$$

where h_r is the radiative heat transfer coefficient (which is dependent on the surface emissivities, temperature and the view factors of the two surfaces exchanging heat) in [$Wm^{-2}\,{}^{o}C^{-1}$] and h_c is the convective heat transfer coefficient (which is a function of the surface temperatures and the indoor air velocity) in [$Wm^{-2}\,{}^{o}C^{-1}$] and the temperatures are in [^{o}C]

B.2.4 Air velocity

Air velocity (v_a) is a measure of the rate of air movement over a specific displacement over a fixed period of time. It plays a crucial role in determining the comfort level of building occupants. A high air velocity, typically above 0.2m/s, can lead to discomfort, particularly in cold temperatures as it can have a cooling effect on the human body [52] whereas high air velocities are beneficial when the air temperature is high. In such scenarios, even small amounts of air movement can cause discomfort due to the enhancement of the cooling effect. It is important to consider the impact of air velocity on thermal comfort in building design and operation to ensure the well-being of the occupants. [53].

B.2.5 Relative humidity

The Relative humidity (RH) is the ratio between the actual water vapour concentration and the maximum possible concentration (at saturation) of water vapour in air at a given temperature. It is usually expressed in % [54].

$$RH = 100\frac{p_w}{p_{sat}} \tag{B.3}$$

where p_w is the actual partial pressure of water vapour and p_{sat} is the partial pressure of water vapour in saturated air at a given temperature.

Various studies have suggested that a relative humidity of 30-60 % can be considered comfortable for humans. Furthermore, relative humidity of more than 70% can provoke discomfort to humans as when the relative humidity exceeds 70%, it can impede human thermoregulation due to the decrease in evaporative cooling capacity of sweat on the skin. This can lead to an increase in perceived temperature and discomfort [55].

B.2.6 Clothing Insulation

The thermal insulation provided to an individual by their clothing, quantified in terms of the unit of measurement known as "clo" (where 1 clo = 155 $m^{2o}C.W$), is referred to as *clothing insulation.*

B.2.7 Metabolic heat rate

The *Metabolic heat rate* or activity level $\dot{M}$ is the net heat flowing from a human body in a unit of time and it depends on various factors such as age, sex, and activity of a person. It is usually expressed in *met* units (1 met = 58.2 $W.m^{-2}$). Moreover, the value is always positive irrespective of the ambient conditions.

C Fundamentals of Building Energy modeling

C.1 Building modeling approaches

The development of an accurate thermal energy-flow model of a building is crucial for the control and optimization of energy sources, as outlined in the introductory chapter. These models are used for a variety of purposes, including energy demand estimation, sizing of heating, ventilation, and air conditioning equipment, optimization, fault detection, and model-based control [56]. According to Boodi et al., the dynamics of energy flow are primarily influenced by several factors such as:

- Thermal, physical and geometric properties of the building
- Indoor energy gains
- Occupancy behavior and interaction with the building
- Location and orientation of the building
- External factors such as ambient temperature, wind speed, solar irradiance and cloud coverage

A wide range of modeling approaches have been investigated to accurately represent the dynamics of energy flow, and these can be broadly classified into three paradigms: white-box, grey-box, and black-box modeling. Each paradigm has its own set of advantages and disadvantages and has been the subject of extensive research in the literature. These studies emphasize the importance of validating the models using standard validation methods, which will be discussed in the following section.

C.1.1 White-box modelling

White-box modeling is a method of modeling that utilizes the laws of physics, thermodynamics, and heat transfer phenomena in the form of differential equations (as discussed in section 2.1) to be solved. These models are parametric in nature and are theoretically infinite-dimensional due to a lack of segregation into nodes which makes them computationally expensive to solve.

However, common assumptions such as homogeneous heating of components make the

model finite-dimensional. These models can be complex due to their non-linear and continuous nature, requiring a significant amount of computational time and effort. Techniques such as discretization and linearization can be employed to reduce the complexity of the model while maintaining accuracy. One commonly used modeling structure in white-box modeling is the RC network analogy. In this approach, resistance symbolizes the thermal resistance to the flow of energy caused by conduction, convection, etc. while the capacitance term represents the capacity to store energy in the component, or the thermal inertia of the system. The development of accurate white-box models necessitates expert knowledge of building components' physical properties, location, and occupancy behavior, as well as accurate data on external disturbances such as climatic conditions and dynamics of building occupancy.

To address the challenges associated with white-box modeling, a variety of simulation tools have been developed for Building energy simulation (BES) and dynamics, such as EnergyPlus [57] and Transient System Simulation Tool (TRNSYS) [58]. These tools are highly optimized solvers that provide high levels of solution accuracy while minimizing computation time. They are capable of producing highly complex and robust models for energy demand prediction.

BES models may have difficulty modeling controllers and optimizing building systems. Co-simulation environments, such as Building Controls Virtual Test Bed (BCVTB) [59] and Modelica Library Extension (MLE+) have been developed to integrate white-box models with control techniques developed in software such as MATLAB, Python, or Modelica. But, it is important to note that these co-simulation software can be computationally expensive due to inefficiencies in the integration scheme [8]. Thus, white-box modeling using BES tools can be suitable for building energy demand estimation, construction optimization, and fault detection, but for optimal control of building's energy systems, it is preferable to develop a model directly in MATLAB, Python or Modelica because of its ability to allow real-time computation.

C.1.2 Black-box modeling

Black-box models are developed using large datasets by optimally relating input parameters, disturbances to the system, and controllable inputs to the building performance output data [60]. This approach does not require a deep understanding of the building's thermodynamic behavior. Since the model is primarily driven by data, it is generally less complex, but it is also known for its high accuracy and computational efficiency.

However, since the model is only driven by data, the internal processes remain unknown and difficult to understand, which reduces the scalability and the degree of control. Additionally, the accuracy of the model is dependent on the quantity and quality of data fed into the system. This data can be obtained from various sources such as :

- Real-time data collected by sensors
- Data collected from BES tools

- Standardized data sets published by ASHRAE

Black-box modeling has been the subject of extensive research over the past decade, and these models have been found to be suitable for building energy demand prediction and model-based control, but they are not ideal for control due to a lack of knowledge about internal processes [61]. The models can be broadly categorized into parametric and non-parametric, and based on complexity, they are classified as linear and non-linear. The choice of statistical model is selected based on the required accuracy and available computational load.

C.1.3 Grey-box modeling

Grey-box modeling is a hybrid approach that combines the principles of physics-based white-box models and data-driven parameter estimation of black-box modeling. The physical model of a building is represented in the form of differential equations, which are then discretized and simplified through state-space dimensionality reduction and linearization. Grey-box modeling structure uses the simplified Resistor-Capacitor (RC) network analogy. The simplified RC network is a linear network that is easily scalable by adding more building components. Data to calibrate these models can be obtained from the same sources as for the black-box modeling approach. The main advantage of the grey-box approach is that it requires less data to optimize the model. Additionally, these lumped/simplified RC networks have a better working range than white-box approximation techniques [62].

C.2 Numerical validation methods

Model validation is a crucial step in ensuring the robustness and performance of the control strategy. Several metrics have been proposed to evaluate the validity of an MPC model, including model accuracy, robustness, and complexity. It is important to note that the choice of the model prediction error measure depends on the application and the objective of the MPC [63].

1. *Mean Absolute Error (MAE)* is defined as the average of the absolute differences between the predicted and measured outputs over a certain time horizon.
2. *Mean Squared Error (MSE)* is defined as the average of the squared differences between the predicted and measured outputs over a certain time horizon.
3. *Root Mean Squared Error (RMSE)* can be obtained by taking the square root of the MSE, which gives a measure of the error in the same units as the measured and predicted outputs.
4. *Normalized Root Mean Squared Error (NRMSE)* can be computed by normalizing the RMSE by the range of the measured outputs, providing a measure of the error relative to the system's dynamic range.
5. *Correlation coefficient (R)* measures the correlation between the predicted and measured outputs. A value of 1 indicates a perfect correlation, while a value of -1 indicates a perfect negative correlation.

The goal is to reduce significant errors, and using Root mean squared error (RMSE) can be effective because it gives more weight to larger errors. When conducting validation, it's necessary to evaluate and compare values across different ranges and NRMSE can be a valuable approach for this purpose.

C.2.1 Normalised Root-mean-square error (NRMSE)

The NRMSE is particularly useful in situations where the range of the measured outputs is variable. The normalization of the error by the range of the measured outputs allows for a fair comparison of the model's performance across different operating conditions, and it is particularly useful when the measured outputs have different units or when comparing the performance of different models. [63]

Furthermore, the NRMSE provides a measure of the model prediction error relative to the system's dynamic range, which can be more informative in situations where the absolute error is not informative on its own. For example, in some control systems, small errors may be acceptable, while in others, even small errors may cause significant problems. In various studies, an NRMSE value of lesser than 0.2 has been regarded as an acceptable value.

$$RMSE = \sqrt{\frac{1}{N}\sum_{i=1}^{N}(y(i) - \hat{y}(i))^2} \tag{C.1}$$

$$NRMSE = \frac{RMSE}{y_{max} - y_{min}} \tag{C.2}$$

C.3 Conclusion

Different approaches have been employed to develop accurate building models, with the grey-box modeling approach being extensively studied due to its simplicity in control and the availability of building data. MATLAB is a commonly used software platform for developing building models, despite the intricacy of thermodynamic properties involved. Modeling convection coefficients and solar irradiance is a significant challenge. Researchers have conducted substantial research to develop accurate modeling techniques and convection correlations. Additionally, complex algorithms have been analyzed to model solar irradiance on tilted surfaces. The Perez model has been recognized as the most suitable choice for modeling solar irradiance.

Once a model is developed, it is necessary to validate it to ensure that it accurately represents the thermodynamics of the building. Several performance parameters are considered during model validation. Since the aim is to minimize significant errors, RMSE can be a useful metric because it assigns more weight to larger errors. When evaluating and comparing values across different ranges during validation, NRMSE can be a valuable approach for this purpose, and an NRMSE of 0-0.2 is regarded as an acceptable range.

D Phase Change Materials: An Overview

Research in modeling of PCM employs both numerical and experimental methodologies, although there is no consensus on the optimal numerical approach as it is dependent on the specific system configuration and analysis being conducted. However, there remains a need for further research on developing robust models for predictive control and optimization, particularly in regard to the hysteresis properties of PCMs [64].

D.1 Characteristics of PCMs

A PCM possesses a set of unique characteristics that make them suitable for thermal energy storage applications. These include:

1. A specific phase change temperature, at which the material undergoes a transition from solid to liquid or vice versa.

2. A high thermal energy storage density, which allows for the storage of large amounts of thermal energy in a small volume.

3. A significant latent heat of fusion or solidification, corresponds to the amount of thermal energy absorbed or released during the phase change process.

4. The presence of hysteresis, which is the phenomenon of different phase change temperature ranges during heating and cooling.

5. Non-toxicity and Durability to withstand repeated charge-discharge cycles over an extended period.

6. Low thermal conductivity, which results in prolonged storage of thermal energy.

7. Low cost for some PCMs, making them readily available.

A compilation of the PCM properties for various classifications, as reported in scholarly literature, that are appropriate for the construction of applications in accordance with European climatic conditions are presented in Table D.1.

PCM type	Melting temperature (^oC)	Heat of fusion (W/m.K)	Density(Kg/m^2)	Ref
Paraffin wax	27–29	245	770 (liquid) 880 (solid)	[65]
CA-MA-PA hydrated salt	18.6	128.2	N/A	[66]
PureTemp 23	22.2-24.2	170.71	830 (liquid) 910 (solid)	[67]
RT-18	26-29	190	756	[68]
$CaCl_2.6H_2O$	20-23	310	1800	[69]
HS29	20-23	310	1530 (liquid) 1680 (solid)	[70]

Table D.1: Thermo-Physical properties of PCM

D.2 PCM Incorporation techniques

In an active system, the PCM is typically used in conjunction with a heating or cooling system, such as a refrigeration or heating system. The PCM is charged with heat energy by the system during periods of excess heat production or low thermal demand, and then released when the demand for heat is high or the heat production is low. In a passive system, the PCM is typically used in conjunction with natural ventilation or radiators to charge and discharge the PCM . As such, the thermal performance of the PCM is primarily dependent on the convective heat transfer between the air and the PCM.

For a climate such as the Netherlands, PCMs are mainly utilized in two ways:

- Absorb the cold from external air during summer nights and release it during the following day
- Absorb the heat from the return air during autumn/winter when the system overproduces the heating demand

D.3 Choice of PCM: Calcium Chloride Hexahydrate

Traditionally, the most widely utilized PCM for temperature regulation in buildings has been based on paraffin. However, the flammable nature of this substance has resulted in its un-

desirable use in building applications. Recent advancements in the field have resulted in the development of salt hydrate-based PCMs, which offer several significant benefits over their paraffin-based counterparts. These PCMs are non-flammable, non-toxic, and free from harmful properties, and can be specifically designed to suit a specific temperature range.

The PCM utilized in the panels is CCH, which is encased within crystal storage panels made of high-density polyethylene The PCM has a melting point range of 20-23 degrees Celsius. The overall thermal storage capacity of the panel related to the phase change process is calculated to be 310 kJ/kg. The utilization of CCH is justifiable due to its elevated Latent heat, Non-Flammablity and broad Operating Temperature Range.

D.4 Modeling of Phase Change materials

Research has shown that PCM can be modeled with high accuracy using a linear phase change (as described by the Scheil-Gulliver equation [71]) in between 20 to 23^{o}C.

The Scheil-Gulliver equation is a mathematical model that describes the solidification kinetics of a liquid metal. The equation relates the solid fraction, f, and the undercooling, ΔT, which is the difference between the liquidus temperature (the temperature at which a metal commences solidification) and the solidification temperature [72]. The equation is represented as:

$$f = 1 - (\frac{\Delta T}{\Delta T_m})^{(1/n)} \tag{D.1}$$

where ΔT_m is the maximum undercooling, which is the difference between the liquidus temperature and the solidification temperature (the temperature at which a metal is fully solid), and n is a constant that is dependent on the material and the cooling rate.

The Scheil-Gulliver equation is based on the assumption that solidification proceeds at a constant rate and that the solid and liquid phases are in equilibrium. It also presumes that the solidification process is diffusion-controlled, meaning that the rate of solidification is determined by the diffusion of atoms or molecules from the liquid to the solid phase. The Scheil-Gulliver equation can be utilized to predict the solid fraction of liquid metal as a function of cooling rate and undercooling. The PCM material selected for this thesis is CCH, and its specifications include a melting temperature range of 3 degrees Celsius (ΔT_m = 3 ^{o}C) and a phase change exponent of 1 (n = 1) as experimentally verified by Peter can den Engel et. al [25].

E Control Systems in buildings

Building control systems, also known as building automation systems or BEMS, are designed to monitor and control the indoor climate of buildings to improve operational performance and ensure the comfort of occupants. These systems typically use centralized, integrated networks of hardware and software to monitor and control indoor conditions. Two main types of building control schemes for indoor environments are conventional controllers and intelligent controllers. Conventional controllers use simple control algorithms, whereas intelligent controllers use more advanced algorithms and have the ability to adapt to changes in the environment.

E.1 Conventional controllers

Building control systems are a fundamental aspect of building energy management, as they play a critical role in achieving energy efficiency and sustainability. Several standard control schemes, such as On-Off control, Proportional-integral (PI), and Proportional-integral-derivative (PID) controllers, have been widely utilized in building control [73]. However, these control systems have demonstrated poor performance in various applications and disturbed environments, and have not provided an optimal control strategy.

The use of on/off controllers, specifically, is commonly utilized for regulating indoor temperature; however, this approach is known to result in significant energy consumption and wastage because of instabilities and frequent overshooting of set points.

P, PI, and PID controllers are closed-loop/feedback controls that lack direct knowledge of the system being controlled and possess constant parameters [73]. These controllers have been found to provide poor control performance for processes that are noisy and nonlinear, with large time delays when used alone. The performance of these controllers can be improved through the cascading of multiple PID controllers or linking feedback and feedforward controllers. However, even with these enhancements, the system could be unstable. Therefore, control designers and engineers have turned to optimal, predictive, and adaptive techniques to improve control performance and stability.

E.2 Intelligent controllers

In the 1990s, a significant amount of research was focused on advanced energy and comfort management controls [73]. The main research trends that emerged in this field include:

1. Learning-based methods: These methods include the use of artificial intelligence, fuzzy systems, and neural networks, such as fuzzy control with conventional controls, Adaptive fuzzy neural network (ANFIS) systems, etc.
2. MPC technique: This technique follows the principles of classical controls and uses mathematical models to predict the behavior of the system.
3. Agent-based control systems: These systems use autonomous agents to manage and control building systems.

These research trends aimed to improve the performance and energy efficiency of building control systems, through the implementation of advanced control algorithms, and self-learning and adaptability capabilities. While it is intriguing to determine the most effective implementation of intelligent control, this study will focus on analyzing the application of the Model Predictive Control strategy.

E.3 Model Predictive Control

Model Predictive Control (MPC) is an advanced control strategy that optimizes system control based on a mathematical model. It combines control theory, optimization, and prediction to achieve desired performance while considering system constraints.

MPC operates by making predictions about the system's future behavior and generating an optimal control sequence accordingly. This sequence is then applied to the system within a specific time frame, and the process is repeated periodically. By continuously updating the control sequence using new measurements and predictions, the control action can be adjusted dynamically to optimize the system's behavior.

The key steps involved in MPC are as follows:

- System Modeling: Develop a mathematical model of the system based on known system dynamics, describing the relationship between inputs and outputs.
- Objective Function Formulation: Define an objective function that captures the desired control objectives, incorporating performance criteria and potential penalties for constraint violations.
- Prediction: Utilize the system model to predict the system's future behavior over a defined time horizon by applying the current control sequence and estimating future states and outputs.

- Optimization: Formulate an optimization problem aimed at finding the optimal control sequence that minimizes the objective function while adhering to system constraints. The optimization algorithm seeks the control sequence that yields the best predicted performance.

- Constraint Handling: Account for constraints such as physical limits, safety boundaries, or operational restrictions during the optimization process. Adjust the control sequence to ensure that the predicted system behavior remains within the acceptable limits.

- Control Action: Implement the first control action from the optimal control sequence on the system. Periodically repeat the process by updating the control sequence based on new measurements and predictions.

In MPC, a mathematical model of the process is used to predict its behavior and generate control signals to achieve a desired outcome [74]. The control signal is obtained by minimizing an objective function while taking into account constraints on the system. The minimization is performed iteratively over a finite prediction horizon. MPC is applied using a receding horizon approach where the control signals are recalculated at each iteration based on a moving prediction horizon, but only the first step of the control is implemented.

This approach enables a more adaptable and quick-responding control strategy and also helps overcome the limitations of unstable solutions and a lack of feedback [8]. Figure E.1 illustrates a simplified layout of MPC strategy.

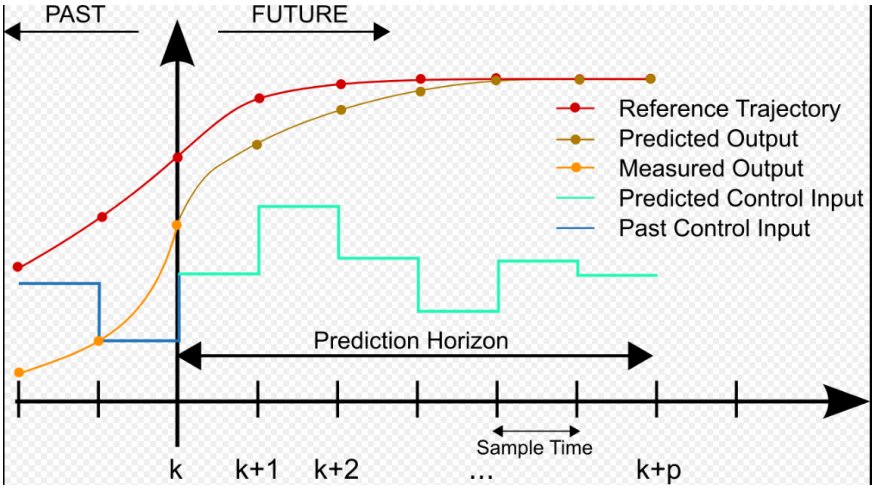

Figure E.1: Simplified layout of MPC strategy

E.4 Model Predictive Control of PCMs in HVAC systems

The control strategy for HVAC systems that utilize PCMs requires the monitoring of the temperature of the PCM and the regulation of the flow of heat to and from it. This is typically accomplished through the manipulation of a heat transfer fluid, such as water or a refrigerant that is in thermal communication with the PCM. The control algorithm should take into account not only the properties of the PCM material, but also the overall performance, energy consumption, and thermal comfort of the building's inhabitants.

A research by Gholamibozanjani et.al [75] presents the results of a numerical study that investigated the use of a MPC strategy to control the heating process using a heat exchanger containing PCM and a solar air collector. The study also looked at the effect of different parameters such as prediction horizon, time step, PCM content in the heat exchanger, and simulation length on the performance of the MPC strategy. The results showed that a greater prediction horizon, smaller time step and a higher amount of PCM content in the heat exchanger were more beneficial in terms of cost savings for electricity.

The research by Serale et.al [76] presents an innovative MPC algorithm for managing energy systems based on latent heat exchange using PCMs. The algorithm incorporates the correlation of experimental specific heat capacity data of the PCM slurry as a piecewise-affine function [76]. The results of the study showed that the MPC algorithm was able to optimize a defined objective function by anticipating the building energy demand and weather disturbances, resulting in energy savings of up to 19.2% compared to a rule-based controller.

E.5 Feasibility of MPC

MPC is well-suited for this research as the control decision should not only consider the present input parameters, but also the future states. Each model used in MPC comprises of the dynamics, weather conditions, occupancy, and disturbances at each step [73]. The prediction model can be created using the modeling approaches discussed in the previous section.

The feasibility of the optimization is constrained by the limitations of the actuators and other constraints. The complexity of the optimization is determined by the objective function, constraints, and the complexity of the model. It is important to note that complex optimization problems are usually computationally expensive, thus there is a trade-off between control performance and computational effort.

E.6 Selection of objectives and constraints

The objective function represents the ultimate goal of the optimization process. The function is minimized in order to achieve convergence toward the goal. In the context of indoor climate control, the goals are often related to occupants' comfort, such as air temperature, air exchange rates, and the relative humidity of air. Alternatively, the energy consumption can also serve as an objective function in the optimization problem. Numerous studies have demonstrated that minimizing the energy consumption while ensuring that comfort criteria are maintained as constraints, is an effective method to formulate the MPC problem [77].

In MPC, constraints can be broadly classified into two categories: hard constraints and soft constraints. Hard constraints are limiting factors that must be adhered to in order to obtain a feasible solution. For instance, in building control applications, hard constraints may include temperature limits and maximum heating/cooling power limits. These constraints are considered mandatory and must be satisfied for the MPC algorithm to be considered successful. Whereas soft constraints are objectives or preferences that the MPC algorithm should aim to satisfy but can be traded off with other objectives. For instance, soft constraints in building control applications can be occupant's comfort or energy efficiency of the HVAC components.

However, there is no universally optimal objective function or constraint for a given MPC problem as every system has unique dynamics and end-goal. Literature has presented various tried and tested methods that can be used. Therefore, one can experiment with a range of combinations of objectives and constraints to determine the most effective solution. It is worth noting that the choice of algorithm, methodologies and tuning method may vary depending on the specific application, the complexity of the system, the computational resources available and other factors.

E.7 MPC problem classes

In this section, an overview of the most significant classes of MPC problems will be presented. These MPC problems are differentiated by the type and structure of the corresponding optimization problem that must be solved through direct methods. Direct methods, in this context, refer to the process of translating the Optimal Control Problem into an Optimization Problem and subsequently obtaining its solution utilizing numerical optimization techniques[8].

E.7.1 Linear MPC

Linear model predictive control (LMPC) is a widely used technique in which the prediction model and the constraints are linear, and the objective function is either linear or quadratic.

One of the key advantages of linear MPC is its ease of integration through recursive substitution of consecutive state variables into large prediction matrices [8]. The prediction matrix is then incorporated into the objective function to form a Hessian matrix, and for the optimization problem to be convex, the Hessian matrix should be positive semi-definite [78]. The computational complexity of this dense linear optimization problem scales with $f(N^3 n_u^3)$ where N is the control horizon and n_u is the number of inputs [79].

Linear MPC has been widely researched in both academic and industrial settings due to its efficient implementation and scalability. Studies have demonstrated the ability to implement linear MPC with thousands of parameters and optimization variables [80]. However, it should be noted that heat transfer phenomena are non-linear in nature and various methods have been proposed to linearize them with a high degree of accuracy [81]. Due to its efficiency and scalability, Linear MPC is considered to be a viable option for indoor climate control.

E.7.2 Nonlinear MPC

In Nonlinear model predictive control (NLMPC), either the prediction model or the objective function is nonlinear. This can be the case when modeling heat transfer phenomena, as they can be non-linear (such as radiation and convection), and many research studies have used non-linear models to develop accurate building energy models.

Unlike Linear MPC, the optimization problem in Nonlinear MPC is not convex, which means that the solution space contains multiple local minima. Therefore, the solvers used for linear optimization problems can no longer ensure that the solution is a global minimum [78]. However, advanced solvers have been developed, such as fminbbnd, fminsearch and fmincon in MATLAB, which can start from multiple initial points and ensure that the solution found is a global minimum.

Nonlinear MPC has great potential in the building sector as it can provide improved accuracy over linear models [82]. However, the main disadvantage is the high computational demand. Nevertheless, Nonlinear MPCs are gaining increasing importance in this sector due to their improved accuracy [83] [84]. Non-linear MPC is chosen to capture the non-linearities in irradiances and convection relations.

E.7.3 MPC solvers

The use of solvers in commercial applications has seen significant advancements in recent years, with a variety of techniques being utilized to address optimization problems of varying complexity and scale. These are briefly discussed below:

- Mixed-Integer Nonlinear Programming (MINLP): MINLP is a type of optimization that combines nonlinear programming with integer constraints, which restrict some or all of the decision variables to integer values.

- Nonlinear Programming (NLP): NLP is a type of optimization used for solving objective functions that are not linear, subject to nonlinear constraints.
- Sequential quadratic programming (SQP): SQP is an iterative optimization algorithm that solves non-linear constrained optimization problems by approximating the objective function and constraints with quadratic models.
- fminunc: This function is used for solving unconstrained optimization problems with smooth objective functions.
- fmincon: This function is used for solving constrained optimization problems with linear or nonlinear constraints.
- patternsearch: This function is used for finding the global minimum of a function without requiring gradient information. It is suitable for optimization problems with non-smooth and discontinuous objective functions.
- Genetic Algorithm (GA): This function is used for solving optimization problems with discrete variables, integer variables, or mixed-integer variables. It is suitable for global optimization problems.
- fgoalattain: This function is used for solving multi-objective optimization problems where the objective functions need to be minimized or maximized subject to constraints.

Since the number of variables in the optimization problem is relatively small, with fewer than a hundred variables, fmincon is a suitable optimization algorithm to use because it can handle both linear and non-linear constraints and provide faster convergence compared to other solvers. It is particularly useful when the optimization problem is non-linear with constraints that can be expressed as inequalities and is highly flexible and provides a variety of options for controlling the optimization process. Moreover, fmincon is a well-established solver that has been extensively tested, and is known for its robustness.

E.8 Conclusion

In recent decades, extensive research efforts have focused on optimizing the control of BEMS by implementing advanced control strategies, such as MPC. MPC is favored due to its capability to consider the future state of the system and optimize control signals based on predicted disturbances. Various combinations of hard constraints and optimization functions have been investigated and evaluated in the literature. However, it is widely recognized that there is no universal solution that can be applied to all scenarios.

Given that convection and radiation terms introduce non-linearities in the equations, a non-linear model of the building was deemed necessary to effectively capture its thermodynamic behavior. As the number of variables in the optimization problem is relatively small, with fewer than a hundred variables, fmincon is a suitable optimization algorithm to employ.

Bibliography

[1] Maohui Luo, Xiang Zhou, Yingxin Zhu, and Jan Sundell. Revisiting an overlooked parameter in thermal comfort studies, the metabolic rate. *Energy and Buildings*, 118:152–159, 2016.

[2] Yukio Narukawa, Masatsugu Ichikawa, Daisuke Sanga, Masahiko Sano, and Takashi Mukai. White light emitting diodes with super-high luminous efficacy. *Journal of physics D: Applied physics*, 43(35):354002, 2010.

[3] Miguel de Simón-Martín, Cristina Alonso-Tristán, and Montserrat Díez-Mediavilla. Diffuse solar irradiance estimation on building's façades: review, classification and benchmarking of 30 models under all sky conditions. *Renewable and Sustainable Energy Reviews*, 77:783–802, 2017.

[4] Delia D'agostino, Paolo Zangheri, and Luca Castellazzi. Towards nearly zero energy buildings in europe: A focus on retrofit in non-residential buildings. *Energies*, 10(1):117, 2017.

[5] www.rijksoverheid.nl/actueel/nieuws/2020/12/18/beng-eisen-treden-van-1-januari-2021-in-werking Ministerie van Binnenlandse Zaken en Koninkrijksrelaties. Beng-eisen treden van 1 januari 2021 in werking, Dec 2020.

[6] Ministerie van Binnenlandse Zaken en Koninkrijksrelaties www.nieman.nl/specialismen/energie-en-duurzaamheid/beng-eis-vanaf 01-01-2021/. Beng eis vanaf 01-01-2021, July 2021.

[7] René van der Loos and www.dgmr.nl/kennis/publicaties/verandering-van-beng/ Kuijpers, Ieke. Beng is veranderd, maar wat betekent dat nu echt?, Feb 2019.

[8] Ján Drgoňa, Javier Arroyo, Iago Cupeiro Figueroa, David Blum, Krzysztof Arendt, Donghun Kim, Enric Perarnau Ollé, Juraj Oravec, Michael Wetter, Draguna L Vrabie, et al. All you need to know about model predictive control for buildings. *Annual Reviews in Control*, 50:190–232, 2020.

[9] Kees van der Linden, Atze C Boerstra, Arjen K Raue, and Stanley R Kurvers. Thermal indoor climate building performance characterized by human comfort response. *Energy and Buildings*, 34(7):737–744, 2002.

[10] Poul O Fanger et al. Thermal comfort. analysis and applications in environmental engineering. *Thermal comfort. Analysis and applications in environmental engineering.*, 1970.

[11] Richard De Dear and Gail Schiller Brager. Developing an adaptive model of thermal comfort and preference. 1998.

[12] AC Van der Linden, Atze C Boerstra, Arjen K Raue, Stanley R Kurvers, and RJ De Dear. Adaptive temperature limits: A new guideline in the netherlands: A new approach for the assessment of building performance with respect to thermal indoor climate. *Energy and buildings*, 38(1):8–17, 2006.

[13] MJP Arets. Thermische behaaglijkheid: eisen voor de binnentemperatuur in gebouwen: een nieuwe richtlijn voor thermische behaaglijkheid in (kantoor) gebouwen, 2004.

[14] Richard J De Dear. A global database of thermal comfort field experiments. *ASHRAE transactions*, 104:1141, 1998.

[15] A Auliciems. Psycho-physiological criteria for global thermal zones of building design. *Int J Biometeorol*, 26:69–86, 1981.

[16] J Fergus Nicol and Michael A Humphreys. Adaptive thermal comfort and sustainable thermal standards for buildings. *Energy and buildings*, 34(6):563–572, 2002.

[17] PJW van den Engel, RMJ Bokel, Eleonora Brembilla, LA de Araujo Passos, and Peter Luscuere. Converge: Low energy with active passiveness in a transparent highly occupied building. In *CLIMA 2022-14th REHVA HVAC World Congress*. TU Delft Open, 2022.

[18] Rakesh P Borase, DK Maghade, SY Sondkar, and SN Pawar. A review of pid control, tuning methods and applications. *International Journal of Dynamics and Control*, 9(2):818–827, 2021.

[19] Williams H McAdams. Heat transmission. Technical report, 1954.

[20] RK MacGregor and Ashley Francis Emery. Free convection through vertical plane layers—moderate and high prandtl number fluids. 1969.

[21] Stuart W Churchill and Humbert HS Chu. Correlating equations for laminar and turbulent free convection from a vertical plate. *International journal of heat and mass transfer*, 18(11):1323–1329, 1975.

[22] Thomas Joseph Ceha, Luigi Antonio de Araujo Passos, Simone Baldi, and Bart De Schutter. Model predictive control for optimal integration of a thermal chimney and solar shaded building. In *2021 29th Mediterranean Conference on Control and Automation (MED)*, pages 21–26. IEEE, 2021.

[23] Theoretical considerations on natural ventilation by thermal buoyancy. Technical report, American Society of Heating, Refrigerating and Air-Conditioning Engineers . . . , 1995.

[24] Luigi Antonio de Araujo Passos, Peter van den Engel, Simone Baldi, and Bart De Schutter. Dynamic optimization for minimal hvac demand with latent heat storage, heat recovery, natural ventilation, and solar shadings. *Energy Conversion and Management*, 276:116573, 2023.

[25] Peter van den Engel, Michael Malin, Nikhilesh Kodur Venkatesh, and Luigi Antonio de Araujo. Performance of a phase change material battery in a transparent building. *Fluid Dynamics and Materials Processing*, 19(3):783–805, 2023.

[26] DG Erbs, SA Klein, and JA Duffie. Estimation of the diffuse radiation fraction for hourly, daily and monthly-average global radiation. *Solar energy*, 28(4):293–302, 1982.

[27] Jamie M Bright. Solcast: Validation of a satellite-derived solar irradiance dataset. *Solar Energy*, 189:435–449, 2019.

[28] Bertil Thomas and Mohsen Soleimani-Mohseni. Artificial neural network models for indoor temperature prediction: investigations in two buildings. *Neural Computing and Applications*, 16:81–89, 2007.

[29] Sophie Obyn and Geoffrey Van Moeseke. Variability and impact of internal surfaces convective heat transfer coefficients in the thermal evaluation of office buildings. *Applied Thermal Engineering*, 87:258–272, 2015.

[30] Jeannette Rosbach, Machiel Vonk, Frans Duijm, Jan T Van Ginkel, Ulrike Gehring, and Bert Brunekreef. A ventilation intervention study in classrooms to improve indoor air quality: the fresh study. *Environmental health*, 12(1):1–10, 2013.

[31] Jesper Kragh, Jørgen Rose, Toke Rammer Nielsen, and Svend Svendsen. New counter flow heat exchanger designed for ventilation systems in cold climates. *Energy and Buildings*, 39(11):1151–1158, 2007.

[32] ASHRAE Handbook. *HVAC systems and equipment*, volume 39. chapter, 1996.

[33] *International Energy Conservation Code® and ANSI/ASHRAE/IES Standard 90.1-2019: Energy Standard for buildings except low-rise residential buildings*. International Code Council, Inc., 2021.

[34] Ion Hazyuk, Christian Ghiaus, and David Penhouet. Optimal temperature control of intermittently heated buildings using model predictive control: Part i–building modeling. *Building and Environment*, 51:379–387, 2012.

[35] KN Shukla, Saroj Rangnekar, and K Sudhakar. Comparative study of isotropic and anisotropic sky models to estimate solar radiation incident on tilted surface: A case study for bhopal, india. *Energy Reports*, 1:96–103, 2015.

[36] Pierre Ineichen, Olivier Guisan, and Richard Perez. Ground-reflected radiation and albedo. *Solar Energy*, 44(4):207–214, 1990.

[37] PG Loutzenhiser, H Manz, C Felsmann, PA Strachan, TH Frank, and GM Maxwell. Empirical validation of models to compute solar irradiance on inclined surfaces for building energy simulation. *Solar Energy*, 81(2):254–267, 2007.

[38] Carlos Toledo, Ana Maria Gracia Amillo, Giorgio Bardizza, Jose Abad, and Antonio Urbina. Evaluation of solar radiation transposition models for passive energy management and building integrated photovoltaics. *Energies*, 13(3):702, 2020.

[39] B Liu and R Jordan. Daily insolation on surfaces tilted towards equator. *ASHRAE J.;(United States)*, 10, 1961.

[40] Pericles S Koronakis. On the choice of the angle of tilt for south facing solar collectors in the athens basin area. *Solar Energy*, 36(3):217–225, 1986.

[41] John E Hay. A revised method for determining the direct and diffuse components of the total short-wave radiation. *Atmosphere*, 14(4):278–287, 1976.

[42] T Muneer. Solar irradiance and illuminance models for japan i: Sloped surfaces. *International Journal of Lighting Research and Technology*, 27(4):209–222, 1995.

[43] Richard Perez, Pierre Ineichen, Robert Seals, Joseph Michalsky, and Ronald Stewart. Modeling daylight availability and irradiance components from direct and global irradiance. *Solar energy*, 44(5):271–289, 1990.

[44] Matjaz Prek. Thermodynamic analysis of human heat and mass transfer and their impact on thermal comfort. *International journal of heat and mass transfer*, 48(3-4):731–739, 2005.

[45] BW Olesen and PO Fanger. The skin temperature distribution for resting man in comfort. *Archives des sciences physiologiques*, 27(4):385–393, 1973.

[46] Diana Enescu. A review of thermal comfort models and indicators for indoor environments. *Renewable and Sustainable Energy Reviews*, 79:1353–1379, 2017.

[47] Gül Koçlar Oral, Alpin Köknel Yener, and Nurgün Tamer Bayazit. Building envelope design with the objective to ensure thermal, visual and acoustic comfort conditions. *Building and Environment*, 39(3):281–287, 2004.

[48] Salvatore Carlucci, Francesco Causone, Francesco De Rosa, and Lorenzo Pagliano. A review of indices for assessing visual comfort with a view to their use in optimization processes to support building integrated design. *Renewable and sustainable energy reviews*, 47:1016–1033, 2015.

[49] Sachin Nikam and VN Bartaria. Indoor environment in air conditioned spaces a review. *International Journal of Advanced Technology and Engineering Research*, 2(4):226–230, 2012.

[50] Stephan A Konz and Steven Johnson. *Work design: Industrial ergonomics*, volume 1. Holcomb Hathaway Pubs, 2000.

[51] Jose Luis Torres and Marcelo Luis Martin. Adaptive control of thermal comfort using neural networks. In *Argentine Symposium on Computing Technology*, pages 1–12, 2008.

[52] Hui Zhang, Edward Arens, Sahar Abbaszadeh Fard, Charlie Huizenga, Gwelen Paliaga, Gail Brager, and Leah Zagreus. Air movement preferences observed in office buildings. *International journal of Biometeorology*, 51(5):349–360, 2007.

[53] Rama Haritha Bandarupalli. Numerical simulation of thermal comfort and contaminant transport in rooms with ufad system. 2007.

[54] Edward Finucane. *Definitions, conversions, and calculations for occupational safety and health professionals*. CRC Press, 2010.

[55] Tomonobu Goto, Jørn Toftum, R De Dear, Povl Ole Fanger, et al. Thermal sensation and comfort with transient metabolic rates. *Indoor Air*, 1:1038–1043, 2002.

[56] Zakia Afroz, GM Shafiullah, Tania Urmee, and Gary Higgins. Modeling techniques used in building hvac control systems: A review. *Renewable and sustainable energy reviews*, 83:64–84, 2018.

[57] Drury B Crawley, Linda K Lawrie, Frederick C Winkelmann, Walter F Buhl, Y Joe Huang, Curtis O Pedersen, Richard K Strand, Richard J Liesen, Daniel E Fisher, Michael J Witte, et al. Energyplus: creating a new-generation building energy simulation program. *Energy and buildings*, 33(4):319–331, 2001.

[58] William A Beckman, Lars Broman, Alex Fiksel, Sanford A Klein, Eva Lindberg, Mattias Schuler, and Jeff Thornton. Trnsys the most complete solar energy system modeling and simulation software. *Renewable energy*, 5(1-4):486–488, 1994.

[59] Michael Wetter. A modular building controls virtual test bed for the integrations of heterogeneous systems. 2008.

[60] Zhenghua Chen, Mustafa K Masood, and Yeng Chai Soh. A fusion framework for occupancy estimation in office buildings based on environmental sensor data. *Energy and Buildings*, 133:790–798, 2016.

[61] Abhinandana Boodi, Karim Beddiar, Malek Benamour, Yassine Amirat, and Mohamed Benbouzid. Intelligent systems for building energy and occupant comfort optimization: A state of the art review and recommendations. *Energies*, 11(10):2604, 2018.

[62] Damien Picard, Ján Drgoňa, Michal Kvasnica, and Lieve Helsen. Impact of the controller model complexity on model predictive control performance for buildings. *Energy and Buildings*, 152:739–751, 2017.

[63] PG Voulgaris and DT Verwer. Model validation of nonlinear systems using a frequency-domain approach. *Automatica*, 39(3):543–557, 2003.

[64] Yuekuan Zhou, Siqian Zheng, and Guoqiang Zhang. A review on cooling performance enhancement for phase change materials integrated systems—flexible design and smart control with machine learning applications. *Building and Environment*, 174:106786, 2020.

[65] Xiaoqin Sun, Jovana Jovanovic, Yuan Zhang, Siyuan Fan, Youhong Chu, Yajing Mo, and Shuguang Liao. Use of encapsulated phase change materials in lightweight building walls for annual thermal regulation. *Energy*, 180:858–872, 2019.

[66] Cheng Liu, Yanping Yuan, Nan Zhang, Xiaoling Cao, and Xiaojiao Yang. A novel pcm of lauric–myristic–stearic acid/expanded graphite composite for thermal energy storage. *Materials Letters*, 120:43–46, 2014.

[67] Lidia Navarro, Aran Solé, Marc Martín, Camila Barreneche, Lorenzo Olivieri, José Antonio Tenorio, and Luisa F Cabeza. Benchmarking of useful phase change materials for a building application. *Energy and Buildings*, 182:45–50, 2019.

[68] Romeu Vicente and Tiago Silva. Brick masonry walls with pcm macrocapsules: An experimental approach. *Applied Thermal Engineering*, 67(1-2):24–34, 2014.

[69] Peter van den Engel, Michael Malin, Nikhilesh Kodur Venkatesh, and Luigi Antonio de Araujo Passos. Performance of a phase change material battery in a transparent building. *Fluid Dynamics &amp Materials Processing*, 19(3):783–805, 2023.

[70] S Kumar, S Arun Prakash, V Pandiyarajan, NB Geetha, V Antony Aroul Raj, and R Velraj. Effect of phase change material integration in clay hollow brick composite in building envelope for thermal management of energy efficient buildings. *Journal of Building Physics*, 43(4):351–364, 2020.

[71] David A Porter and Kenneth E Easterling. *Phase transformations in metals and alloys (revised reprint)*. CRC press, 2009.

[72] Martin Eden Glicksman. *Principles of solidification: an introduction to modern casting and crystal growth concepts*. Springer Science & Business Media, 2010.

[73] Pervez Hameed Shaikh, Nursyarizal Bin Mohd Nor, Perumal Nallagownden, Irraivan Elamvazuthi, and Taib Ibrahim. A review on optimized control systems for building energy and comfort management of smart sustainable buildings. *Renewable and Sustainable Energy Reviews*, 34:409–429, 2014.

[74] Jan Marian Maciejowski. *Predictive control: with constraints*. Pearson education, 2002.

[75] Gohar Gholamibozanjani, Joan Tarragona, Alvaro De Gracia, Cèsar Fernández, Luisa F Cabeza, and Mohammed M Farid. Model predictive control strategy applied to different types of building for space heating. *Applied energy*, 231:959–971, 2018.

[76] Gianluca Serale, Massimo Fiorentini, Alfonso Capozzoli, Paul Cooper, and Marco Perino. Formulation of a model predictive control algorithm to enhance the performance of a latent heat solar thermal system. *Energy conversion and management*, 173:438–449, 2018.

[77] Frauke Oldewurtel, Alessandra Parisio, Colin N Jones, Dimitrios Gyalistras, Markus Gwerder, Vanessa Stauch, Beat Lehmann, and Manfred Morari. Use of model predictive control and weather forecasts for energy efficient building climate control. *Energy and buildings*, 45:15–27, 2012.

[78] Eduardo F Camacho and Carlos Bordons Alba. *Model predictive control*. Springer science & business media, 2013.

[79] Gianluca Frison and John Bagterp Jørgensen. A fast condensing method for solution of linear-quadratic control problems. In *52nd IEEE Conference on Decision and Control*, pages 7715–7720. IEEE, 2013.

[80] Kenneth R Muske and James B Rawlings. Model predictive control with linear models. *AIChE Journal*, 39(2):262–287, 1993.

[81] Damien Picard, Filip Jorissen, and Lieve Helsen. Methodology for obtaining linear state space building energy simulation models. In *11th international modelica conference*, pages 51–58, 2015.

[82] Thomas Binder, Luise Blank, H Georg Bock, Roland Bulirsch, Wolfgang Dahmen, Moritz Diehl, Thomas Kronseder, Wolfgang Marquardt, Johannes P Schlöder, and Oskar von Stryk. Introduction to model based optimization of chemical processes on moving horizons. In *Online optimization of large scale systems*, pages 295–339. Springer, 2001.

[83] M Castilla, JD Álvarez, JE Normey-Rico, and F Rodríguez. Thermal comfort control using a non-linear mpc strategy: A real case of study in a bioclimatic building. *Journal of Process Control*, 24(6):703–713, 2014.

[84] Cara R Touretzky and Michael Baldea. Nonlinear model reduction and model predictive control of residential buildings with energy recovery. *Journal of Process Control*, 24(6):723–739, 2014.